UNIVERSITY OF OKLAHOMA

GRADUATE COLLEGE

INTEGRATED INTERPRETATION OF BOREHOLE MICROSEISMIC DATA FROM HYDRAULIC FRACTURING STIMULATION TREATMENTS

A DISSERTATION

SUBMITTED TO THE GRADUATE FACULTY

in partial fulfillment of the requirements for the

Degree of

DOCTOR OF PHILOSOPHY

By

CARLOS LUIS CABARCAS BEJARANO
Norman, Oklahoma
2014

INTEGRATED INTERPRETATION OF BOREHOLE MICROSEISMIC DATA FROM HYDRAULIC FRACTURING STIMULATION TREATMENTS

A DISSERTATION APPROVED FOR THE
CONOCOPHILLIPS SCHOOL OF GEOLOGY AND GEOPHYSICS

BY

Dr. Roger Slatt, Chair

Dr. Kurt Marfurt

Dr. Shankar Mitra

Dr. Gloria Romero

Dr. Jeffrey Callard

In memory of Dora Bejarano, mi mama, una mujer virtuosa

Acknowledgements

God has given me multiple blessings such as a countless number of academic opportunities. Among these gifts (for which I am extremely grateful) was the chance to complete the dissertation work presented within this book. I pray God will allow me to make the most of these opportunities to better serve him.

I would also like to thank everyone who contributed to this project. In particular, I would like to explicitly show my gratitude to my advisor, Dr. Roger Slatt, for his guidance and encouragement allowed me to pursue my goals and successfully reach the finish line. Special thanks also go to my advisory committee: Dr. Kurt Marfurt, Dr. Shankar Mitra, Dr. Jeffrey Callard and Dr. Gloria Romero, who kindly supported my aspirations since the very early stages of this dissertation.

The entire staff of the ConocoPhillips School of Geology of Geophysics, the Mewbourne College of Earth and Energy, the Graduate College, and my alma mater, The University of Oklahoma, also deserves my sincere appreciation. Among such an extraordinary group of people, I have to expressly recognize the support of Donna Mullins, who always went above and beyond her job duties, not only on my behalf but—to the best of my knowledge—to serve the best interest of each and every student that has ever reached out to her for help.

I would also like to state my praise and appreciation of Hilcorp Energy Company's management for permission to publish this work, as well as its support of the application of new technologies. I must also thank the Society of Exploration Geophysicists, the American Association of Petroleum Geologists, and the Society of

Petroleum Engineers, because these professional groups have played a key role on my intellectual growth, providing the venues, resources and tools to develop, share and discuss the ideas presented within this publication. Likewise, I would like to appreciate and recognize my gratitude to Dawn Henderson for proofreading numerous drafts of this manuscript, making it a more appealing piece of writing.

On a more personal note, I would like to offer special thanks to all my OU friends and colleague students whom made this journey more enjoyable. In particular, I would like to recognize the explicit and implicit encouragement received from Dr. Oswaldo Davogustto, Dr. Paul McColgan, Dr. Roderick Perez and Dr. Norelis Rodriguez, for their words lifted me up on more than one occasion, while their actions kept pushing me back into the pathway to success. Richard Brito also deserves my gratitude as I could have not finished this project without his help. In the same spirit, I would like to express sincere gratitude to my family, a source of motivation and cheer to achieve my academic goals. Among all people whom I am proud to call family, Heather and Robert Grimm (Mom and Bob) deserve a very special recognition, for their love has always been given to me unconditionally and without them this work, and probably my whole life, would have been completely different. Similarly, I would like to acknowledge the encouragement received from my beloved son, Carlos Jesus, who arrived to this world on the later stages of this project, injecting me with the energy I needed to finish it. Finally, my greatest appreciation goes to the love of my life, Dr. Maricel Marquez. She is my better half, but she definitely deserves more than half of the credit for this dissertation.

Table of Contents

List of Tables

List of Figures

Abstract

Sequence stratigraphic principles provide means to interpret the geological framework and likelihood of finding hydrocarbon–bearing rocks. In this work, I show that they can also be used to predict and better interpret the microseismic response associated with a hydraulic fracturing stimulation treatment.

In order to test my hypothesis, first I recognize the presence in the subsurface of brittle-ductile couplets, based on a sequence stratigraphic framework provided by gamma ray stacking patterns. Then, I use my geological model to better interpret the microseismic response recorded during a single stage fracture stimulation treatment monitored from three strategically located observation wells. I analyzed and compared hydraulic fracturing results inferred by individual processing of microseismic data acquired from horizontal and vertical sensor arrays, as well as the results from simultaneously processing the signals recorded by all three sensors. At the end, I show how the triple array simultaneous solution provides the most useful data set to interpret the stimulation treatment based on the good fit between the microseismic events locations obtained under this approach and the theoretical expectation from the aforementioned sequence stratigraphic framework.

Additionally, this document summarizes significant findings obtained while working on my dissertation. I discovered that despite its widespread use, there are several issues associated with the implementation of microseismic technology, which may lead to erroneous interpretations of the treatment results. In this publication, I discuss several examples of common pitfalls, including poor data recording, velocity

model artifacts, processing constraints and display limitations. These findings underscore the importance of the interpreter’s role in ensuring a high quality outcome from a microseismic hydraulic fracturing evaluation. Moreover, I demonstrate that microseismic data can also serve to identify subsurface geological features such as faults and natural fractures zones through the use of magnitude vs. distance plots.

The results from this dissertation not only improve current hydraulic fracturing microseismic interpretation workflows, but they also translate into significant costs savings associated with more efficient hydrocarbon developing campaigns.

CHAPTER 1: Introduction

Integration of geologic, geophysical and petroleum engineering concepts is not an easy task, but the exploration and production industry recognized long ago that it is perhaps the best approach to tackle the challenges of hydrocarbon extraction. This dissertation presents several examples of technology advancement based on data integration. For Instance, I make the case for using a sequence stratigraphic framework (a robust geological model) while implementing borehole microseismic monitoring (a geophysical tool) to assess the effectiveness of a hydraulic fracturing treatment (a common petroleum engineering operation). The biggest advantage of this approach is not only that it is simple and easy to use, but also, as I demonstrate in this work, it can significantly enhance the quality of the interpretation of hydraulic fracturing treatment results.

Development of resource plays is taking a crucial role in the energy supply chain. Capital investments associated with these operations reach billions of dollars annually. Therefore, improvement in the workflows currently in place by the industry, carefully outlined in this dissertation, may have a positive impact far beyond the academic requirements that this work intends to fulfill.

In particular, this dissertation studies how the interpretation of borehole microseismic data benefits from implementing an integrated analysis, ultimately impacting well spacing strategies, estimated ultimate recovery, and total development costs.

Chapter 1 introduces fundamental principles of the technologies used within this dissertation; hydraulic fracturing, borehole microseismic monitoring and sequence stratigraphy. Chapter one also elaborates on the geological characteristics of the Eagle Ford formation, because I developed most of the ideas presented in this dissertation implementing borehole microseismic while evaluating hydraulic fracturing performed on the Eagle Ford.

Chapter 2 underscores the fact that it is common practice to overlook fundamental principles during the location of microseismic events, leading to potentially erroneous hydraulic fracturing assessments. Examples of microseismic results qualitatively illustrate this assertion, showing poor data recording, velocity model artifacts, processing constraints and inadequate display choices made during practical applications of the technology. My intent is to raise awareness of some common pitfalls while also providing recommendations to increase the value of a microseismic monitoring job implementation.

Chapter 3 shows how a simple modification to the velocity model, accounting for a 4.5-degree dip supported by geological data, significantly impacts the event final locations during a borehole-based hydraulic fracturing monitoring treatment. These results underscore the importance of integrating all available data and implementing well known quality controls before using microseismic monitoring data for hydraulic fracturing evaluation.

Chapter 4 validates and supports the use of microseismic-derived Magnitude vs. Distance Plots (MDP) as a tool to discriminate between fault reactivation (i.e. stimulation failure), and successful hydraulic fracturing treatments in the absence of additional subsurface data. Moreover, when combined with other independent measurements such as 2D or 3D reflection seismic sections, as also shown in this chapter, MDP’s could unequivocally characterize the reactivation of a fault based on the recognition of microseismic event of relatively higher amplitude sometimes associated with a distinctive inferred azimuth change.

Chapter 5 describes how I used a sequence stratigraphic framework to analyze the microseismic response from a single stage hydraulic fracturing treatment monitored by three observation wells. The stratigraphic model that I built, represented by brittle-ductile couplets identified from gamma ray stacking patterns, was key to the stimulation evaluation. Ultimately, my results underscore the value of using proper geological principles on microseismic data analysis.

Chapter 6 summarizes the main ideas presented within this dissertation and provides some recommendations for future research and advancement of the microseismic monitoring technique to support the exploitation of resource plays.

1.1 Basics of Hydraulic Fracturing

In this dissertation hydraulic fracturing refers to the mechanism of injecting fluids and other additives at high-pressure to increase the flow paths between hydrocarbon bearing rocks and a wellbore, which would not otherwise produce economically without being stimulated.

For simplicity, a hydraulic fracture can be conceptualized as the geometric body illustrated in Figure 1.1.1 (Martin and Valko, 2007), which can be completely characterized by its height (h_f), width (w_f), and half-length (x_f). In reality, the geometry of a hydraulic fracture is more complex, resembling more the cartoon representation shown in Figure 1.1.2 (Paillet, 1985). Observations made from “mine-back” experiments (Cipolla et al., 2008), coupled with recent fracture images taken via downhole video camera (King, 2012), presented in Figures 1.1.3 and 1.1.4, respectively, provide evidence of this more complex geometry. The schematic in Figure 1.1.5 (Cipolla et al. 2008), depicts possible fracture growth patterns in a hard rock formation: simple fracture, complex fracture, complex fracture with fissure opening, and complex fracture network. Daneshy (2013) suggests an off-balance structure, which combines the geometries of a simple and complex fracture into a single pattern, as seen in Figure 1.1.6.

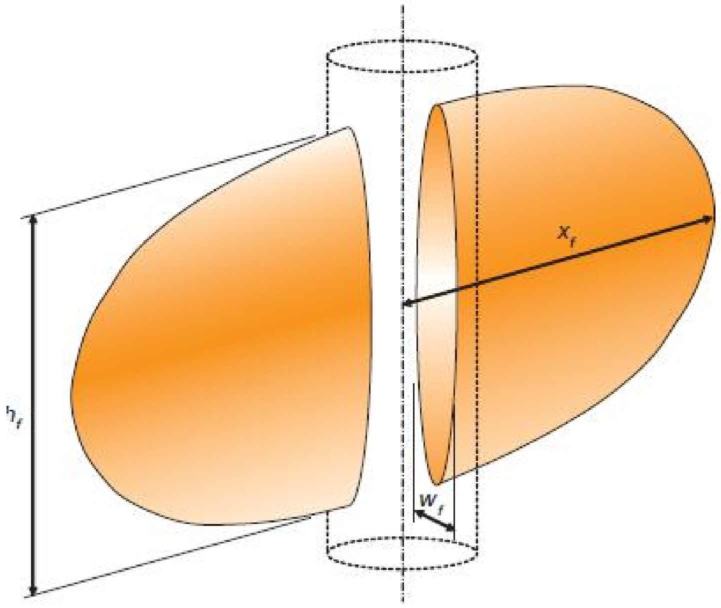

Figure 1.1.1. Geometric characteristics of an idealized hydraulic fracture; height (h_f), half-length (x_f) and width (w_f) (after Martin and Valko, 2007).

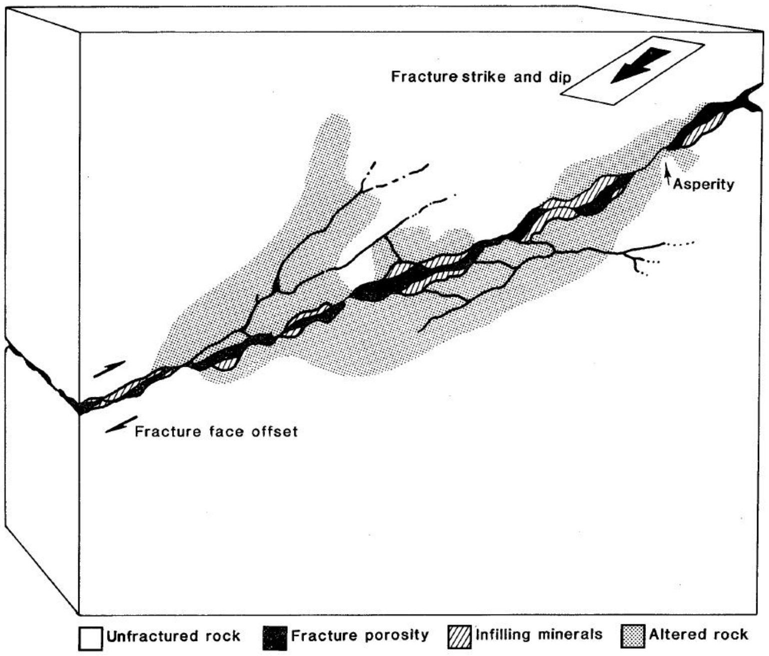

Figure 1.1.2. Schematic representation of a more realistic fracture model described by unfractured rock and altered rock associated with displacement along a rough surface geometry, fracture porosity and infilling minerals (after Paillet, 1985).

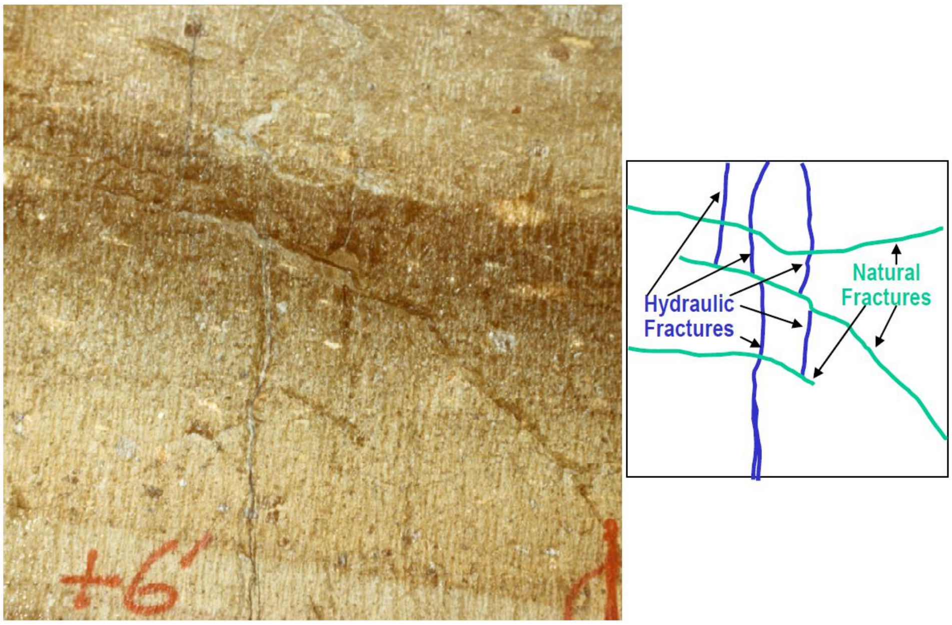

Figure 1.1.3. Fracture complexity as observed in a “mine-back” experiment and its associated schematic representation (after Cipolla et al., 2008).

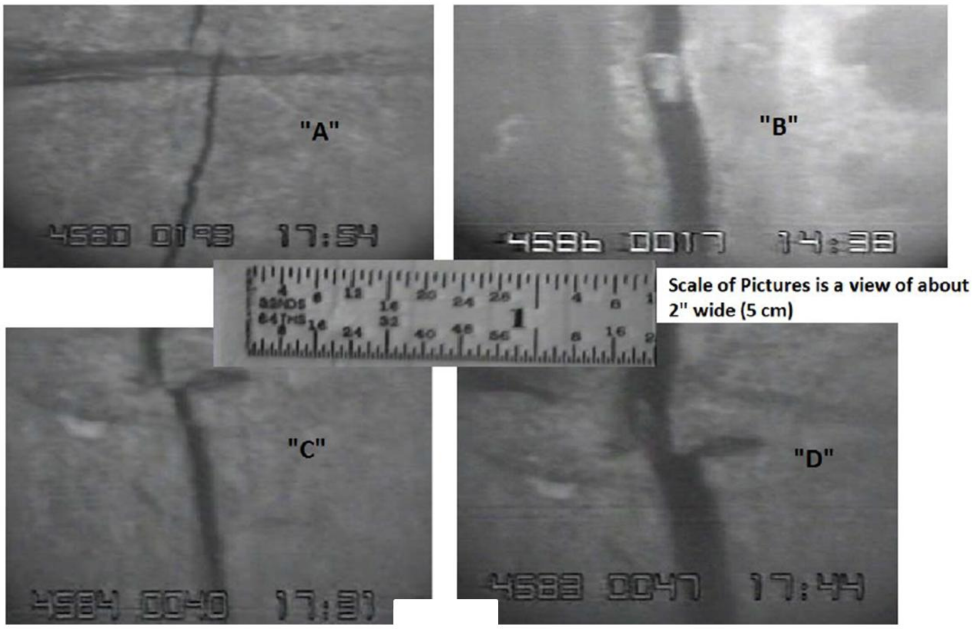

Figure 1.1.4. Hydraulic fracture photos from vertical wells open hole completions taken using Amoco downhole camera. A) Fracture shift in the presence of a ¼ in (6mm) shale barrier. B) ¼ in (6mm) wide fracture in a limestone with a rock fragment in its interior. Widening of a fracture due to increasing pressure is observed in C) before and D) after the pressure increase (after King, 2012).

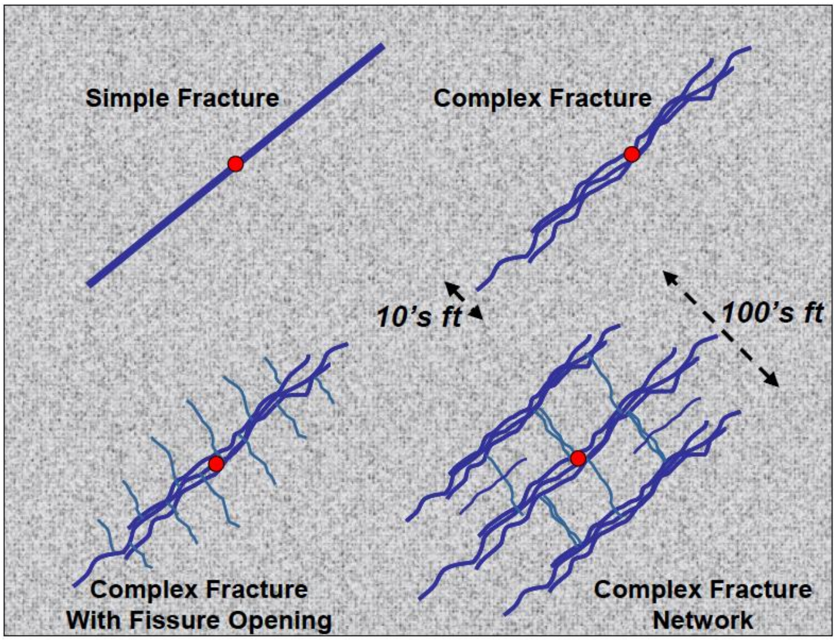

Figure 1.1.5. Schematic representation of fracture types at different complexity levels, i.e. Simple fracture, complex fracture, complex fracture with fissure opening, and complex fracture network (after Cipolla et al., 2008).

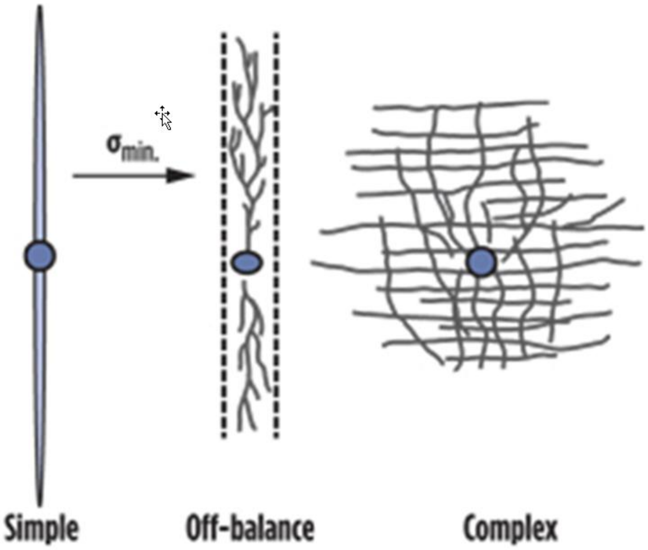

Figure 1.1.6. Plan view of different types of fracture growth patterns (after Daneshy, 2013).

A successful hydraulic fracturing treatment is one in which a fracture is initiated and propagated under pressure, and it stays open due to the presence of a proppant agent (e.g., sand, bauxite or ceramic), once the pressure is released. Although many variations exist, the general process usually involves the following steps:

1. First, inject a pad of fracturing fluid to initiate the stimulation treatment. The pad is usually a fixed volume of a viscosified fluid designed to create fracture geometry.
2. Continue fluid injection with the addition of propping agents (i.e., a mixture also known as slurry) to propagate the fracture, and introduce proppant within it.
3. Reduce injection pressure, allowing the fracture to close on the proppant.
4. Initiate the wellbore flow back to remove excess fracturing fluid and proppant.

Two main sets of parameters control hydraulic fracturing results; those related to the stimulated formation, referred to as reservoir parameters; and those related to the stimulation itself, known as treatment parameters (Daneshy, 2013). Reservoir parameters such as permeability, non-propped conductivity, horizontal stress, horizontal stress orientations, Poisson's ratio, and Young's modulus, are inherent to the formation of interest. On the other hand, treatment parameters such as fracturing fluid viscosity, pumping rate, treatment volume, pad size, and proppant size, concentration, and sequence in the pumping schedule (ramp schedule), can be designed to maximize the results of the hydraulic fracturing stimulation (Daneshy, 2013).

When it comes to fracturing fluids, choices are extensive. Nitrogen and propane have been used in multiple occasions to stimulate tight formations but most commonly a combination of water and smaller amounts of other fluids (i.e., gels, friction reducers, crosslinkers, breakers, scale inhibitors, biocides, and surfactants) are used in most of the commercial hydraulic fracturing jobs (Economides and Nolte, 2000).

Proppants also come in multiple forms (Figure 1.1.7), but usually the selection is determined by cost and availability. In principle, the role of the proppant agent is to keep the fracture open against the formation pressure, so that a fluid conduit from the reservoir into the wellbore is preserved. In reality, proppant crushing and embedment over time results in diminished fracture conductivity and productivity loss. A schematic representation of the hydraulic, propped and flowing lengths within a fracture is shown in Figure 1.1.8.

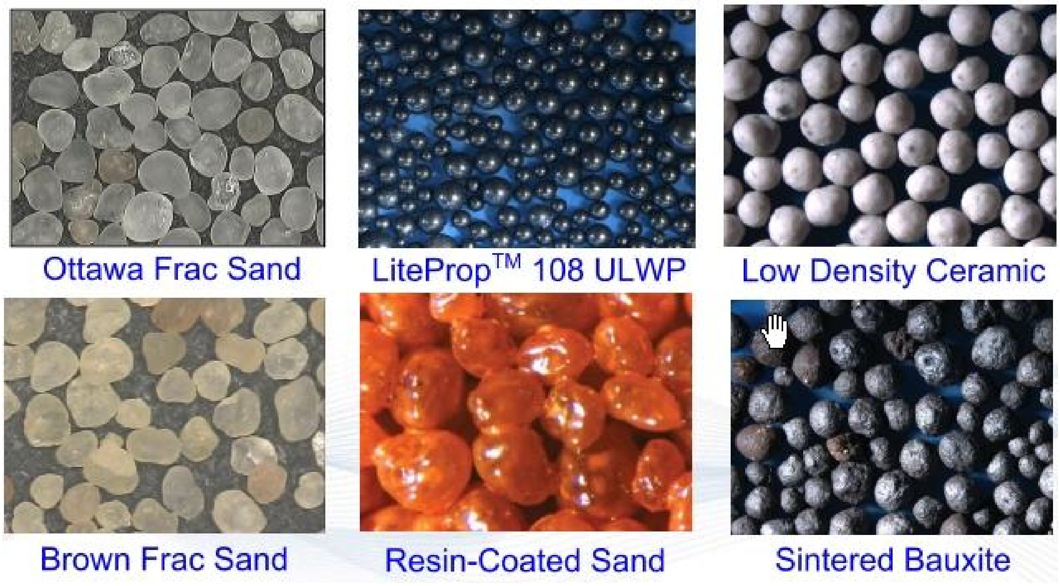

Figure 1.1.7. Common types of proppants (after LaFollette, 2010).

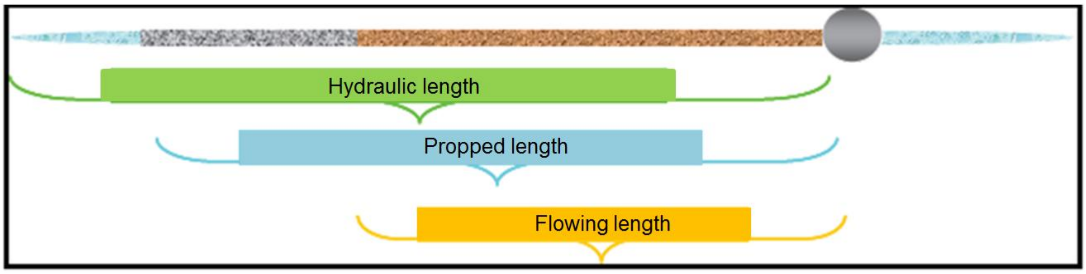

Figure 1.1.8. Schematic representation of different fracture dimensions on their proper length relationship, i.e. the hydraulic length is larger than the propped length, which is larger than the flowing length (after Maxwell and Cipolla, 2011).

The optimization of hydraulic fracturing treatment parameters has been the subject of much work, both in Academia and the Industry. Table 1 shows a compilation of practical observations on some of the most common parameters. As already mentioned, treatment results are highly dependent on the properties of the formation; therefore, it is almost impossible to design a fit-for-all treatment recipe. This has resulted in a trial and error approach to optimizing the stimulation campaigns for individual resource plays.

Table 1. Summary observations from a parameter study (Cohen et. al., 2013).

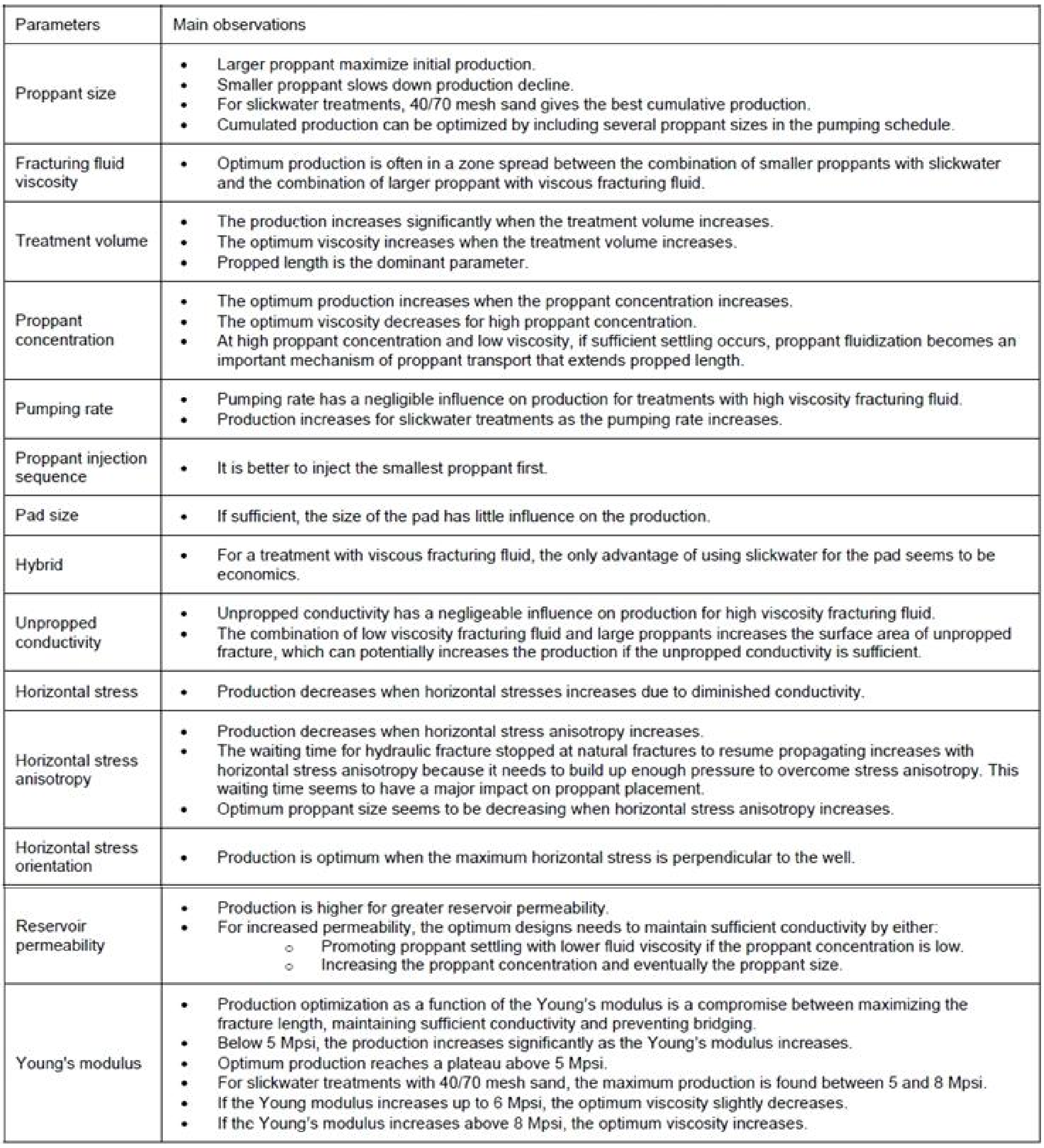

Parameters	Main observations
Proppant size	• Larger proppant maximize initial production. • Smaller proppant slows down production decline. • For slickwater treatments, 40/70 mesh sand gives the best cumulative production. • Cumulated production can be optimized by including several proppant sizes in the pumping schedule.
Fracturing fluid viscosity	• Optimum production is often in a zone spread between the combination of smaller proppants with slickwater and the combination of larger proppant with viscous fracturing fluid.
Treatment volume	• The production increases significantly when the treatment volume increases. • The optimum viscosity increases when the treatment volume increases. • Propped length is the dominant parameter.
Proppant concentration	• The optimum production increases when the proppant concentration increases. • The optimum viscosity decreases for high proppant concentration. • At high proppant concentration and low viscosity, if sufficient settling occurs, proppant fluidization becomes an important mechanism of proppant transport that extends propped length.
Pumping rate	• Pumping rate has a negligible influence on production for treatments with high viscosity fracturing fluid. • Production increases for slickwater treatments as the pumping rate increases.
Proppant injection sequence	• It is better to inject the smallest proppant first.
Pad size	• If sufficient, the size of the pad has little influence on the production.
Hybrid	• For a treatment with viscous fracturing fluid, the only advantage of using slickwater for the pad seems to be economics.
Unpropped conductivity	• Unpropped conductivity has a negligeable influence on production for high viscosity fracturing fluid. • The combination of low viscosity fracturing fluid and large proppants increases the surface area of unpropped fracture, which can potentially increases the production if the unpropped conductivity is sufficient.
Horizontal stress	• Production decreases when horizontal stresses increases due to diminished conductivity.
Horizontal stress anisotropy	• Production decreases when horizontal stress anisotropy increases. • The waiting time for hydraulic fracture stopped at natural fractures to resume propagating increases with horizontal stress anisotropy because it needs to build up enough pressure to overcome stress anisotropy. This waiting time seems to have a major impact on proppant placement. • Optimum proppant size seems to be decreasing when horizontal stress anisotropy increases.
Horizontal stress orientation	• Production is optimum when the maximum horizontal stress is perpendicular to the well.
Reservoir permeability	• Production is higher for greater reservoir permeability. • For increased permeability, the optimum designs needs to maintain sufficient conductivity by either: ○ Promoting proppant settling with lower fluid viscosity if the proppant concentration is low. ○ Increasing the proppant concentration and eventually the proppant size.
Young's modulus	• Production optimization as a function of the Young's modulus is a compromise between maximizing the fracture length, maintaining sufficient conductivity and preventing bridging. • Below 5 Mpsi, the production increases significantly as the Young's modulus increases. • Optimum production reaches a plateau above 5 Mpsi. • For slickwater treatments with 40/70 mesh sand, the maximum production is found between 5 and 8 Mpsi. • If the Young modulus increases up to 6 Mpsi, the optimum viscosity slightly decreases. • If the Young's modulus increases above 8 Mpsi, the optimum viscosity increases.

Hydraulic fracturing treatments can be diagnosed using real-time (e.g., pressure monitoring and microseismic interpretation), and post-treatment methods (e.g., radioactive proppant and liquid tracers surveys).

A more detailed discussion of the use of microseismic data for hydraulic fracturing monitoring is presented in the following sections of this dissertation. The use of pressure data for diagnostic purposes, on the other hand, is based on the relationship between fluid flow (material balance), rock elasticity and fissure creation / propagation. Therefore, net pressure (*Pnet*) inside the fracture can be expressed by Equation 1 (Smith, 2013), which assumes steady state propagation in a linear elastic, isotropic and homogeneous medium; incompressible fluid behavior; and tip growth proportional to fracture toughness (K_{IC}).

$$p_{net} \propto \left[\frac{E'^{4}}{H^{4}} \left(\frac{\mu\, Q\, x_f}{E'} \right) + \frac{K_{Ic-app}{}^{4}}{H^{2}} \right]^{1/4} \qquad \text{(Equation 1)}$$

where,

p_{net} : net pressure inside the fracture
v: Poissons' Ratio
E: Young modulus
E': Plane strain modulus = $E/(1- v^2)$
H: fracture height
μ: fluid viscosity
Q: fluid injection rate
x_f: fracture half-length
K_{Ic-app}: fracture toughness (tip effects)

Figure 1.1.9 shows a schematic representation of a typical monitoring plot, in which bottom hole pressure (BHTP), shut-in tubing pressure (STP), slurry rate and proppant concentration are plotted versus time (Martin and Valko, 2007). In general, gradual pressure changes are representative of events inside the fracture (slurry/proppant movement), whereas sharp pressure changes signal near wellbore events (Daneshy, 2013). Pressure and rate measurements are continuously recorded during the fracturing operation, and plotted real-time to make decisions on the stimulation treatment.

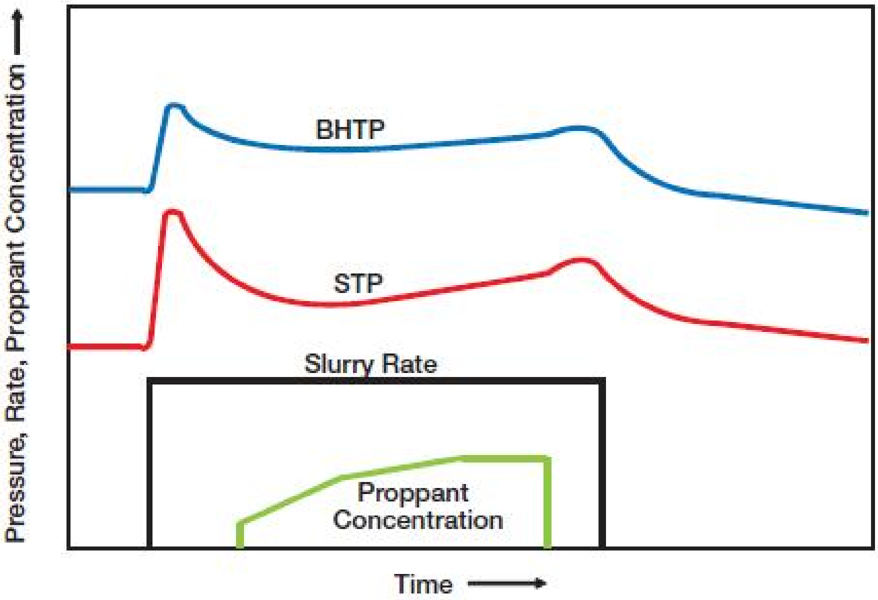

Figure 1.1.9. Schematic representation of a typical hydraulic fracture stimulation plot. The graph is a combined representation of bottom hole pressure (BHTP), shut-in tubing pressure (STP), slurry rate and proppant concentration with respect to time. Values increase in the direction of the arrows (after Martin and Valko, 2007).

Net pressure analysis is relatively inexpensive and the data is readily available, however, it is subject to fracture modeling interpretation. There are a number of fracture simulators commercially available; most of them assume a simple, two-dimensional fracture geometry solution (KGD or PKN models), or a lumped-parameter 3-D solution, which models fracture growth as bi-wing ellipses meeting at the fracture initiation point at the wellbore. It is important to note that the complex nature of fracture growth and fracture network development in shale reservoirs, limits the applicability of two-wing fracture models in these environments (Economides and Martin, 2007).

No matter the completion design and the completion system chosen (e.g., plug and perf, or sliding sleeves, Figure 1.1.10), hydraulic fractures will always propagate perpendicular to the orientation of the least principal stress (Hubbert and Willis, 1957) as illustrated in Figure 1.1.11. Therefore, once the least principal stress direction is known, a development program supported by horizontal wells tends to be more efficient than with vertical wells, because drilling and completion of a horizontal well should be a less expensive option than the exploitation of the same reservoir drainage area using multiple vertical wells, as schematically shown in Figure 1.1.12.

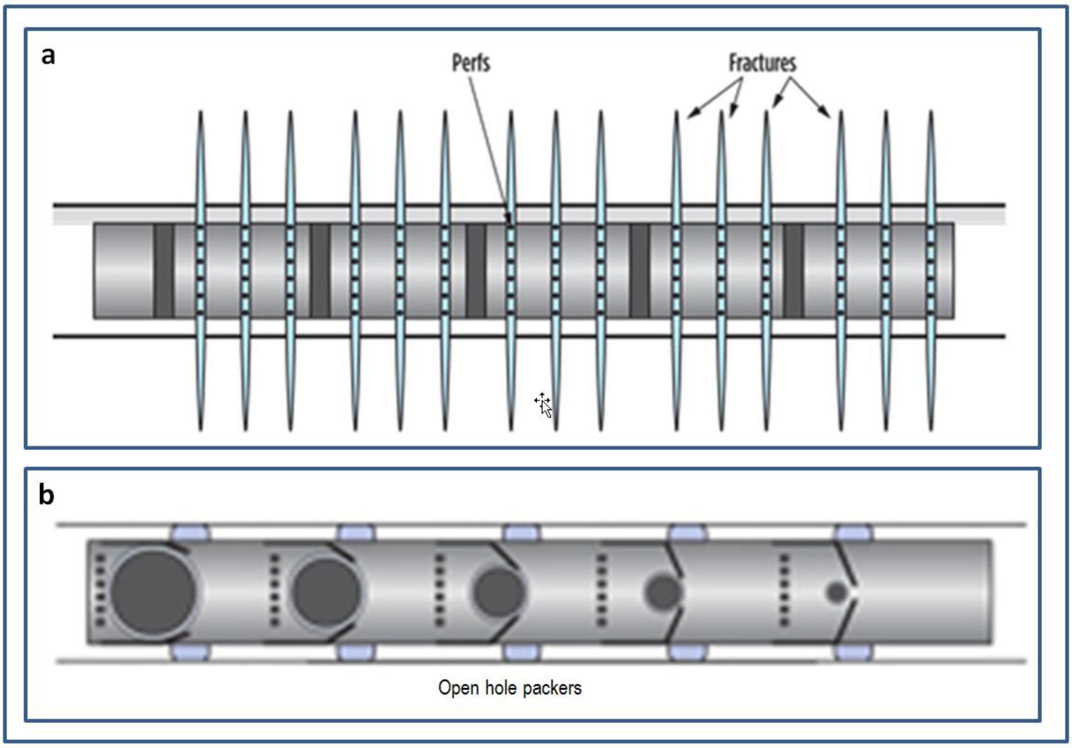

Figure 1.1.10. Schematic of completion systems a) Plug and perf b) Ball-activated sliding sleeve (after Daneshy, 2013)

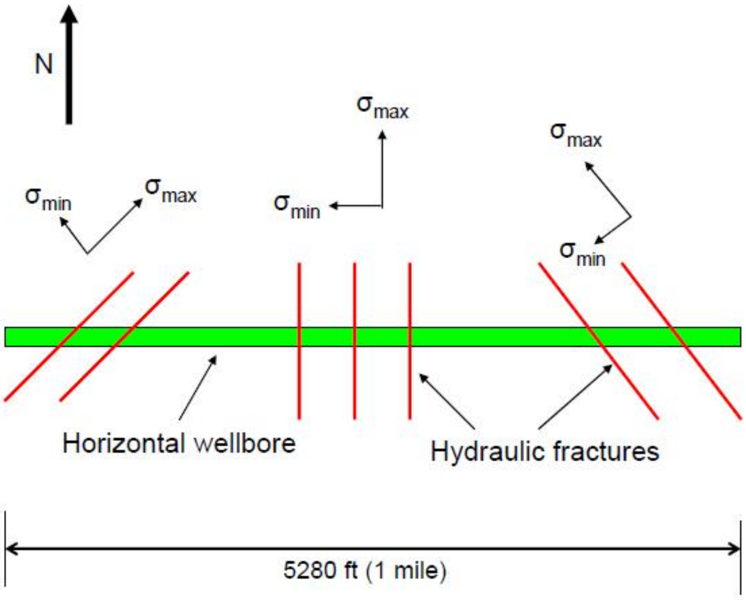

Figure 1.1.11. Schematic representation of hydraulically induced fractures orientations (red lines) with respect to a hypothetical horizontal wellbore (green bar) and horizontal stress directions. Notice that as the induced fractures are open perpendicular to the minimum horizontal stress the azimuth of these fractures will always be parallel to the maximum horizontal stress (after Miskimins, 2008).

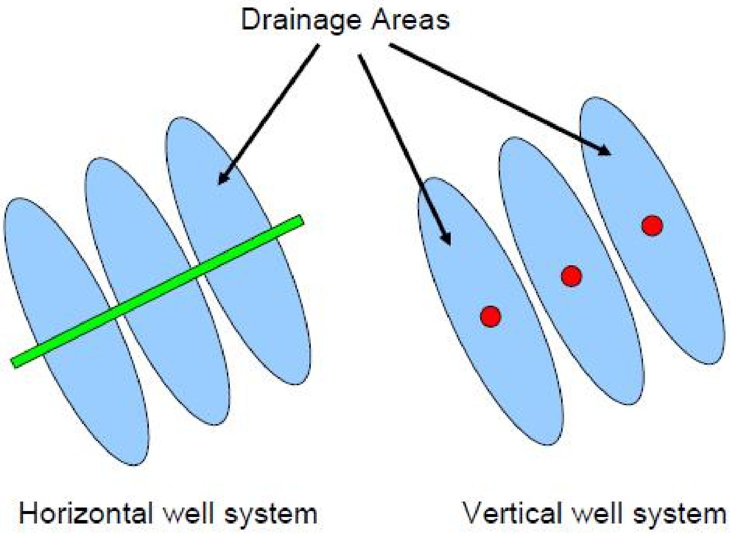

Figure 1.1.12. Hypothetical representation of the drainage areas (blue ellipsoids) associated with three hydraulic fracturing treatments on a horizontal wellbore (green line) as compare to the drainage area of three individual stimulations treatments on vertical wells (red dots) (after Miskimins, 2008).

1.2 Borehole microseismic monitoring of hydraulic fracturing.

Borehole microseismic is an indirect diagnostic technique that uses low magnitude seismic signals, registered at a monitor well, to study induced subsurface activity from a varied type of operations. For example, microseismic is commonly used to monitor typical operations of geothermal fields, to manage steam or CO_2 injection for enhanced oil recovery, and to study reservoir compaction due to production operations (Maxwell et al., 2010b). Recently, borehole microseismic has gained popularity in the monitoring of hydraulic fracturing, which is currently its most common application.

During hydraulic fracturing, microseismic monitoring consists in capturing, processing, and analyzing seismic signals originated at plane of weakness disturbed by the stress changes, and pore pressure increases associated with the injection of fracturing fluids, fracture growth, and fluid leak-off into the stimulated formation (Warpinski, 2009a). Figure 1.2.1, modified from House and Shemeta (2008), shows schematically the relative subsurface location with respect to the hydraulic fracture of these shear slippages commonly known as microseismic events. As pointed out by multiple authors (e.g. Pearson, 1981, and, Cipolla et al., 2011), a mostly tensile mechanism is involved in fracture opening, and does not generate much seismic activity. Therefore, it is necessary to analyze the perturbations occurring at the periphery of the hydraulic fracture to better estimate the characteristics of the stimulated fracture itself (Cipolla et al., 2011).

The parameters controlling the amount of energy used to generate the hydraulic fracture are injection rate and the amount of fluid introduced into the formation. Because the release and capture of seismic energy is only secondary to the main hydraulic fracturing process, and the method does not employ a controlled seismic source, microseismic monitoring is usually referred to as passive seismic.

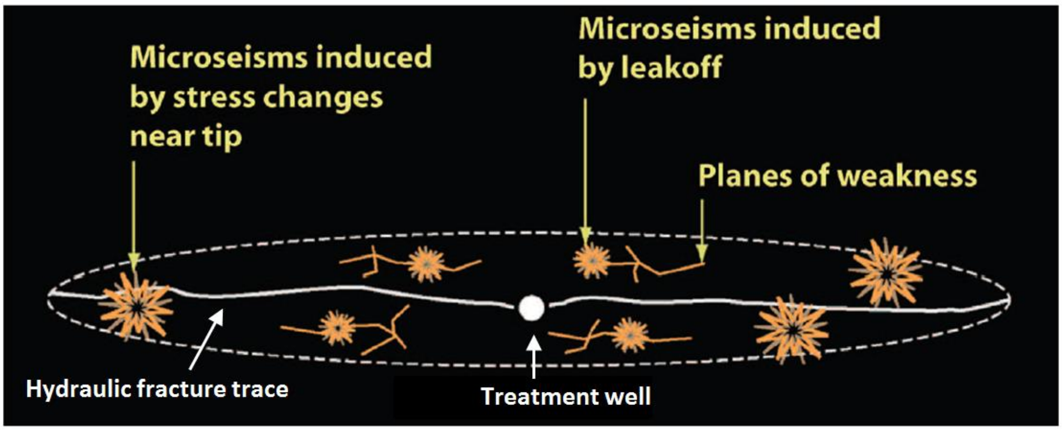

Figure 1.2.1. Schematic representation of a hydraulic fracture and its surroundings. Creation of a hydraulic fracture (continuous white trace) introduces stress and pore pressure changes that originate shear slippages (i.e. microseismic events - brown asterisks) at natural planes of weakness (brown traces) on a halo embracing the stimulated fracture (dashed white trace) (Modified from House and Shemeta, 2008).

During hydraulic fracturing, microseismic information is recorded by very sensitive sensors (either geophones or accelerometers) positioned inside one or multiple boreholes located nearby a treatment well, usually between 45 and 1500 m (150 and 5000 ft). Arrangements of 8 to 12 multicomponent sensors are common for these type of operations, although a few service companies may provide arrays of more than 40 sensors. Regardless of the final sensor configuration, data gets recorded at sample rates of 0.5 ms or less, because of the relative high frequencies of microseismic events (between 100 and 700 Hz), and is transmitted continuously to the surface by fiber-optic wire line (House and Shemeta, 2008).

Figure 1.2.2 shows a typical representation of an earthquake seismogram and typical observations that can be made on it as the P-wave arrival time and S-wave arrival time. Microseismic signals are plotted in a similar way, with time increasing to the right on the horizontal axis, and positive to negative amplitudes displayed from top to bottom on the vertical axis. Following such analogies, Figure 1.2.3 illustrates a seismic record with relatively high signal to noise ratio and Figure 1.2.4, on the other hand, shows a typical event from a borehole microseismic experiment.

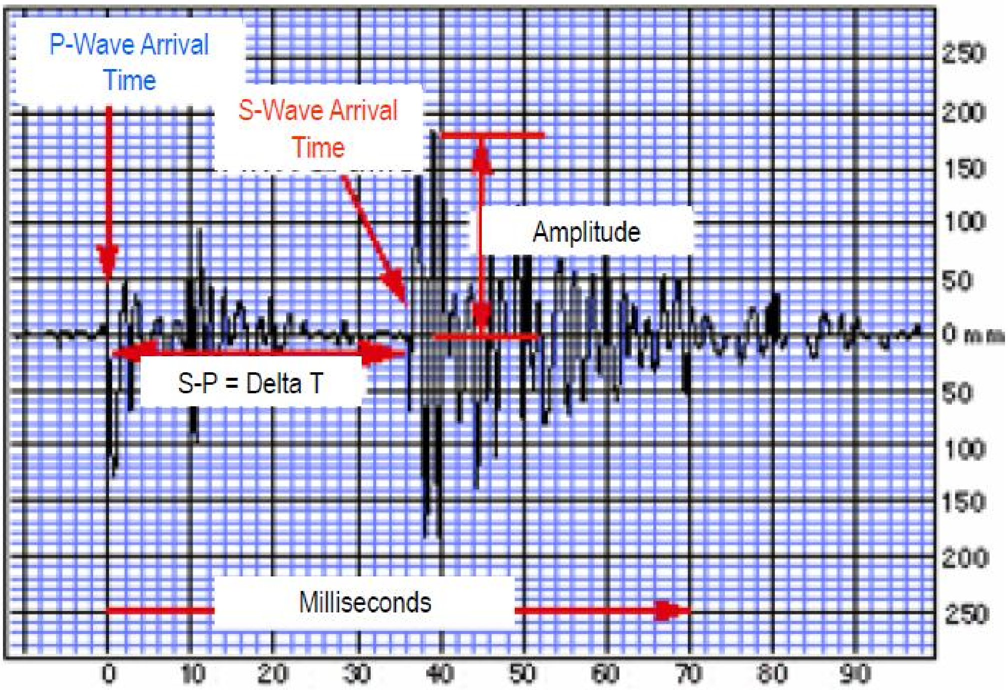

Figure 1.2.2. Seismogram example - Typical representation of a seismic signal. This time plot (milliseconds in the horizontal axis increasing trough the right) connects amplitude values (vertical axis) registered at a fixed sampling rate. From a seismogram, it is possible to select P-wave and S-wave first arrival time, and the time difference between them (Delta T), as shown in the figure (after Geology Labs online, University of California; www.sciencecourseware.org/glol/).

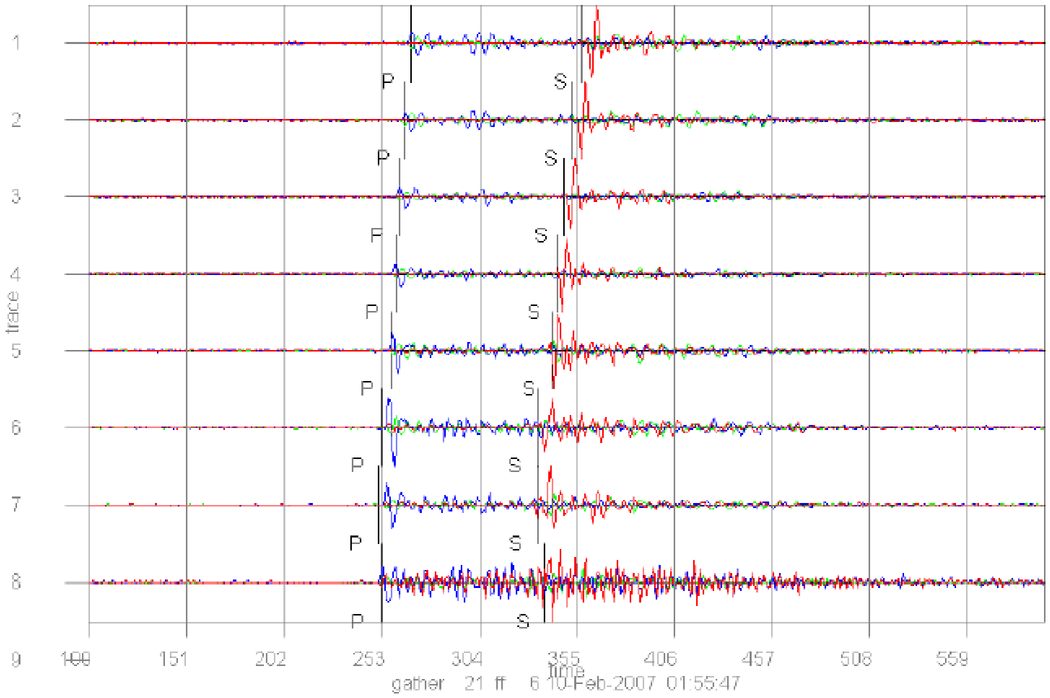

Figure 1.2.3. Example of high signal to noise (S/N) seismograms generated during a microseismic project. Data from each component is plotted on top of each other. Blue traces display the information from the vertical component, while red and green traces present the data from the two horizontal components. For each sensor display, the horizontal axis represents recording time in milliseconds, while the vertical axis displays negative and positive values with respect to a horizontal zero base line. P-wave and S-wave first arrival time are also indicated. A vertical wellbore contains all sensors; sensor 1 being the shallowest and sensor 8 the deepest following the vertical label (after Woerpel et al., 2010).

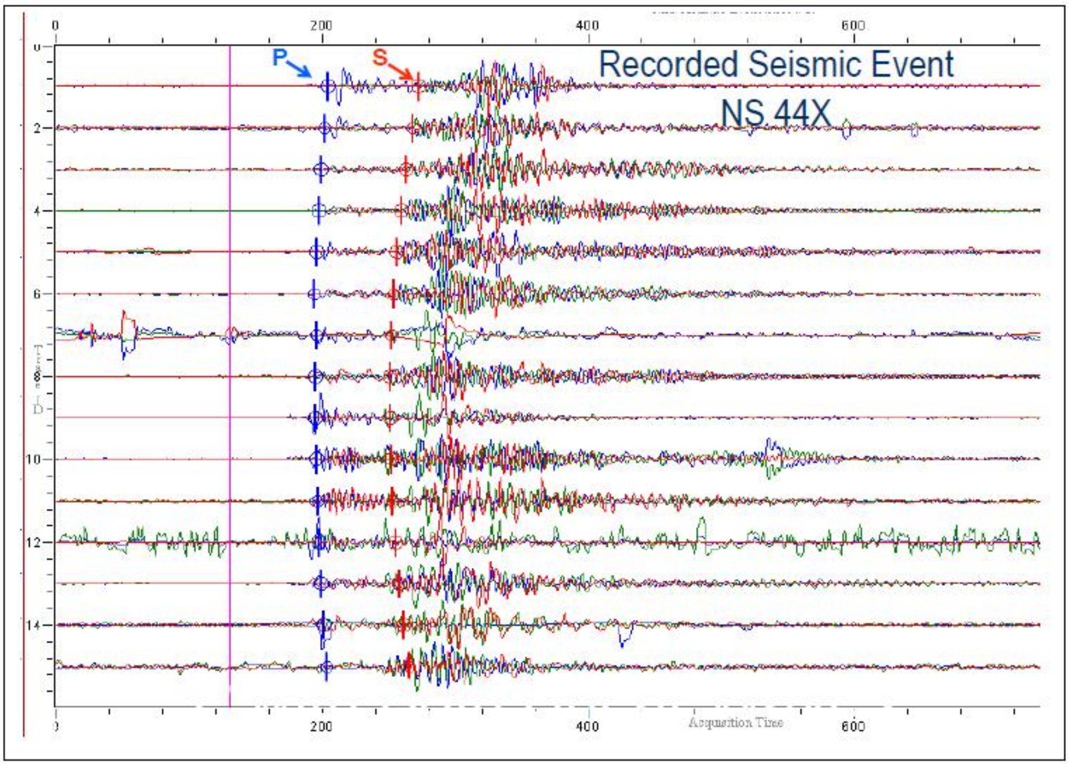

Figure 1.2.4. Example of a typical microseismic record conformed by traces from fifteen borehole tri-component sensors. Microseismic data from each component is plotted on top of each other. Blue traces display the information from the vertical component of geophones, while red and green traces present the data from the two horizontal components. For each sensor display, the horizontal axis represents recording time (in milliseconds) increasing to the right, while the vertical axis displays negative and positive values with respect to a horizontal zero base line. P-wave and S-wave first arrival time are also indicated. A vertical wellbore contains all sensors; sensor 1 being the shallowest and sensor 15 the deepest following the vertical label (after Forrest et al., 2010).

Once microseismic signals are recorded, and traces (waveforms) are available, it is possible to analyze the data following multiple approaches to estimate the location of microseismic events. To this end, one of the most commonly used inversion techniques consists of running a computer algorithm to first separate individual microseismic events (also referred as triggers) from the continuous signal records, and then automatically select P-waves and S-waves first arrival times for each trace. A degree of waveform filtering, as well as enhanced event detection sequences, commonly accompany and further enhance these automatic-picking algorithms. The result from this process is later evaluated by a seismic analyst, whom occasionally selects manually each single event in the presence of very low signal to noise ratio seismograms. Once the analyst is comfortable with the time picks, it is possible to compute the traveltime difference between P-waves and S-waves, which together with a predetermined velocity model, provide the estimated distance from the sensor array to the origin of the seismic source in the subsurface, also referred to as the microseismic hypocenter, foci, or simply microseismic event location.

The velocity model implemented in the location workflow described above is commonly derived from dipole sonic compressional (Vp) and shear (Vs) velocity logs, as the one shown in Figure 1.2.5, calibrated with information obtained from the hydraulic fracturing operation. One of such calibration methods, described in the work of Warpinski et al. (2005a), consists in recording the precise time of perforation (or string shot) firing in addition to its seismic signal, and then modifying the original velocity model accordingly in order to better match the known location of the perforations.

The calibration phase is required because in general, vertical velocities measured by the sonic tool are different from the horizontal velocities of a layered subsurface. Moreover, seismic signals propagate in radial patterns, thus requiring more than horizontal and vertical components of the velocity to completely describe the microseismic signal travel path. Therefore, none of the calibration approaches currently in use fully compensate for the intrinsic anisotropic characteristic of the stimulated zone of interest in resource plays (Eisner et al., 2011).

The use of sonic logs to build the velocity model carries significant upscaling uncertainties as pointed out by Chesnokov et al. (2011). Similar issues arise when the velocity model is built using data from surface seismic experiments because velocities obtained from the surface, as well as from log measurements, suffer from well-known and difficult to compensate dispersion issues (Liner, 2012).

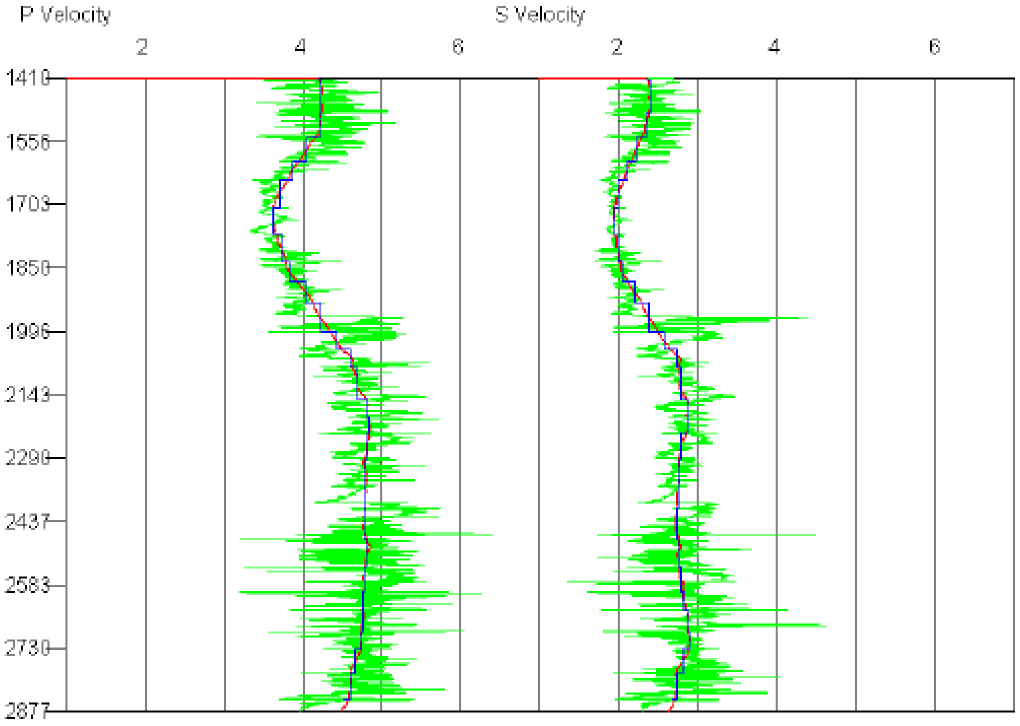

Figure 1.2.5. Smoothed (red line), and blocked (blue line) representations of P-wave and S-wave sonic logs (green lines). The vertical axis represents depth in meters, and the horizontal axis velocity in km/s (after Woerpel et al., 2010).

The azimuth of the hypocenter, on the other hand, is estimated via hodogram analysis, which is an amplitude analysis on a Cartesian plot of the differences recorded from the multicomponent sensors as presented schematically on Figure 1.2.6 (House and Shemeta, 2008).

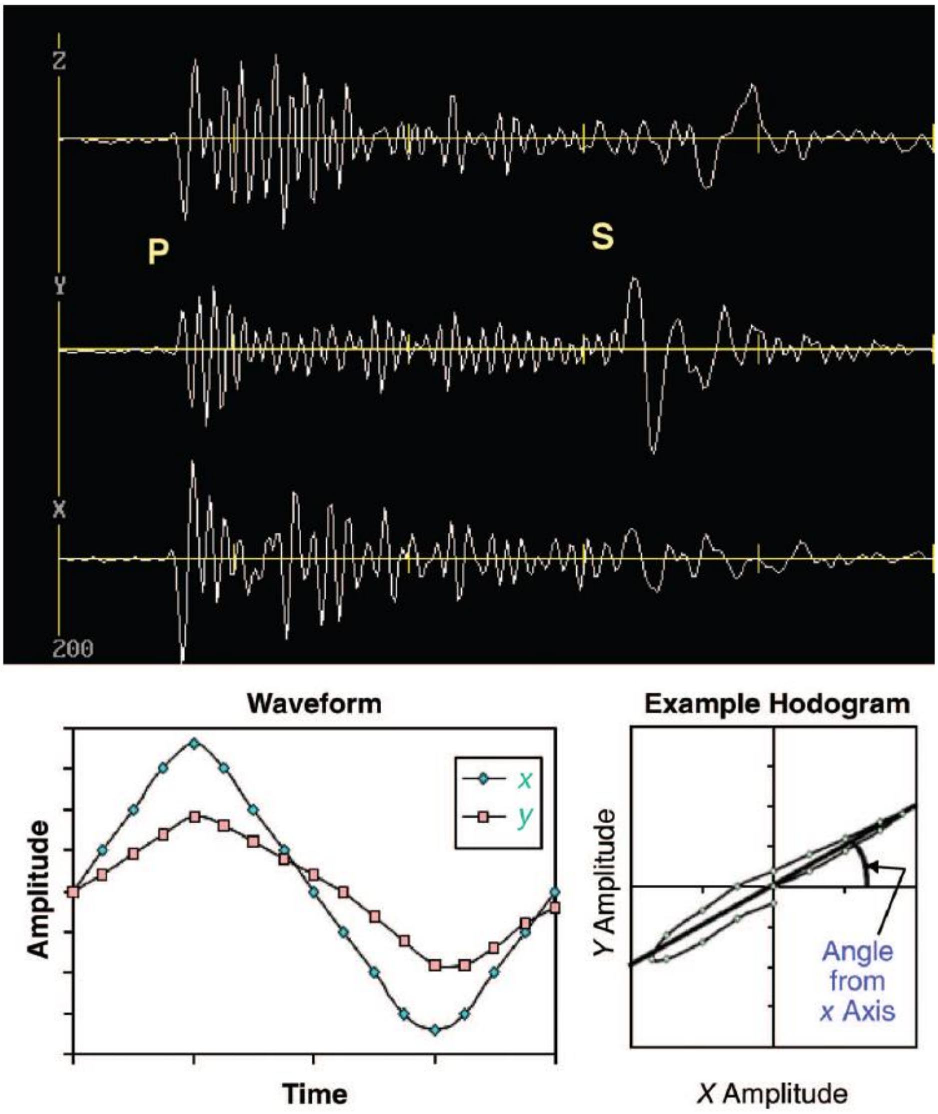

Figure 1.2.6. Z, Y and X geophone component waveforms associated with a single microseismic event. Amplitude comparisons of each component during time (lower left) provide polarization information, while cross plotting amplitudes variations on a particular time window / period provides the event direction (hodogram analysis, lower right) (after House and Shemeta, 2008).

1.3 Fundamentals of Sequence Stratigraphy

For more than five decades, sequence stratigraphy has proven to be a key tool of the exploration and production geoscientist providing the basis to predict and characterize spatial and temporal relationships between the different members of the petroleum system (i.e. source, seal and reservoir rocks). This chapter summarizes a few sequence stratigraphic principles, as they are fundamental to this dissertation. For detailed information on the topic I refer the reader to the works of Payton (1977), Van Wagoner et al. (1990), Posamentier and Allen (1999), Emery and Myers (1996), and Catuneanu et al. (2011). Those publications introduced and further discussed most of the concepts described in the following paragraphs. Slatt (2006) also presents a comprehensive review of the sequence stratigraphic concepts together with numerous examples describing the application of this theory to the search and exploitation of hydrocarbons.

Sequence stratigraphy refers to the study of genetically related sedimentary packages within a chronostratigraphic context (Van Wagoner et al., 1990). Based on a sequence stratigraphic framework subsurface data may be analyzed on a much more informative manner than just following lithologic rock typing. For example, Figure 1.3.1 shows common differences between lithostratigraphic and cronostratigraphic interpretations of a gamma ray (GR) log.

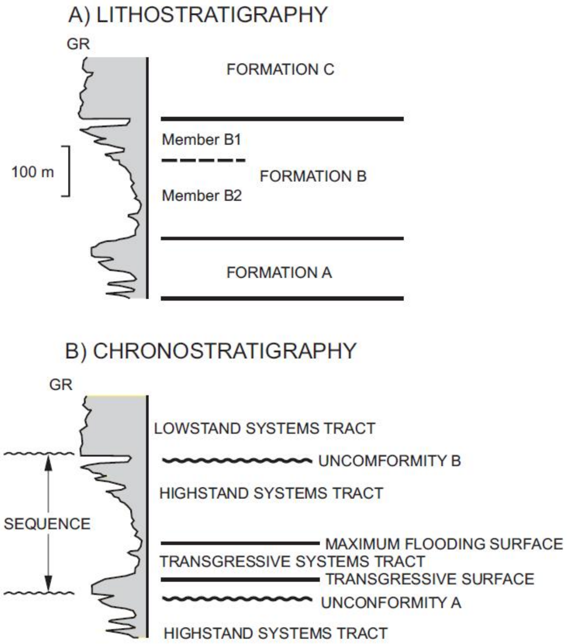

Figure 1.3.1. Tops interpreted in a GR log section based on A) lithostratigraphic and B) chronostratigraphic approaches. Tops for formations A, B, and C, and members B1 and B2, only bear lithological differences. On the other hand, unconformities A and B delimit a full sequence and together with a transgressive surface and a maximum flooding surface, convey information related to major stratigraphic events and their associated components. These sedimentary assemblages, denominated Lowstand, Transgressive and Highstand System Tracts, provide a better insight to the type of environment, processes and energy associated with the lithological packages inferred from the GR log, becoming a powerful tool to correlate multiple sections and predict geological occurrences far from the location of well control (after Slatt, 2006).

The lithostratigraphic description presented in Figure 1.3.1A is independent of a depositional reference time-frame, and is mainly supported by lithological characteristics. Following such an interpretation approach, it is possible to identify three formations (Formations A, B, and, C) as well as two formation members (B1 and B2). The chronostratigraphic description in Figure 1.3.1B, on the other hand, provides relatively more detail into possible environments and processes framing the deposition of the same stratigraphic unit, by identifying the presence of time correlative stratal surfaces and delineating a complete stratigraphic sequence. In this context, a sequence is defined as “a relative conformable, genetically related succession of strata that are bounded (at their top and base) by unconformities or their correlative conformities” (Slatt, 2006), associated with time-specific relative sea level cycles. The deposition of a sequence is mainly controlled by relative fall and rises of sea level also influenced by location specific tectonic characteristics and sediment supply. Therefore, recognizing a sequence carries a series of stratigraphic implications of great value in the characterization of a geologic package.

Figure 1.3.2 shows a schematic relative sea level curve, conformed by a falling limb and a rising limb, and the characteristic sedimentary assemblages associated with specific times for this particular cycle.

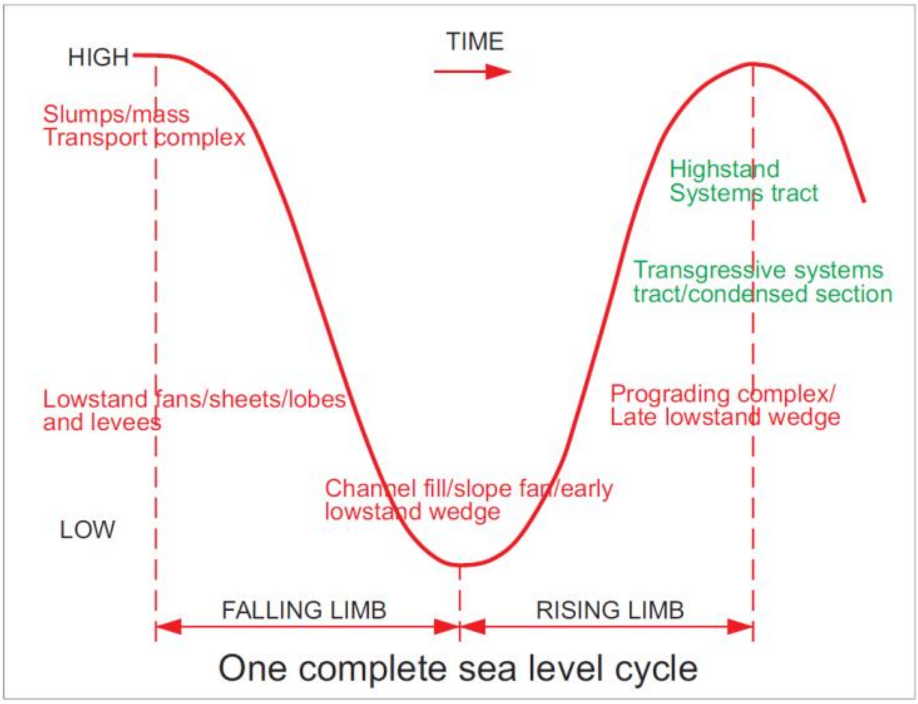

Figure 1.3.2. Simplified relative sea level curve (solid red line) diagram – fall and rise. Because relative sea level changes between high and low (Y axis) as time progress (towards the right on the X axis) the figure represents a complete sea level cycle. As sea level changes major sedimentary assemblages form with time. During sea level fall and following early rise (1) Slumps/mass transport complex, (2) Lowstand fans/sheets/lobes and levees, (3) channel fill/slope fan/early lowstand wedge and, (4) Prograding complex/late lowstand wedge get deposited respectively establishing the Lowstand System Tract (red labels). Then, as the sea level keeps rising, sediments accumulations form the Transgressive System Tract (TST) and the Highstand System Tract respectively. See text for expanded description (after Slatt, 2006).

According with sequence stratigraphic principles, as the sea level falls at the beginning of a relative sea level cycle, aerial exposure of the shelf and wide-ranging relatively low eustatic levels (i.e. low sea levels) do not allow much sediments to accumulate on the shelf, shoreline and non-marine environments, thus originating an unconformity which becomes a sequence boundary (SB). As time progresses, sediments associated with usually drastic falls in sea levels accumulate on top of the sequence boundaries, and as the sea level begin to rise, more sediments continue to fill the stratigraphic column. It is following this succession that mass transport deposits and basin floor fans, followed by slope fans and a prograding complex fill the deeper portions of the basin. These four elements form the sedimentary assemblage known as the Lowstand System Tract (LST), which encompasses most of the deep-water sediment accumulations. Figure 1.3.2 illustrates schematically the spatial and temporal relationships of elements forming the LST.

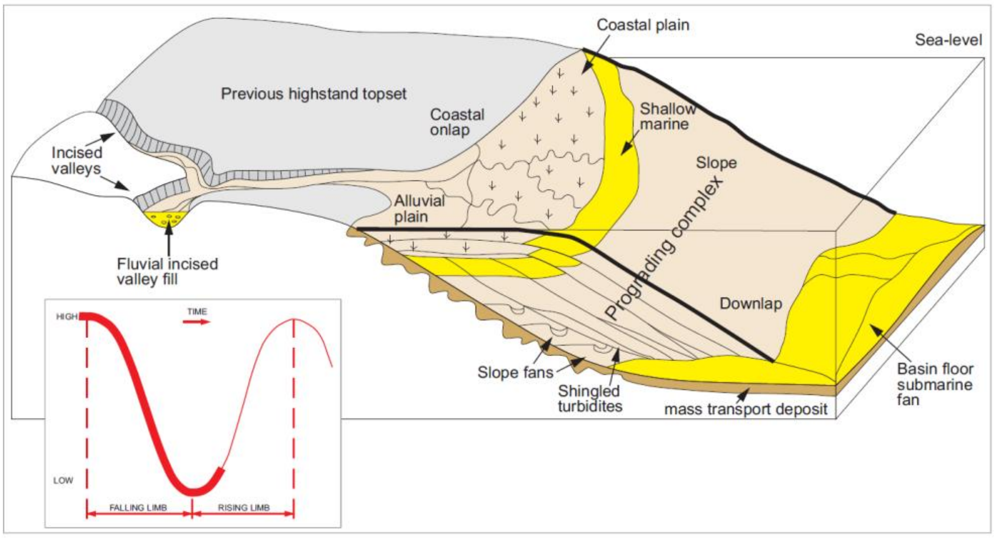

Figure 1.3.3. Schematic shelf to basin three-dimensional representation illustrating major stratigraphic elements associated with the sudden fall and early rise of sea level within a relative sea level cycle (Lowstand System Tract). During this stage sediments are deposited beyond the shelf break as deep water and slope architectural elements, while the shelf is mostly exposed. The corresponding highlighted portion of the relative sea level curve associated with the diagram is also included for reference (lower left corner red insert) See text for expanded description (after Slatt, 2006).

As the relative sea level rapidly continues its rise and sediments keep accumulating, a new system tract begins to form as shown in Figure 1.3.4. Previously exposed areas of the shelf cut by incised valleys eventually get capped by a sedimentary succession, which in these valleys usually begins with fluvial sediments and is followed by estuarine deposits. In the same time frame, typical coastal deposits such as (1) barrier islands, (2) lagoon – eolian – beach, (3) shoreface strata and, (4) ebb and flood tidal delta also begin to accumulate. Relatively minor amounts of sediments reach deep waters during this time interval, and those that make it that far are usually particles of relatively small size. The sediments deposited during this period of time constitute the Transgressive System Tract (TST).

The progression described above originates a condensed stratigraphic section conforming the vertical upper portion of the TST, a relatively thin, sometimes organic rich layer associated with fine grain sediments accumulated during a relatively long period of geological time. Indeed, sediment particle sizes collectively display a relative decrease from the bottom of the LST to the top of the TST recognized at multiple scales. The TST phase is over when the maximum water depth in the shelf is reached and the shoreline is also at its maximum landward position. Because of these characteristics, the top boundary of this system tract is called the maximum flooding surface (mfs). Figure 1.3.4 illustrates schematically spatial and temporal relationships of the TST elements.

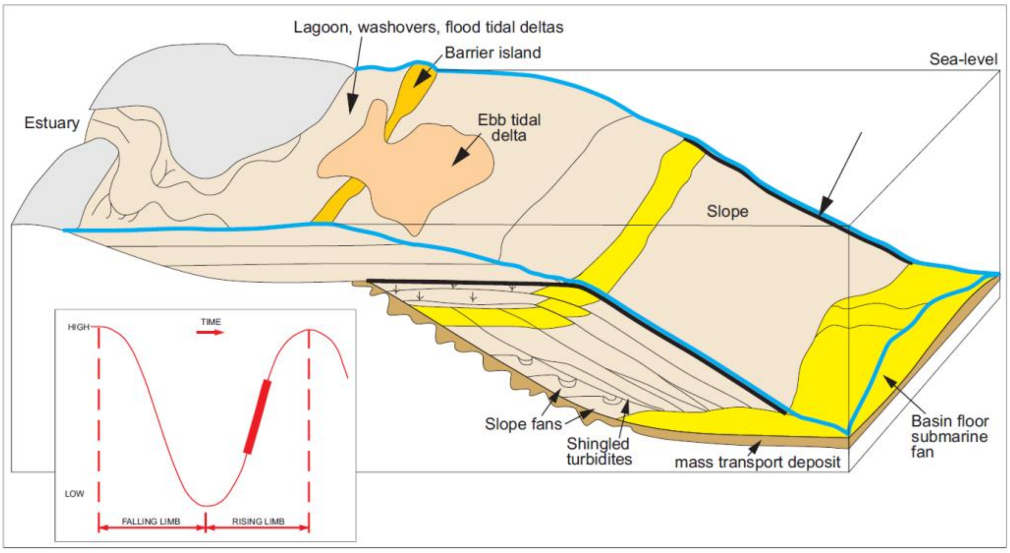

Figure 1.3.4. Schematic shelf to basin three-dimensional representations illustrating major stratigraphic elements associated with the early and relatively fast-rate increase in sea level within a relative sea level cycle (Transgressive System Tract). Is within this phase that a condensed section is formed, and bounded at its top by a maximum flooding surface (mfs), when minimal sedimentation is registered in deep water. The corresponding highlighted portion of the relative sea level curve associated with the diagram is also included for reference (lower left corner red insert) See text for expanded description (after Slatt, 2006).

As the sea level continues to rise, more space becomes available in the shelf for sediments to accumulate (a characteristic state denominated an increase in accommodation space) supporting sediments progradation seaward, as schematically presented in Figure 1.3.5. During this phase, deltas form where rivers are abundant, and interdeltaic shorelines develop in their absence. The sediment accumulations associated with this period of time are said to be part of the Highstand System Tract (HST). Because of its regressive character, the downlapping signatures of the HST sediments on top of the mfs are very descriptive of this phase. During this stage very few sediments reach deep water and the general transgressive pattern in grain size, characteristic of LST and TST assemblages, revert to a coarsening upward HST trend related to higher energy processes while depositional environments shift in the basinward direction.

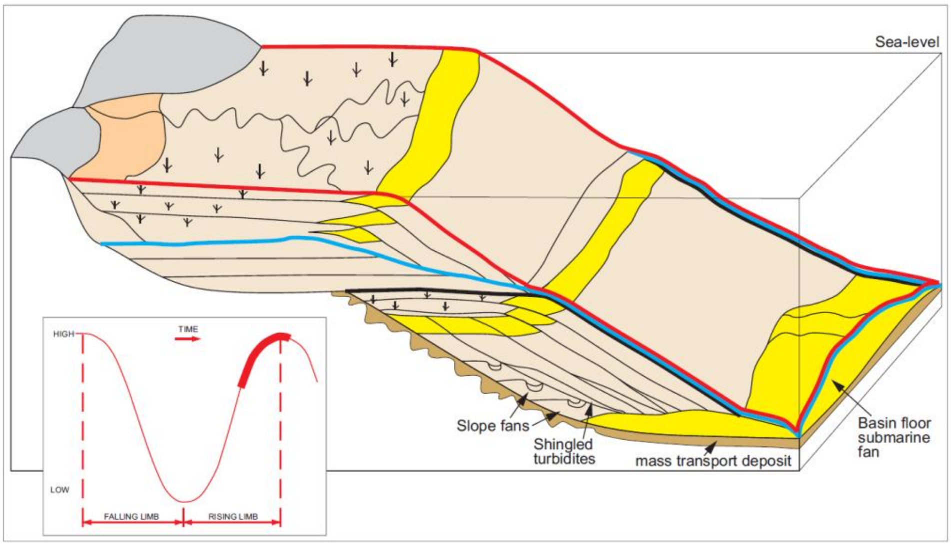

Figure 1.3.5. Schematic shelf to basin three-dimensional representation illustrating major stratigraphic elements associated with the final rising stage of a relative sea level cycle (Highstand System Tract). In this phase sediments prograde seaward when the rate of deposition exceeds the rate at which space for sediments to accumulate increase. Again no much sediment reaches the deeper portions of the basin. The corresponding highlighted portion of the relative sea level curve associated with the diagram is also included for reference (lower left corner red insert). See text for expanded description (after Slatt, 2006).

The presence of a stratigraphic hierarchy in sequence stratigraphy is also relevant. Particles stack together forming a lamina, and lamina sets form beds. Following this pattern, relatively conformable succession of genetically related beds, bounded by a marine flooding surface or a correlative surface forms a parasequence (Van Wagoner, 1990) and parasequence sets, grouped in progradational, agradational or retrogradational patterns, according with relationships between the rate of deposition and the rate of accommodation, become the building blocks of a sequence.

The cyclicity described in previous paragraphs is caused by multiple factors such as the formation and breakup of supercontinents, continental ice growth and decay, Milankovich glacioesutatic cycles and astronomical forces (Payton, 1977), thus they are also observed at multiple scales or as commonly refer in the sequence stratigraphic jargon, different orders. First and second orders are usually related to basin analysis, while third order is typical of exploration plays and prospects. Fourth and higher orders refer to variations observed at the reservoir and smaller scales. These sequence orders are typically associated with the specific time components shown in Figure 1.3.6.

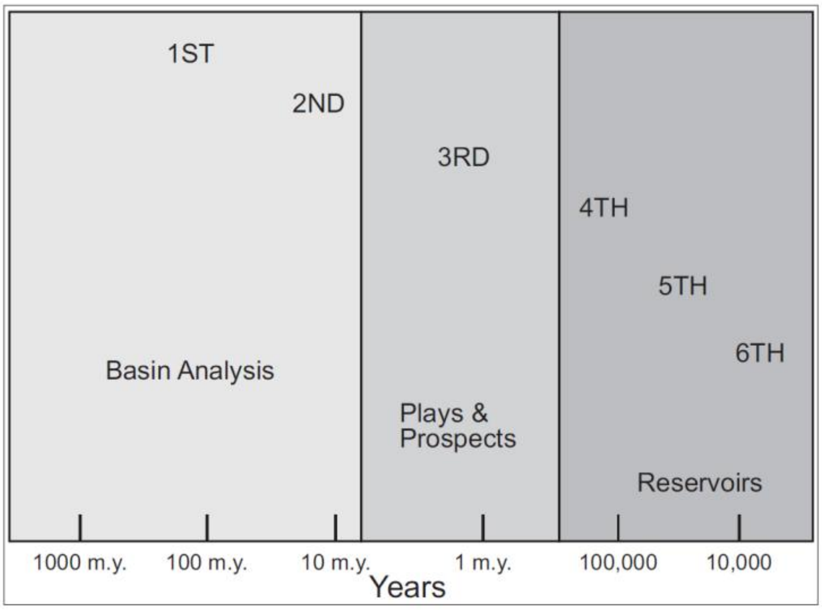

Figure 1.3.6. Scale of variations of relative sea level. Hundreds and tents of millions of years cycles represent first and second order variations associated with basin scale analysis. Millions of years cycles represent third order variations typically associated with play and prospect analysis. Cyclicity at higher levels, for example fourth, fifth and sixth order cycles, associated with variations in the scales of hundreds of thousands, tens of thousands and thousands years respectively, are more descriptive of the reservoir scale (after Slatt, 2006).

In general, several orders of variations act simultaneously, in conjunction with other factors such as tectonic influences (e.g. subsidence) and sediment supply, originating a more complex interaction pattern, schematically presented as an example in the composite relative sea level curve modified by subsidence presented in Figure 1.3.7.

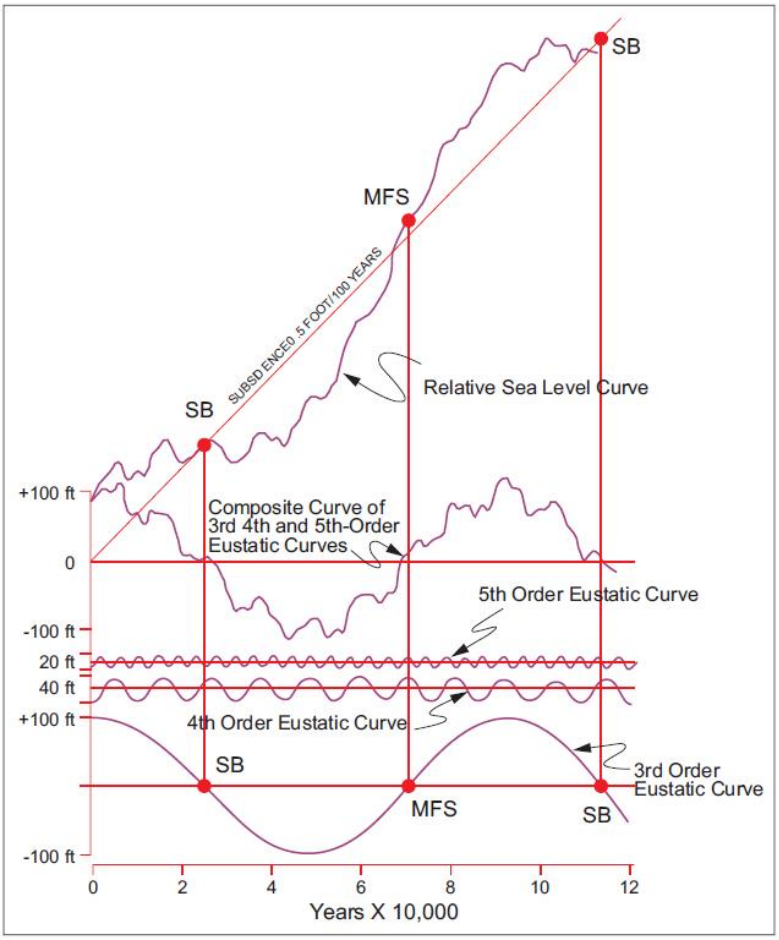

Figure 1.3.7. Schematic representation of relative sea level variations with time (top curve). This curve was formed by adding the effects of basin subsidence at a constant rate (.5 foot / 100 year) to the composite curve from fifth, fourth and third order eustatic cycles (also shown from top to bottom respectively). The horizontal axis represents time in tens of thousands of years, while each curve has its own associated vertical axis (in feet) representing the height variations of relative sea level. Third order sequence boundaries (SB) and its associated maximum flooding surface (MFS) have a significant impact on the overall depositional pattern while small order variations may impose major constraints at the reservoir scale (after Slatt, 2006).

As Figure 1.3.7 shows, third order SB and mfs have a significant impact on the overall shape of the curve (i.e. play and prospect scale), but higher order variations probably impose major constrains at the reservoir scale where other stratigraphic elements are probably more relevant.

The superposition of multiple orders is clearly observed when analyzing logs responses within a sequence stratigraphic framework. In particular, because high GR counts readings may be interpreted as associated with flooding surfaces, the identification of these markers serves to recognize multiple orders GR parasequences (GRP) as presented in the work of Singh (2008). For instance, Figure 1.3.8 presents three GRP identified by the upward-decreasing, upward-increasing, and constant GR count on log signatures also supported by the respective visual recognition of the associated grain size changes in core samples from three different sections of the Barnet Shale. Singh's work (2008) thus suggests that GR patterns are useful to identify parasequences according with a sequence stratigraphic framework.

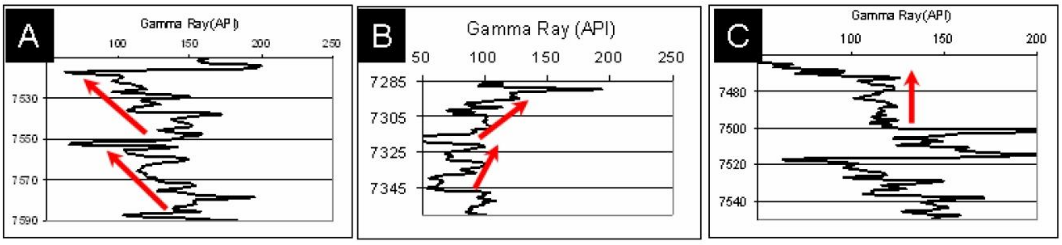

Figure 1.3.8. Barnet Shale example of A) upward-decreasing, B) upward-increasing, and C) constant GR API count useful to delimit parasequences from log readings (after Singh, 2008).

Sequence stratigraphic analysis extends beyond log examination and is applicable to data of multiple scales, from basin long seismic profiles, to outcrop, to core (Van Wagoner et al., 1990). The use of sequence stratigraphic principles in the analysis of surface reflection seismic data (also known as seismic stratigraphy in a 2D sense, or seismic geomorphology when related to 3D interpretation) has proven to be an excellent exploration and development tool for the Oil and Gas industry. In the analysis of surface seismic reflection data, a key principle provided by sequence stratigraphy is that seismic reflections are time significant stratal surfaces (Vail et al., 1977). As the physical properties of rock units change more drastically vertically than laterally, the acoustic response obtained by the seismic reflection method is much more than a simple lithostratigraphic image. Therefore, a surface seismic reflection data set, based on a sequence stratigraphic framework, carries a wealth of information and provides a unique perspective of the subsurface. In this context, the power of sequence stratigraphy, among other things, relies in using the seismic data to predict the presence of certain lithologies away from known control points (Vail et al., 1977).

Sequence stratigraphic principles can also be used to analyze information from core samples integrated with thin sections, log analysis, hydrocarbon systems records and basin history, leading to a more coherent geological interpretation. In exploration of conventional hydrocarbon accumulations, this integration is very useful as it helps to recognize and predict the presence, among other elements, of well-sorted grains of relatively high particle size, typically associated with high porosity and permeability reservoirs. Moreover, during the analysis of unconventional shale plays, where source, reservoir, and seal are essentially the same rock unit, sequence stratigraphy also has a key role. For example, based on sequence stratigraphic principles, Slatt and Rodriguez (2012) recognized several characteristics of currently productive organic-rich shale plays that serve as the base to propose a predictive model, schematically presented in Figure 1.3.8, where condensed sections represent the most prolific candidates for exploration and exploitation of unconventional hydrocarbon resources.

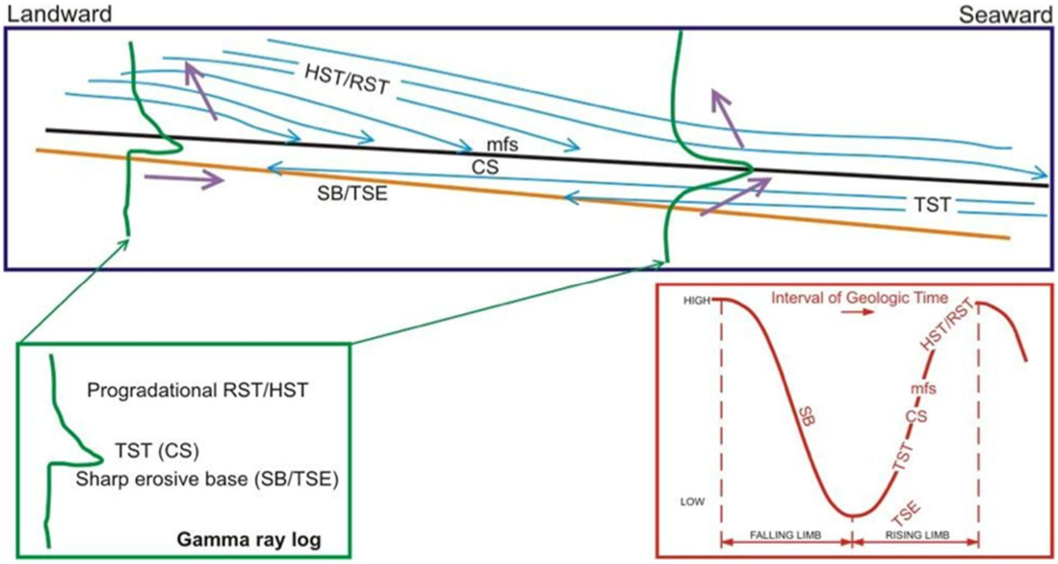

Figure1.3.8. Schematic representation of a general sequence stratigraphic model for shale resource plays. Under this approach, condense sections are the most prolific targets for resource play developments. SB - sequence boundary; TSE - transgressive surface of erosion; TST - transgressive system tract; HST - highstand system tract; mfs - maximum flooding surface; CS - condensed section; RST - regressive system tract (after Slatt and Rodriguez, 2010).

On the development stage of a resource play a sequence stratigraphic framework also provides opportunities to enhance operational strategies by identifying geomechanical characteristics of target zones. For instance, Figure 1.3.9 from Slatt and Abousleiman (2011), illustrates cyclic sets of rocks (brittle-ductile pairs) recognized in Woodford and Barnett shale data, which correlate well with distinctive hydraulic fracture propagation lengths. Slatt and Abousleiman’s observations (2011) suggest a combination of sequence stratigraphy and geomechanics principles to properly map the most prospective sections of a resource play. This should be the preferred approach to select well placement and improve development efforts.

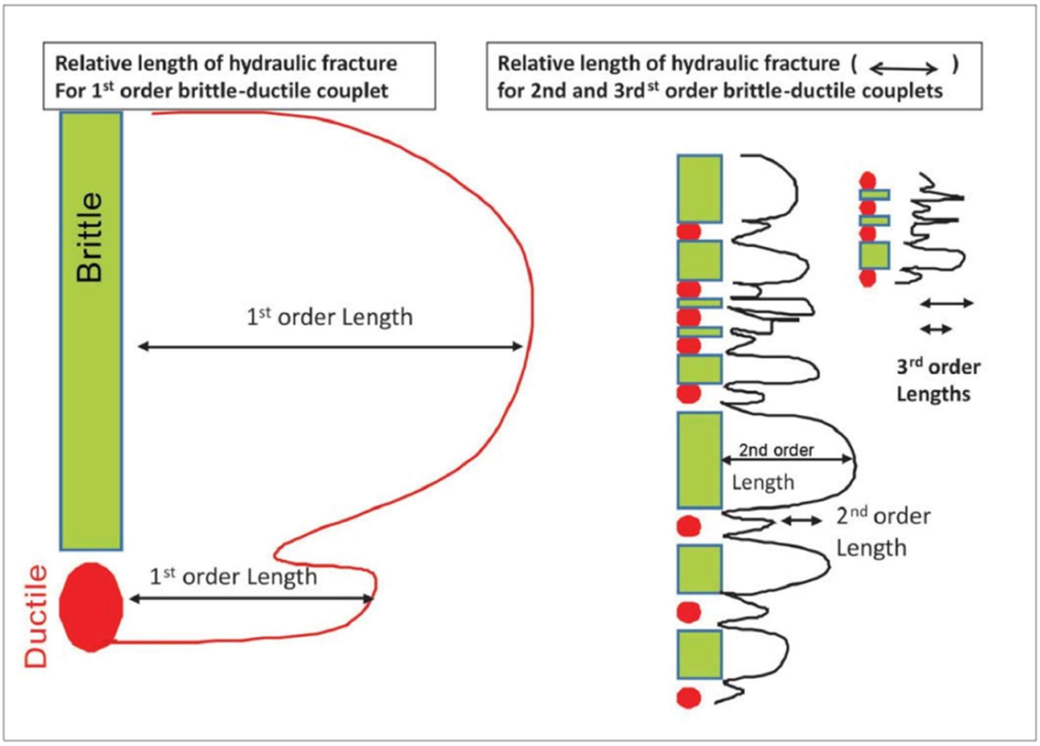

Figure 1.3.9. Schematic hydraulic fractures lengths variations within multiple scales of brittle-ductile couplets (after Slatt and Abousleiman, 2011).

This dissertation builds upon prior knowledge, extending and emphasizing the use of sequence stratigraphic principles to provide an appropriate framework to analyze and interpret borehole microseismic data recorded during hydraulic fracturing operations. It is my hypothesis that in a similar way as sequence stratigraphy is used to interpret depositional settings and the likelihood of finding hydrocarbons–bearing rock units, the same principles could be used to set some expectations regarding the sedimentary column response to hydraulic fracturing stimulation and their associated microseismic response, thus improving the analysis of this diagnostic tool.

1.4 Eagle Ford Geologic Characteristics

Hilcorp Energy Resources (HER), a private oil and gas operator, entered the Eagle Ford play in the summer of 2009 and rapidly initiated an aggressive development campaign. In less than 2 years, HER drilled and completed a total of 97 horizontal wells. These nimble operations concluded on November 1st 2011, when HER sold all its assets to Marathon Oil Corporation. While working for HER, I supported field development through geophysical operations, which provided significant insight to the topics discussed here. This section elaborates on the geological characteristics of the Eagle Ford formation, because I developed most of the ideas presented in this dissertation implementing borehole microseismic while evaluating hydraulic fracturing performed on the Eagle Ford.

Literature related to the rock unit known as the Eagle Ford is abundant. Numerous articles describe its various geological characteristics over a relatively large area, from the regional and outcrop level to the nanometer and molecular scale. These multiscale data-gathering efforts are the result of exploration campaigns at the basin scale, and productivity enhancement studies that depend largely in reservoir properties orders of magnitude smaller. Understanding these various characteristics and their relationships is essential as geologic parameters control the quality of hydrocarbon resources, and impose significant constrains to the most efficient exploitation approaches. This section summarizes analysis from vast amounts of data, usually collected in support of resource play operations, publicly available and in good agreement with proprietary information from the subsurface of the area of interest associated with this dissertation. Ultimately, the geological data within this chapter provides the necessary framework to interpret the microseismic response to hydraulic fracturing of the Eagle Ford and supports the hypothesis that geological information is crucial for the proper evaluation of microseismic data on any formation.

1.4.1 Regional perspective

In 1887, Hill made the first formal reference to the Upper Cretaceous (Cenomanian – Turonian) Eagle Ford strata, and reported the village of Eagle Ford in Dallas County, Texas, as its type locality (Donovan and Staerker, 2010). Outcrop and subsurface studies on age-equivalent rocks often refer to these strata as The Eagle Ford Group, Eagle Ford Formation, and Boquillas-Flags Formation, among other names (Liro et al., 1994; Dawson, 2000; and Lock and Peschier, 2006). For example, Boquillas is its common designation in West Texas publications (Donovan and Staerker, 2010). Although often labeled “The Eagle Ford Shale” (e.g. Martin et al., 2011; Bazan et al., 2010; Inamdar et al., 2010; Stegent et al., 2010; and Fan et al., 2011), this interval consists mainly of intercalated limestones, carbonate-rich mudstones, clay-rich mudstones, and quartzose siltstones (Dawson, 2000; and Minisini et al., 2011).

In Texas, Eagle Ford sediments were deposited in the western portion of the Greater Gulf basin (Hendershott, 2012), i.e. the East Texas basin, the San Marcos arch, and the Maverick basin, on a southwest - northeast trend parallel to the current Texas’ Gulf of Mexico coast strike as shown in the map presented in Figure 1.4.1.

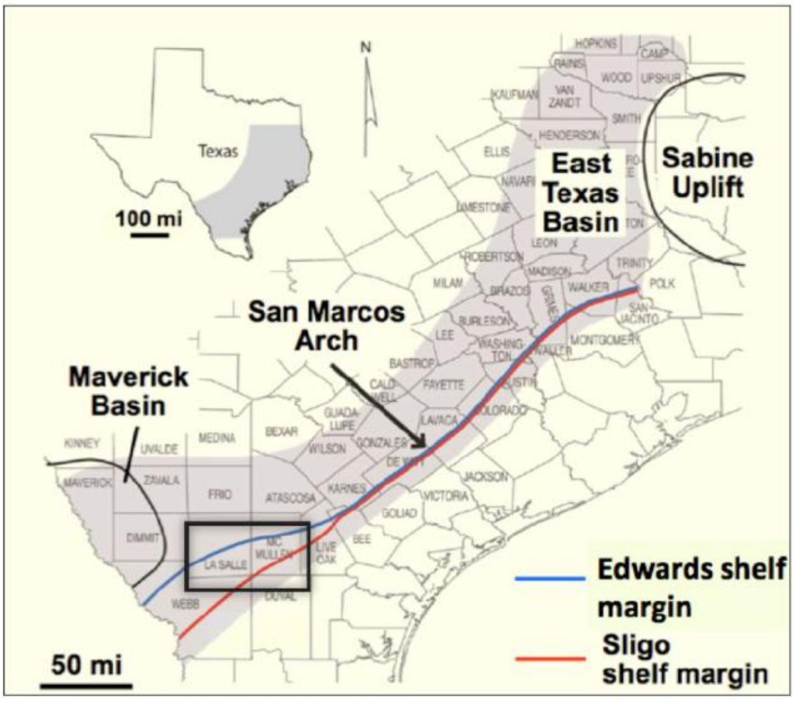

Figure 1.4.1. Spatial extent of the Eagle Ford formation in Texas (grey shadow) along with properly labeled major structural features of the area. Blue and red lines represent the relative positions of the Edwards and Sligo shelf margins respectively. A black box towards the south west underscores the region known as the Hawkville trough were the Eagle Ford was first targeted as a productive interval. Most of the data available in the literature is associated with the Hawkville field, which is located in this region (after Hendershott, 2012).

Figure 1.4.2 shows a schematic perspective of the Cenomanian paleogeography in the area currently occupied by Texas and Mexico. Major geographical features like the relative location of the Cenomanian shoreline, magmatic arcs and the connection with the Western Interior Seaway are all depicted in this figure. During this time, the Sabine Uplift and the Western Interior Seaway were all mayor sources of siliciclastic sediments (Scott, 2010). These conditions were prone to the generation of vast accumulation of carbonate sediments.

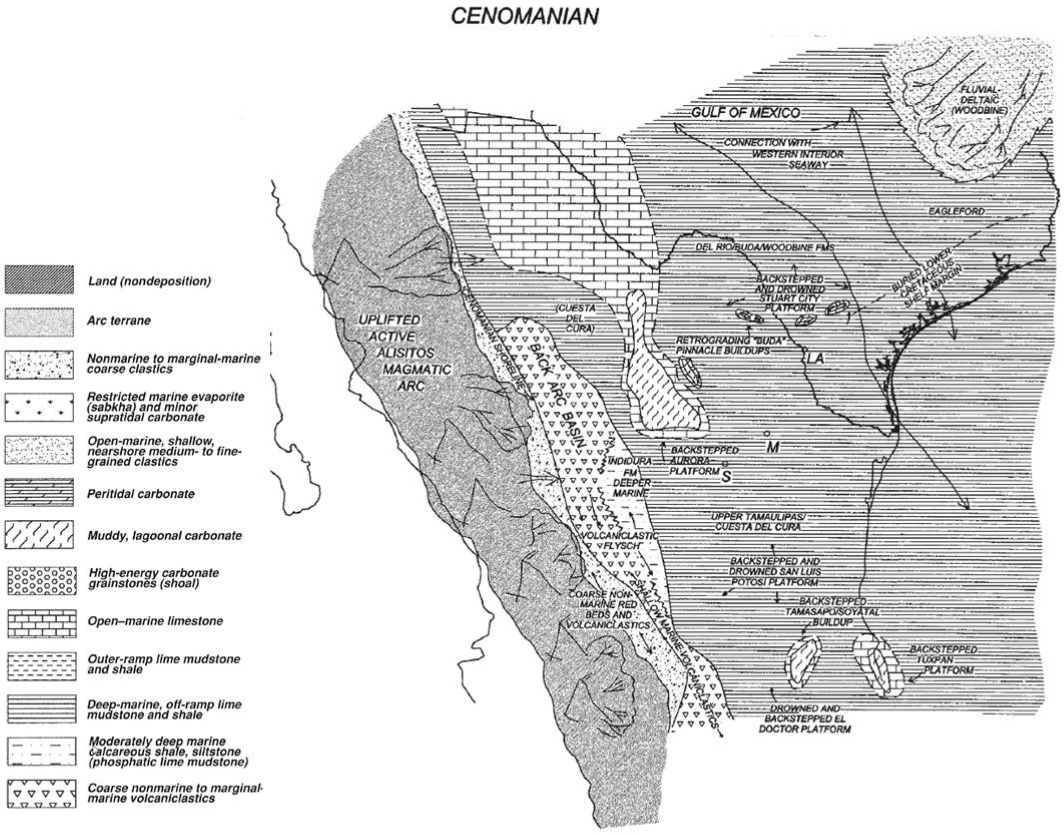

Figure 1.4.2. Cenomanian paleogeography. Notice how the Western Interior Seaway of the Rocky Mountains was connected to the Gulf of Mexico due to first-order and second-order eustatic events supporting the deposition and preservation of deepwater pelagic carbonates and siliciclastics in front of elevated shallow waters, rift-rimmed, Middle Cretaceous platforms. Notice also the presence of active magmatism to the west of current day Texas, which are the source of multiples ash beds found in the Eagle Ford formation (after Goldhammer et al., 1998).

Knowledge of the relative location of the paleogeographic elements presented in figures 1.4.1 and 1.4.2 is key as it provides the basis to understand the different interactions between sediments sources and the depositional environments associated with the Eagle Ford formation. In particular, the presence of two Lower Cretaceous shelf margins, the Edwards (Comanchean) and Sligo (Coahuilan) margins (Figure 1.4.1) delineate the area known as the Hawkville Trough, which may have caused a local mini basin, giving distinctive characteristics to the sedimentary column of this area. Also, some of these structural elements could have influenced the occurrence of natural fractures within Eagle Ford layers. As all these features refer to the geologic time during deposition and preservation of Eagle Ford sediments, current characteristics of the region are also significant. For instance, Figure 1.4.3 illustrates the present day stress field of the area according to the World Stress Map (Hendershott, 2012). This information is extremely important as the current stress field determines fracture orientation, thus impacting drilling and completion operations and the overall efficiency of major development plans.

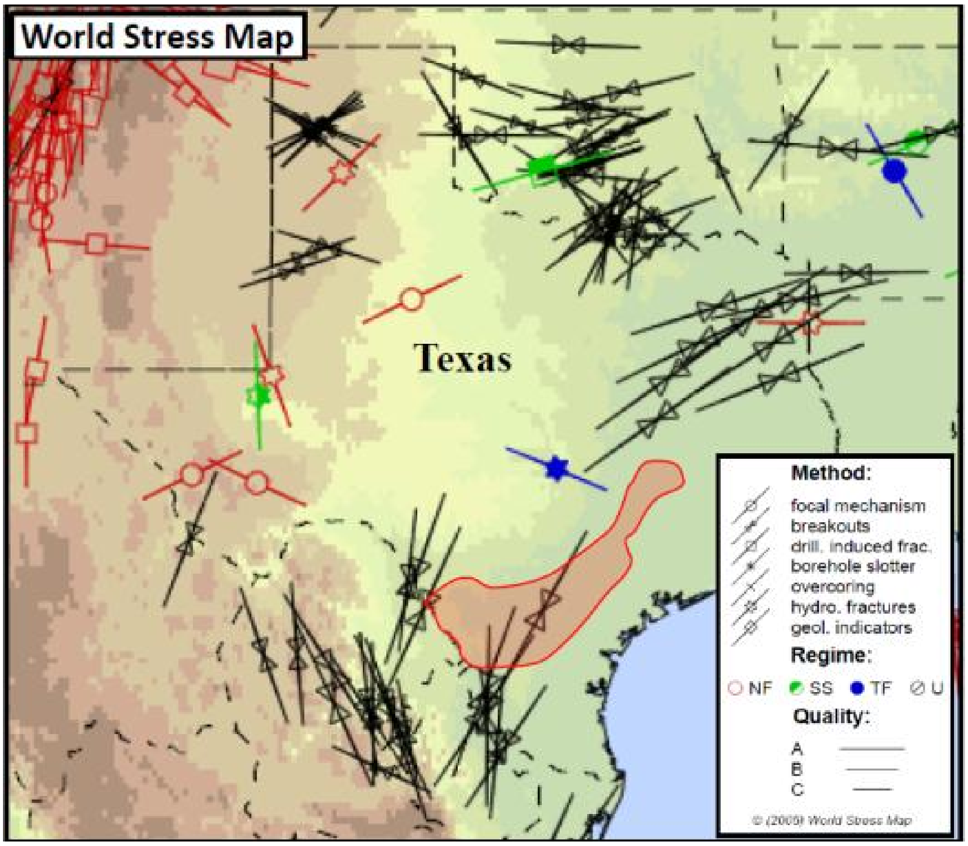

Figure 1.4.3. Texas portion of the World Stress Map. The shaded area represents the Eagle Ford trend associated with a maximum horizontal compressive stress with azimuth southwest – northeast obtained from wellbore breakouts (after Hendershott, 2012).

For a long time the Eagle Ford formation has been recognized as the hydrocarbon source rock for numerous reservoirs of the overlain Austin Chalk and the giant East Texas oil field (Liro et al, 1994). Additionally, in recent years the Eagle Ford has attracted much attention from the Energy Industry as a resource play (Martin et al. 2011) because of its potential to generate and store significant amounts of hydrocarbons in Texas and Mexico (Lock and Peschier, 2006). Moreover, its many carbonate layers make sections of the Eagle Ford significantly brittle and thus, an excellent candidate for hydraulic fracturing. For these reasons, The Eagle Ford has been the subject of significant hydrocarbon exploration and production activities along an area of more than 50 miles wide and 400 miles long, from the Mexico-Texas border to East Texas. Figure 1.4.4 shows the current commercial activity associated with this resource play. Green dots on the northern area represent wells producing hydrocarbon liquids from Eagle Ford rocks associated with relatively shallow depths, low temperatures and low pressures. Gas wells, shown by red dots, usually produce from deeper depths and higher temperatures and pressures. Green and yellow bands depict areas of oil and wet gas/condensate, respectively, while the dry gas area is enclosed by a red band.

The map in Figure 1.4.4 also shows the relatively simple monoclinal structure with a minor south-southeast dip (~1 degree) towards the current position of the Gulf of Mexico (Hendershott, 2012). Major normal faults downward to the coast easily recognized in seismic profiles are also present in the area but have been omitted on Figure 1.4.4 for simplicity. Most faults are post depositional, usually having vertical separations between 8 and 60 m (25 and 200 ft) along the Eagle Ford section (Hendershott, 2012).

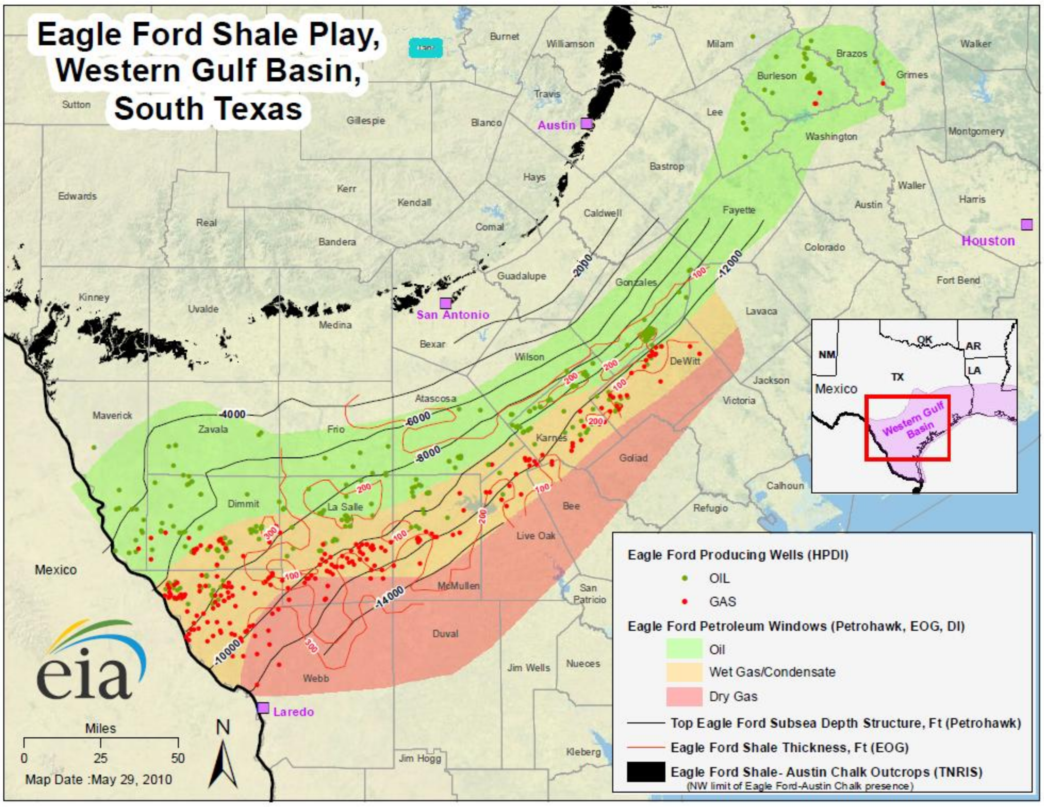

Figure 1.4.4. South Texas map displaying relevant Eagle Ford formation geographic information. (EIA, accessed 2012) The current commercial activity, indicated by the number of oil and gas wells drilled (green and red dots), covers a significant area from the Texas-Mexico border to East Texas. Subsurface contours describing a simple structure (i.e. depths contours without mayor faults) and thickness of the formation overlay green, yellow, and orange bands that correlate with interpreted oil, wet gas, and dry gas hydrocarbons windows, respectively. The map also highlights the position of outcrops where the formation is studied at the surface level.

1.4.2 Outcrop Characteristics

Figure 1.4.5, modified from Lock et al., 2010, shows one of many West Texas road cuts where it is possible to study the Eagle Ford on the surface. This outcrop is correlative to the subsurface section currently targeted for hydrocarbon production. When visible in an outcrop, Eagle Ford rocks usually weathers grey but freshly exposed samples display the descriptive black color and oily smell for which this “black shale” is famous. This is shown in Figure 1.4.5.

Figure 1.4.5. Typical Eagle Ford (Boquillas) formation outcrop in Highway 90, Val Verde County, TX. The inset in the figure shows a close-up view of the outcrop, with weathered (gray) and freshly-exposed (black) rock surfaces. The height of the section is approximately 30 ft. In this picture, it is possible to observe bed-scale facies variations interpreted as outer-shelf deposits by Minisini et al., 2011 (modified from Lock et al., 2010).

Thin volcanoclastic beds recognized throughout the formation (Lock et al., 2010, and, Minisini et al., 2011) are good correlation markers (Minisini et al., 2011). Similarly, flooding surfaces and resistant limestone beds observed on the surface delineate parasequences representing preferential cyclic stacking patterns easily correlated along several miles on the surface (Minisini et al., 2011). It is important to note that detailed fieldwork supports the interpretation of outer-shelf shallow waters as the most likely depositional environment associated with Eagle Ford sediments analyzed from outcrops, based on the predominance of marine fossils and the abundance of lignitic, terrestrial and plant debris (Liro et al., 1994, and, Minisini et al., 2011). Planktonic foraminifera, calcispheres, and Inoceramids (benthonic organisms known to tolerate low oxygen levels) are among the few fauna recognized on these rarely burrowed strata (Liro et al, 1994). These observations suggest anoxic conditions during deposition. Additionally, the observed thin-bedded stratigraphy, composed mainly of small grain size sediments, together with the presence of thin and continuous bentonites beds, implies a low energy setting (below storm wave base) only perturbed episodically. This hypothesis is supported by the limited amount of sandstones and siltstone layers observed in the Eagle Ford (Liro et al, 1994).

In general, subsurface rock samples share most of the characteristics recognized in outcrops. However, the presence of depositional structures such as mass transport deposits, which are found in the outcrop but not recognized in analysis involving subsurface data, suggest that sediments found in the subsurface were probably deposited in more distal portions of the depositional basin and, consequently, deeper water environments (Minisini et al., 2011).

1.4.3 Reservoir Characteristics

Figure 1.4.6, from Stoneburner et al. (2012), shows a typical log response from a vertical well that penetrates the entire Eagle Ford interval. In this particular example, 224 ft of Eagle Ford formation are delimited at the bottom by the Buda limestone, and at the top by the Austin Chalk. Both contacts are unconformable as recognized by the abrupt changes of properties registered via GR, resistivity, porosity and sonic logs. Based on log responses, the Eagle Ford could be divided into upper and lower members, which are also divisions easily observed in outcrops (Donovan and Staerker, 2010). The typically targeted Eagle Ford interval is located within the Lower Eagle Ford member, and it is associated with high resistivity and porosity values, among other properties, as shown in the logs presented in Figure 1.4.6. The geomechanical properties and anisotropy of the zone of interest could also be evaluated via sonic transit time *wireline* logs and associated computed logs, as the compressional transit time (DTC), shear transit time (DTS) and Poisson's ratio displayed in track 4 of the example log shown in Figure 1.4.6.

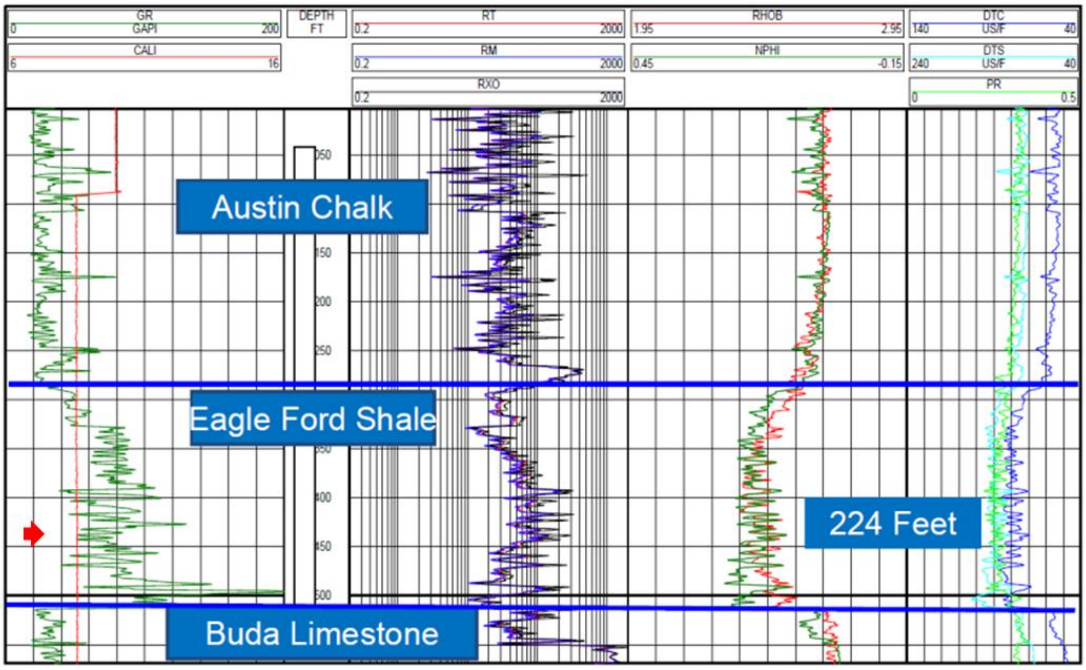

Figure 1.4.6. Typical open borehole logs responses from a vertical well penetrating the Eagle Ford shale play. Track one shows caliper (red) and gamma ray (green) curves. Track two displays resistivity logs; total (red), medium (purple) and shallow (black). Track three contains porosity measurements; density (red) and neutron (green); and Track 4 presents transit time for primary (dark blue) and secondary (cyan) wave pulses as well as computed Poisson ratio (light green) using the previous curves. In this particular example, the Eagle Ford formation is represented by a 68m (224ft) section delimited by the top of Buda Limestone and the base of the Austin Chalk, as clearly marked in the log. Within the Eagle Ford formation, a typical target zone has relatively high gamma ray, resistivity, porosity and transit time as depicted by the red arrow (After Stoneburner, 2012).

A regional southwest-northeast cross-section on a structural strike direction was built correlating logs assemblages such as the one previously presented. This is shown in Figure 1.4.7. The top of the Buda limestone and the base of the Austin chalk are easily correlated due to their unconformable characteristics with the Eagle Ford Formation, as observed on GR and resistivity logs. In the same way, a maximum flooding surface, which divides the Eagle Ford upper and lower members, is also easily tracked regionally. Moreover, Figure 1.4.7 presents the typical South Texas stratigraphic column, because it is possible to recognize the following formations from bottom to top: Edwards, Georgetown, del Rio, Buda, Eagle Ford and Austin Chalk.

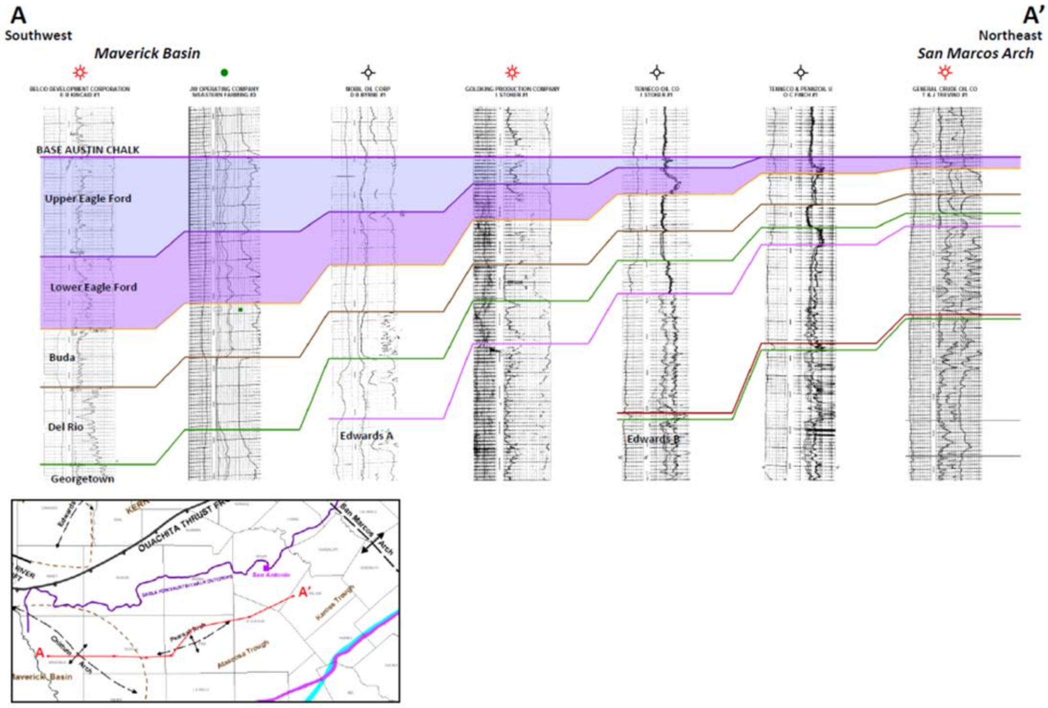

Figure 1.4.7. Regional southwest - northeast cross-section showing log character variability across the Eagle Ford play. GR log is plotted in track 1 while resistivity log is plotted in track 2. Continuous colored lines delimit the boundaries between the Edwards, Georgetown, Del Rio, Buda, Eagle Ford and Austin Chalk formations as annotated. Upper and lower Eagle Ford members are colored blue and purple, respectively. Notice how the Eagle Ford section thickens toward the west, from the San Marcos Arch area to the Maverick basin (Modified from Matsutsuyu, 2011).

The cross section on Figure 1.4.7 easily presents thickness variations across Texas but due to the large spatial extent of the Eagle Ford formation, other geological characteristics also vary significantly along particular geographical areas. Table 2 shows value ranges for some of the most relevant properties of the Eagle Ford formation.

Table 2. Properties of the Eagle Ford Shale (modified from Lyle, 2010; Mullen, 2010; and Borstmayer et al., 2011).

Depth (ft)	4000 – 14000
Gross Thickness (ft)	50 – 300
TOC (%)	2.0 – 6.5
Vitrinite Reflectance (%Ro)	1.0 – 1.27
Total Porosity (%)	3 – 18
Pressure Gradient (psi/ft)	0.43 - 0.84
Permeability (nD)	1 – 800
Water Saturation (%)	1 – 31
Young’s Modulus (psi)	1.00E+06 – 2.00 E+06
Poisson’s Ratio	0.25 – 0.27

The wide range of Eagle Ford properties observed in Table 2 underscore the need for data from specific areas to properly analyze the play. Therefore, the few Eagle Ford characteristics and examples presented in the following paragraphs should not be considered representative of the entire Eagle Ford formation.

1.4.4 Sample Characteristics

Due to the extremely low permeability of the fine-grained sedimentary rocks associated with resource plays, acquiring and analyzing whole core samples becomes essential. Ultimately, cores are the only source of direct and quantitative subsurface rock characteristics, such as those presented in Table 2. For instance, visual descriptions of core supported by photographs and simple measurements (e.g. core spectral gamma ray), serve as a proxy to infer depositional environments and/or fracture density properties. Furthermore, geomechanical, geochemical and petrographic analysis made on smaller core fragments provide insight on properties controlling fluid flow and hydrocarbon quality, while also allowing to quantify rock storage and flow parameters.

Figure 1.4.8 shows a photograph of an Eagle Ford core. A dark thinly laminated lower portion (rich in organic matter) is visually different from the also thinly laminated, but lighter color section above it. The upper portion of the core presented in Figure 1.4.8 contains abundant foraminifera (fossil fragments), as clearly annotated in the figure, associated with an increase in the carbonate content. This characteristic may be associated with a higher tendency to break (brittleness) when the rock is subjected to high stress.

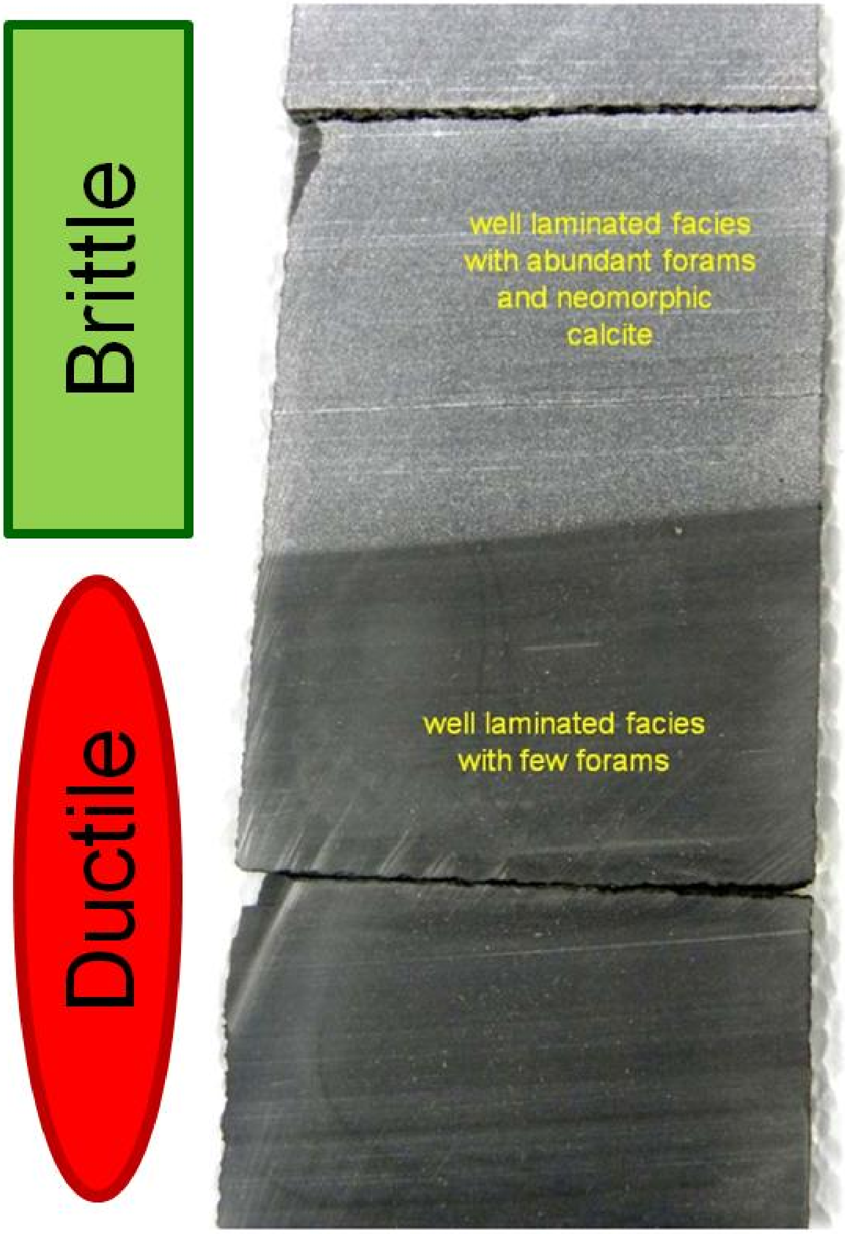

Figure 1.4.8. Eagle Ford core photograph showing clearly the well-laminated character of this section together with the sharp contrast between a foraminifera rich upper portion, and a relatively darker bottom portion with a significant smaller content of foraminifera. A simple visual inspection makes it possible to infer that there are numerous stratigraphic planes of weakness within the entire section and that the upper portion of the core likely represents a more brittle section of the subsurface relative to a more ductile bottom (modified from Lock et al., 2010).

Figure 1.4.9 shows core photographs from some of the typical facies encountered within the Eagle Ford section: limestone, calcareous shale, ash beds and three types of marl with various amounts of planktonic foraminifera, the most pervasive fossil assemblage of the Eagle Ford Section usually agglomerated in thin laminations (Stoneburner, 2012).

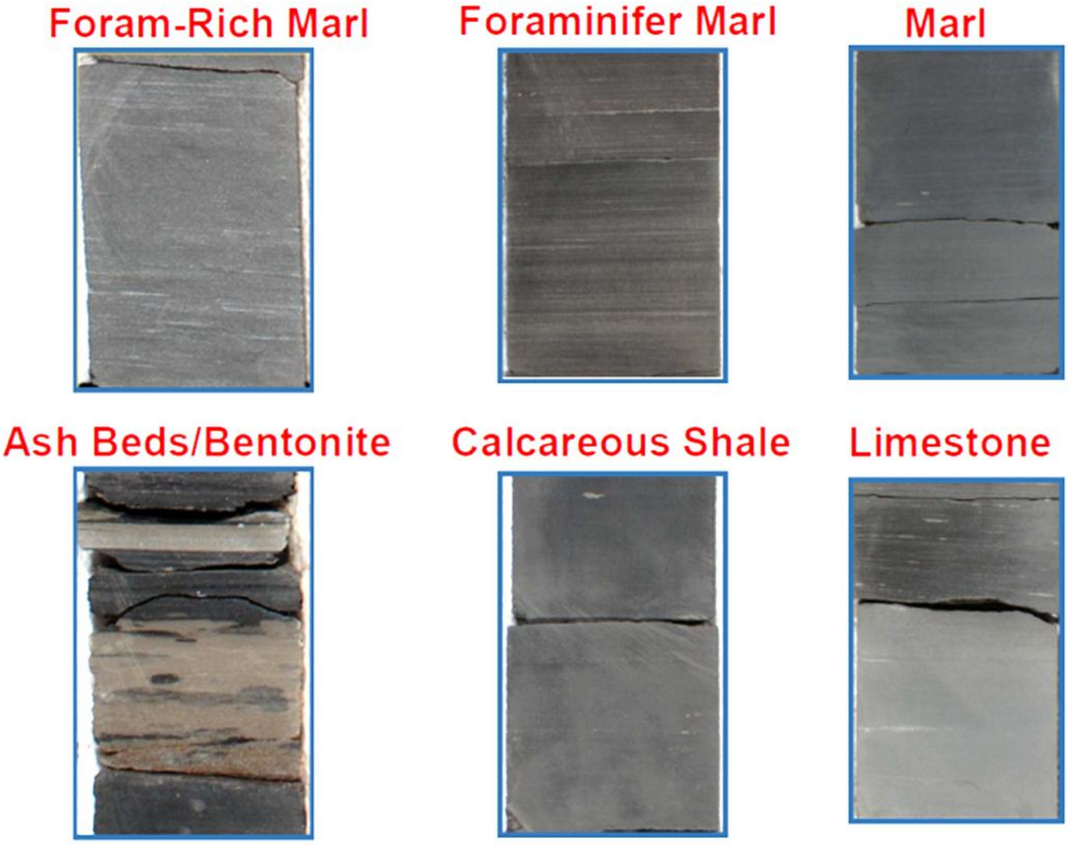

Figure 1.4.9. Core photographs of different rock facies typically encountered in the Eagle Ford formation. Limestones, calcareous shales and marls are the most common rock types. The amount of foraminifera and other fossil organisms found in different layers usually varies as shown in the marls photographs presented at the top. Ash beds/bentonite and other stratigraphycally distinct beds/surfaces are also easily recognized in the core and can also be correlated with log readings (Modified from Stoneburner, 2012).

As seen on cores, mixed siliciclastics and calcareous beds dominate the upper Eagle Ford composition while the darker, organic rich calcareous facies are typical of the lower Eagle Ford. From the perspective of the drilling and completion engineer, it is important to know that the different facies presented in Figure 1.4.9 will react differently to hydraulic stimulation and the organic content varies significantly between these different rock assemblages (Stoneburner, 2012).

From core samples it is possible to interpret depositional environments and estimate porosity, permeability and fluid saturations. For example, Figure 1.4.10 presents porosity measurements made on 353 Eagle Ford samples from 3 different wells. The average porosity from this data set is 7.4%, and although the reported error is +/- 0.02%, the data suggest greater variability in the porosity range.

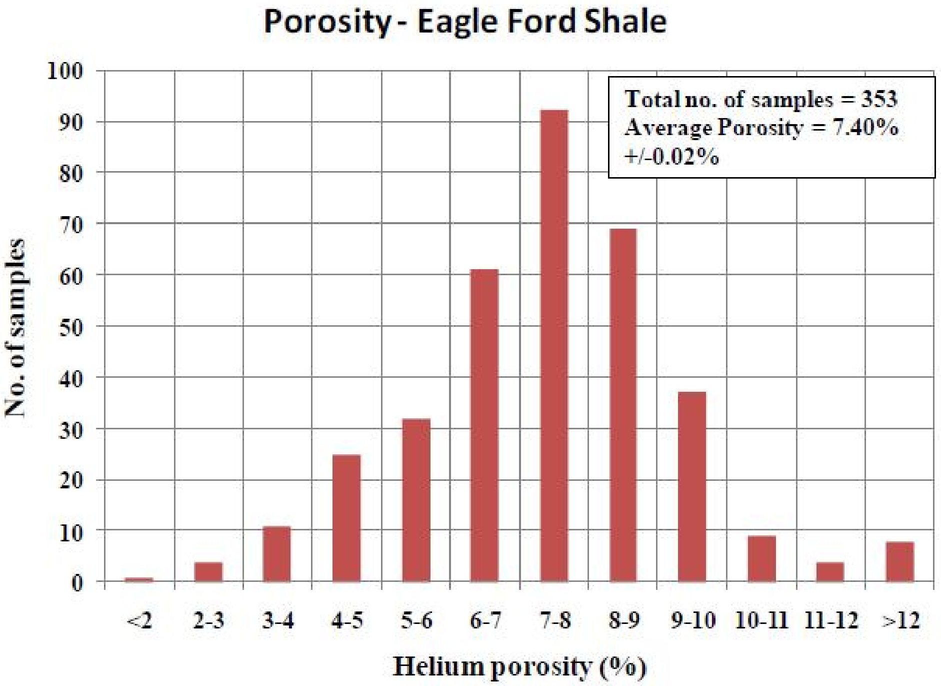

Figure 1.4.10. Histogram of 353 helium porosity measurements made on core samples from three different Eagle Ford wells. Values vary significantly from 1.90% to 20.25% with an average porosity of 7.40% +/- 0.02% (after Sondhi, 2011).

Another approach to compute porosity from an Eagle Ford sample involves a full multiscale analysis as the one presented in Figure 1.4.11. A computed tomography (CT) scan image of a whole Eagle Ford core is first taken to provide, among other things, good records of the original core. Then, a micro CT scan is acquired on a core plug to provide more detailed information via ion milled scanning electron microscope (SEM), ultimately providing porosity, and volume fraction relationships from stacks of two-dimensional high-resolution images. This level of detail is necessary because in fine-grained reservoirs, as the Eagle Ford formation, much of the porosity is in the nanometer scale. Three main types of pores; i.e. organic matter pores, intraparticle pores, and interparticle pores conform the total porosity (Loucks et al., 2012), and thus an accurate value of porosity provides the means to calculate the volume of hydrocarbons in place and the approximate actual value of the resource. For this reason, multiple porosity estimation methods, including the Gas Research Institute (GRI) crushed sample technique (Guidry et al, 1996), as well as the techniques mentioned before, are commonly used during a detailed resource play evaluation. It is important to note that porosity values obtained from different approaches are often associated with a high uncertainty due to the small scale of the measurements and the usual measurement errors of each method. Other parameters, such as permeability, are also prone to large variability and uncertainty because traditional methods of estimating this property, such as direct core analysis or well tests and pressure buildups, are also not appropriate due to the same reasons.

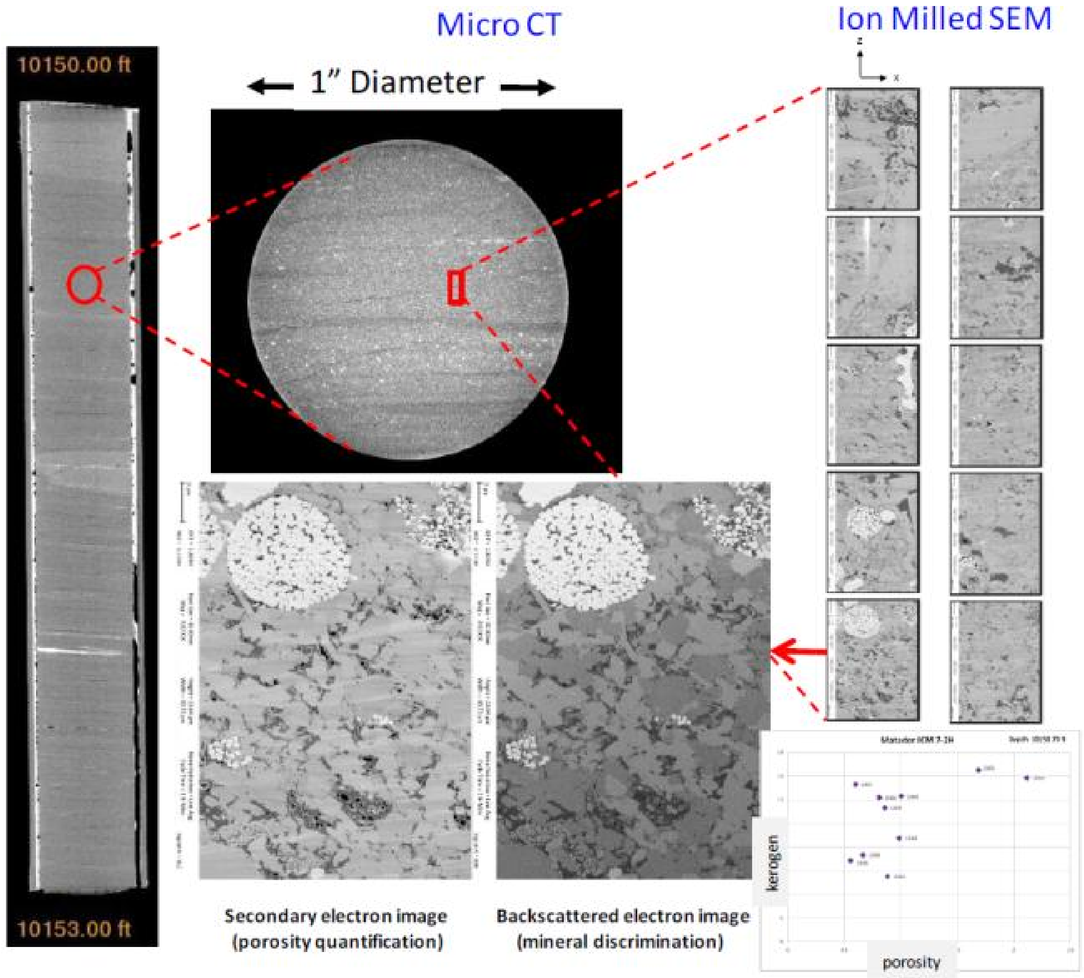

Figure 1.4.11. Representation of a typical workflow for a multiscale core characterization on the Eagle Ford shale. Continuous CT whole-core scans (farthest left) followed by micro CT scan of a selected plug from which samples for ion-milled SEM scans are taken (properly labeled in the Figure). From these images, porosity and mineral composition/kerogen content can be quantitatively determined as shown in the lower right corner of the figure (after Walls et al., 2011).

The access to preserved reservoir core samples provides additional support to the design of multiple completion parameters such as proppant selection and fracturing fluids. Furthermore, measurements made on cores provide the means to verify and calibrate similar rock properties usually derived from log readings.

1.4.4.1 Geomechanical characteristics

Depositional processes, primary and diagenetic composition, pore structure and fabric directly influence the mechanical properties of rocks. Therefore, the term geomechanics is commonly associated with rock studies that take into consideration these elements when analyzing the mechanical properties of rocks. In particular, the term fabric refers to the spatial and geometric configuration of the elements that constitute the rock. The degree of lamination is a typical fabric characteristic, which directly influences the rock anisotropy, strength, and fracture toughness. Slatt and Abousleiman (2011) suggest that laminae/bedding contacts represent planes of weakness for hydraulic fracturing, and sustain their hypothesis in numerous observations from the Barnett and Woodford shales. Eagle Ford samples reflect the same characteristics cited by Slatt and Abousleiman, including the lack of significant authigenic cement along bed/lamination contacts, which weakens the rock at those contacts, and geomechanical properties highly dependent on bedding direction (perpendicular vs. parallel), as well as the presence of layers with fractures perpendicular to the bedding intermixed with non-fractured layers.

Lithofacies stacking patterns represent another fabric characteristic of the Eagle Ford. The facies presented in the core images in Figure 1.4.8 and Figure 1.4.9 are easily recognized in logs measurements once calibrated, and could be interpreted as cyclic patterns associated with eustatic and oxygen levels changes representing the brittle-ductile couplets proposed by Slatt and Abousleiman (2011) at the parasequences and sequence scale.

Geomechanical measurements from core samples are key inputs into drilling and completion designs as they relate to finding sweet spots, mapping fractures and fracture behavior, optimizing hydraulic fracturing, understanding fracturing fluid behavior, selecting proppants, as well as optimizing horizontal drilling and staged completions. In general, results from stress tests at different pressures and temperatures provide the basis to understand rock responses to mechanical changes. Of particular interest are measurements like the Young's modulus and Poisson's ratio, which provide a quantitative measure of how much the rock will deform under stress. In general, a combination of relatively high Poisson's ratio and low Young's modulus is characteristic of ductile rocks (those that suffer plastic deformation under high stress), while low Poisson's ratio combined with high Young's modulus is typical of brittle rocks (those that shatter under high stress). Published values of Young's modulus and Poisson's ratio for the Eagle Ford range between $1x10^6$ - $2x10^6$ psi, and 0.25 - 0.27, respectively (Table 2). These values are characteristic of a relatively brittle section.

In order to better assess the rock response to hydraulic fracturing stimulation other parameters should also be considered. For example, the brittleness index, which combines mineralogy and organic carbon content, is a useful parameter to predict the rock behavior under stress (Jarvie et al., 2007, and Wang and Gale, 2009). Nonetheless, parameters like the brittleness index should be considered in conjunction with detailed geological analysis. The origin of quartz fragments (e.g. biogenic, detrital or digenetic), for instance, impose distinctively different geomechanical characteristics to the rock not always following the general belief that the presence of quartz make the rock more brittle (Slatt, 2011).

1.4.4.2 Geochemical characteristics

For resource plays exploration and exploitation, geochemical analyses are particularly significant, as they provide the basis to quantify the amount and type of hydrocarbons of the specific petroleum system. The assessment of the organic richness, quality, and maturity of targeted intervals provide the basis to make these estimations.

Results from heating rock samples at controlled environment conditions, an experiment known as pyrolysis, provide the parameters to compute Hydrogen Index (HI) and Oxygen Index (OI), which together with the Total Organic Carbon (TOC), provide quantitative information about the rock richness. Organic richness is usually associated with more than 1% total organic content (TOC) and Hydrogen Index (HI) greater than 350 mg HC/g for oil-prone source rocks, while 0.5% TOC values and HI greater than 150 mg HC/g are expected for gas-prone source rocks (Hunt, 1996).

Prospective Eagle Ford sections are particularly organic rich according to TOC measurements such as the one presented in Figure 1.4.12. This TOC histogram shows most of the readings reaching at least the gas prone generation cut off, and an average TOC of 2.45% from 112 samples. TOC also tends to correlate well with GR log API values, which allows, through proper log-core calibration, a good way to estimate TOC (Passey et al., 1990).

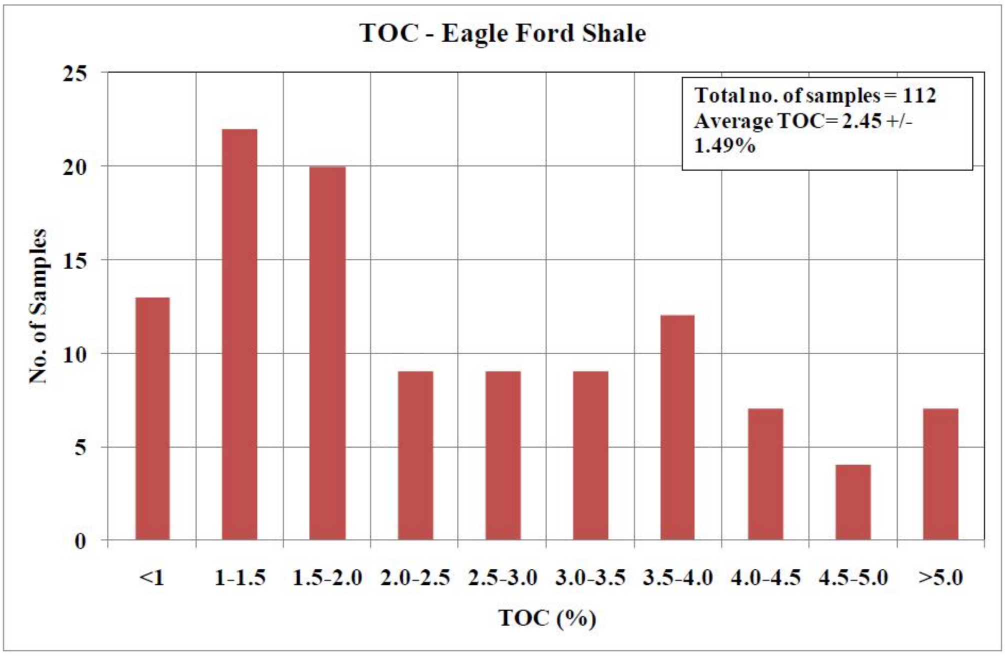

Figure 1.4.12. Histogram distribution of TOC measurements made on 112 samples from three Eagle Ford wells. TOC values vary from 0.06 to 6.32 % (wt %), with an average of 2.45 +/- 1.49% (wt %) (after Sondhi, 2011).

Vitrinite reflectance (%Ro) is a key maturity parameter, with common values for the Eagle Ford ranging between 1.00 and 1.27 as shown in Table 2. These values are characteristics of a mature source rock. The Production Index (PI), another measurement derived from the pyrolysis experiment, also provides an estimation of the maturity of the rock. The temperature at maximum release of hydrocarbon during the pyrolysis experiment (Tmax) is also a good maturity estimator. Figure 1.4.13 presents a graph of Tmax versus HI associated with multiple samples from three Eagle Ford wells. As seen in this Figure, most of the samples from wells A and B fall within the “Mature” region, which is associated with type II-III oil gas prone and type III gas prone, while samples associated with well C are post mature, and fall within the inert type of the dry gas window. This type of analysis over a multitude of samples is what has defined the current hydrocarbons windows presented in Figure 1.4.3.

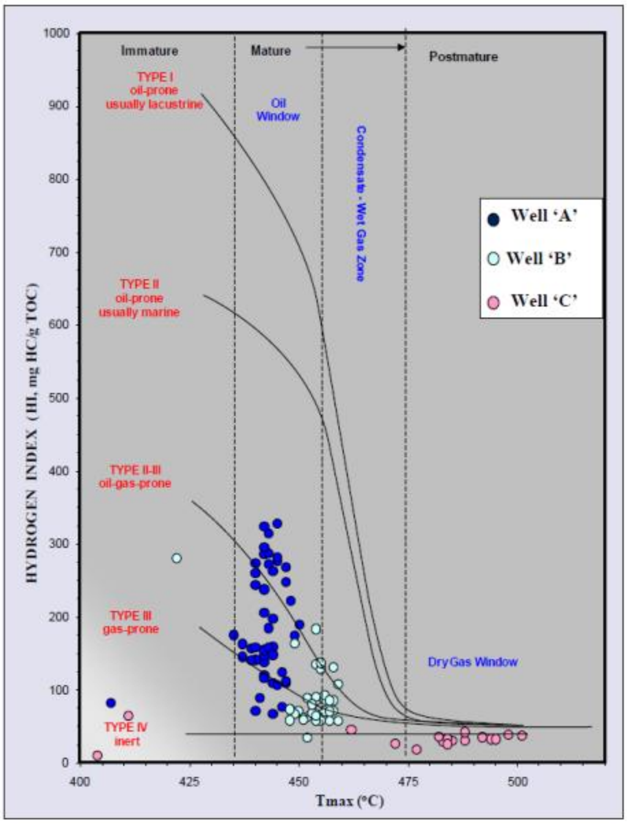

Figure 1.4.13. Crossplot of HI vs. Tmax for multiple samples from three Eagle Ford wells. Well A and B are inferred to be associated with an oil window while measurements from the well C fall clearly within the dry gas window (after Sondhi, 2011).

Lock et al., 2010, reported results from analytical studies on fresh outcrop samples that correlated to the subsurface zone targeted for hydrocarbons exploitation in the Eagle Ford. From their work, TOC measurements varied from 1.99 to 5.7 % as reported on Table 3, together with other useful values from the pyrolysis analysis. Because these measurements were obtained from outcrop samples, they should represent a lower bound of TOC values, as compared to samples that did not suffer weathering. However, a few authors report TOC values as high as 5% from Eagle Ford outcrop samples (e.g. Liro et al., 1994, and Slatt et al, 2012).

Table 3. Eagle Ford Shale Total Organic Content (TOC), and reported values from programmed pyrolysis analysis on five different samples (after Lock et al., 2010).

Sample #	TOC %	S1	S2	S3	T_{max} °C	HI	OI	PI
001 (10/07)	1.99	0.43	13.28	0.52	423	668	26	0.03
002 (10/08)	4.77	1.50	34.95	0.78	423	733	16	0.04
003 (10/28)	3.29	0,77	16.65	0.76	431	506	23	0.04
004 (10/31)	3.09	3.01	22.16	0.50	431	718	16	0.12
005 (KP-01)	5.70	1.46	42.19	0.76	423	741	13	0.03

Visual kerogen analysis also provides the means to characterize the quality of source rocks because kerogen is the sedimentary organic matter that generates hydrocarbons. The atomic ratio of hydrogen to carbon (H/C), and oxygen to carbon (O/C) makes possible to classify distinct types of kerogen and their associated hydrocarbons. Based on this classification, Eagle Ford samples are consistently associated with a type II kerogen, being capable to generate large amounts of oil and gas as shown in Figure 1.4.13. In regards to hydrocarbons accumulations, the Stuart City/Edwards reef margin represents a good regional reference marker, because north of it, Eagle Ford accumulations tend to be oil rich and normally pressured, while south of this boundary, hydrocarbon accumulations, tend to be over-pressured dry natural gas.

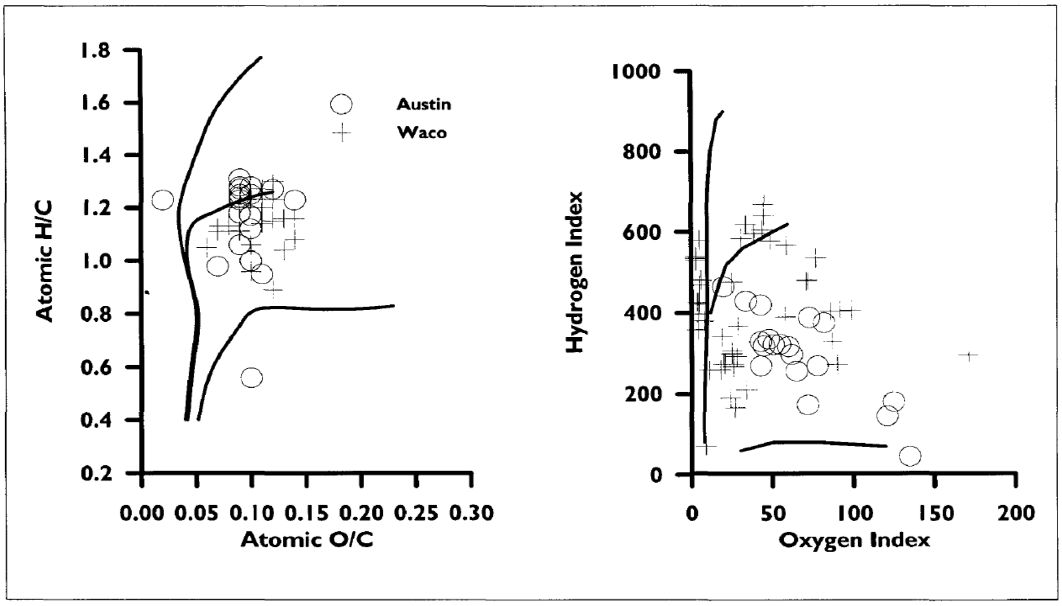

Figure 1.4.14. Comparison of pyrolysis and elemental data for kerogen typing of Eagle Ford samples in Austin and Waco localities. Most of the samples are consistent with type II kerogen (after Liro et al. 1994).

The existence of anoxic or oxic conditions during deposition could also be inferred from geochemical interpretations by analyzing the presence of certain minerals and specific biomarkers as well as by studying the relative hydrocarbon potential (Slatt and Rodriguez, 2012). In particular, the presence of phosphatic nodules on Eagle Ford cores reflect characteristic of transgressive conditions during deposition. Similarly, disseminated pyrite along the Eagle Ford's vertical column clearly delimits cyclic events, revealing that anoxic conditions fluctuated with time.

The Eagle Ford thickness, which could be greater than 100m (30ft), attests to the possibility of large amounts of hydrocarbons still remaining within this resource, for in the presence of thick source rock, above 60m (200ft) the expulsion processes are not as efficient, leading to significant amounts of residual hydrocarbon in place (Slatt and Rodriguez, 2012).

1.4.4.3 Petrographic characteristics

The analysis of rock properties via thin sections, x-ray diffraction (XRD) analysis, and scanning electron microscope (SEM) imaging is referred to as Petrographic Characterization.

Lower Eagle Ford thin sections, as the one shown on Figure 1.4.15, reveal the character of organic rich beds containing variable carbonate concentrations. Carbonates dominate the rock composition, primarily as recrystallized carbonates zones and grainstones lamina mainly composed of calcispheres, planktonic foraminifera and Inoceramid fragments (Lock and Pechier, 2006).

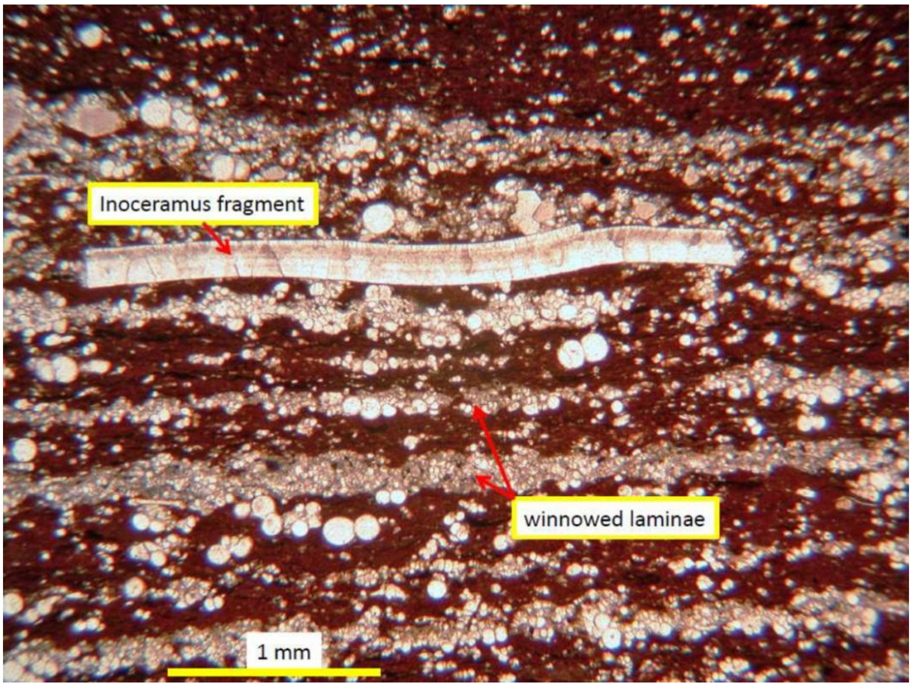

Figure 1.4.15. Eagle Ford thin section from a "black shale" portion of core, which has a distinct organic rich matrix. Here it is also easy to recognized Inoceramus fragments, disperse calcispheres and winnowed laminae of calcispheres and planktonic foraminifera. (after Lock and Pechier, 2006).

Thin section analysis also reveals the presence of fractures, which may serve as natural conduits for fluids to flow, thus enhancing reservoir permeability. Figure 1.4.16 shows two thin sections on natural light (A and C), and fluorescence light (B and D) to highlight the presence of fractures parallel and perpendicular to bedding.

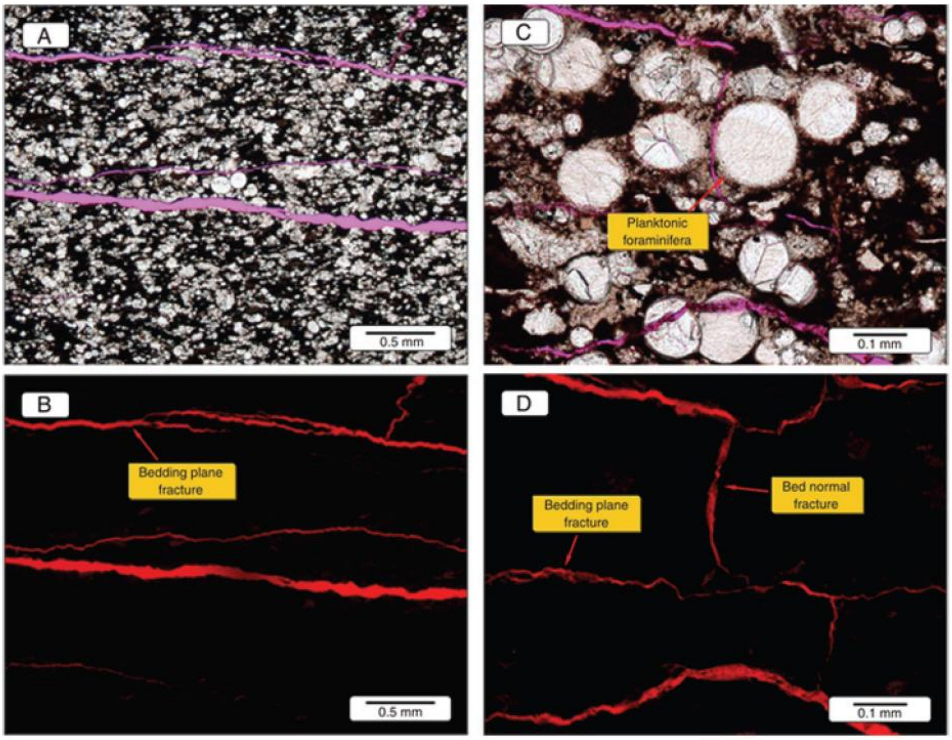

Figure 1.4.16. Eagle Ford thin sections showing fractures normal and along bedding-planes through the use of natural light (A and C) and fluorescence light (B and D) (after Mullen, 2010).

The interaction of X-rays with the crystalline substance of rock samples, referred as XRD analysis, provides particular patterns that characterize and identify their constitutive elements and confirm the observations made in thin sections. In this regard, calcite is the most abundant mineral and it is present as parts of the matrix, fossils fragments, cement filling foraminifer's chambers, and recrystallization material. Figure 1.4.17 shows graphically the volume percentage of various elements for the Buda, Eagle Ford, and, Austin Chalk formations obtained from XRD analysis.

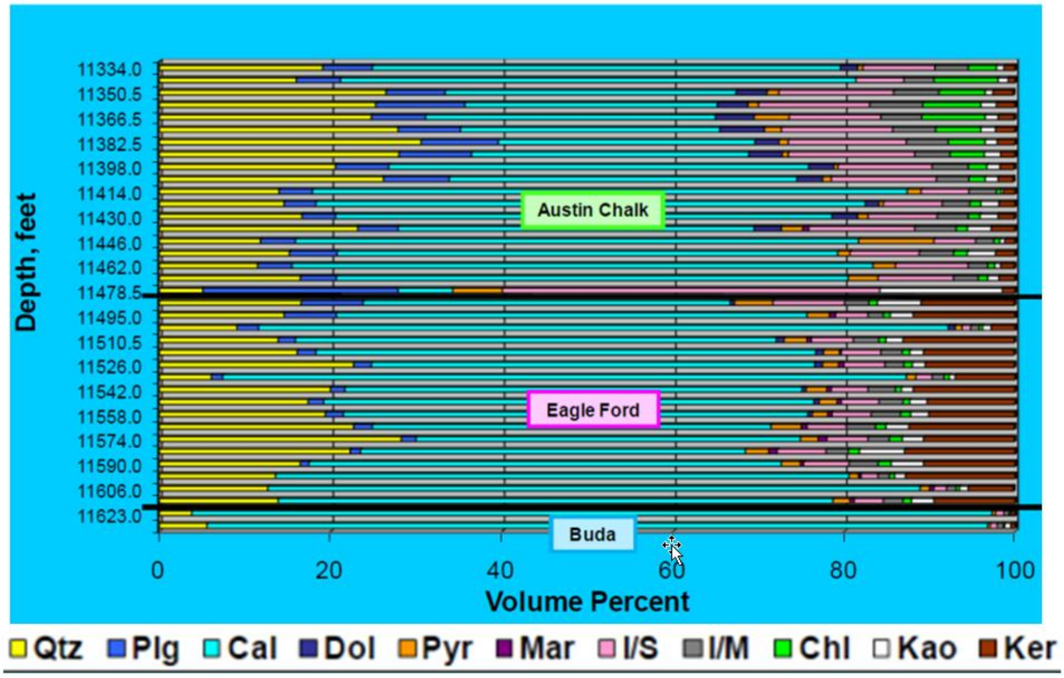

Figure 1.4.17. Mineralogy by XRD of an undisclosed well is penetrating the Eagle Ford Shale play. Quartz (Qtz), plagioclase (Plg), calcite (Cal), dolomite (Dol), pyrite (Pyr), marcasite (Mar), illite/smectite (I/S), illite/mica (I/M), chlorite (Chl), kaolinite (Kao), and kerogen (Ker) (after Stoneburner, 2012).

Most of the Eagle Ford samples reflect a composition very similar to the one presented in Figure 1.4.17 where quartz, plagioclase, calcite, dolomite, pyrite, marcasite, illite/mica, illite/smectite, chlorite, kaolinite, and kerogen represent the major elements of the rock. It is worth noting that the data presented in Figure 1.4.17 is from an area in the Eagle Ford Shale that has a relatively high kerogen content (mostly greater than 6%), and calcite is its major constituent, representing more than 50% of the section. This composition, however, varies considerably from east to west along the basin, as shown in the cross-section presented in Figure 1.4.18. In particular, the changes in the concentration of clay minerals (Illite, smectite, kaolinite and chlorite), together with changes in carbonate, quartz, and kerogen content result in vertical and lateral anisotropy in rock properties that directly affect log and seismic data responses, while also impacting the strength characteristics of the rock.

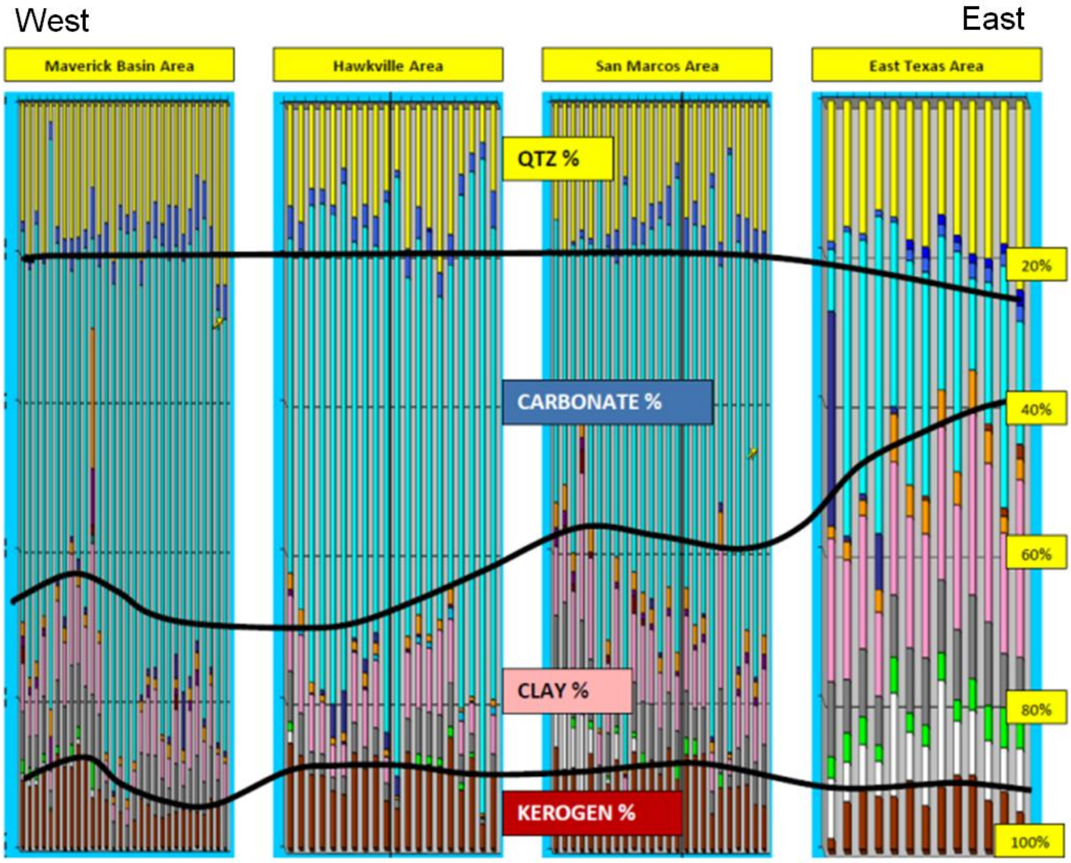

Figure 1.4.18. X-Ray Diffraction (XRD) information from four undisclosed wells penetrating the Eagle Ford Shale play forming a West-East cross section covering approximately 250 miles from the Maverick Basin to the East Texas area (see Figure 1.4.1 to get a relative distance between each area). The percentage of quartz (QTZ%), carbonate, clay and kerogen varies considerably. In particular, notice how the relative percentage of clay and carbonates changes from west to east (after Stoneburner, 2012).

On a fine-grained reservoir like the Eagle Ford, common rock typing based on porosity and permeability relationships is more difficult to perform because of the narrow range of porosities associated with the play and the nanodarcy permeability of the matrix. Therefore it is necessary to study thin sections and SEM images to recognize the effect of depositional processes in the reservoir quality and the relationship between different components of the rock. These analyses allow to understand mineral composition, diagenesis and anisotropy together with a complete characterization of the pore structure affecting the porosity and permeability relationship for each primary producing zone. Moreover, SEM images provide the means to obtain accurate porosity determination and relative permeability quickly in multiple directions, eventually aiding in the properties upscaling process (Walls et al., 2011). Figure 1.4.19 presents SEM images of two Eagle Ford shale samples showing distinctive carbonates, pyrite, kaolinite, and organic material fragments, as well as pore spaces distributed throughout the sample.

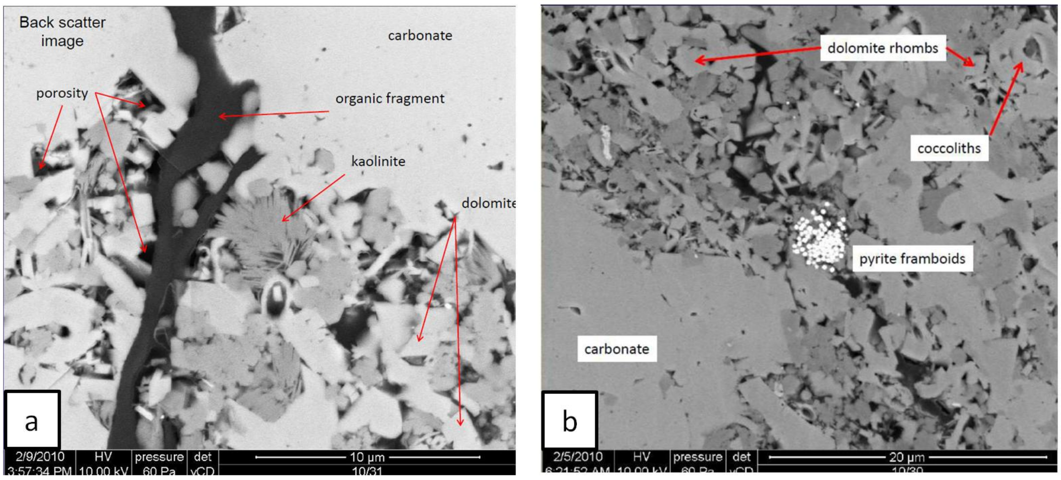

Figure 1.4.19. Eagle Ford shale Back-scatter SEM images showing the presence of carbonate, dolomite and clay (kaolinite) fragments as well as the presence of pyrite framboids, organic matter, fossils (coccoliths) and pore space. Figure a represents a higher resolution image compared to figure b as clearly marked on the figure's scales (modified from Lock et al., 2010).

Ion-milling, a technique typically used to generate relatively smooth surfaces of the samples from which high resolution images of the pore space are taken, should be treated with special care (as well as the results from these processes) because the milling process may significantly affect the sample analyzed, as shown in Figure 1.4.20.

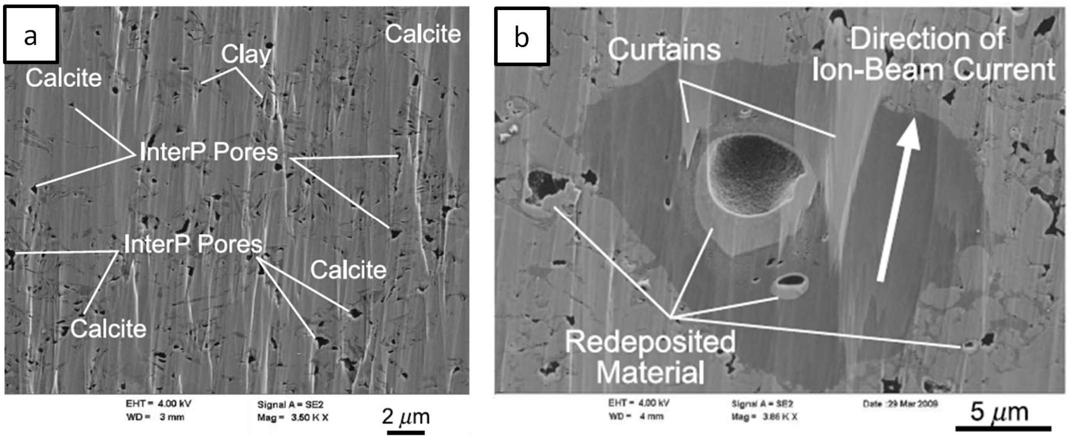

Figure 1.4.20. Eagle Ford shale SEM images highlighting the occurrence of clay and carbonate particles and associated inter particle pores. Figure b represents a higher resolution image compared to Figure a, as clearly marked on each the figure scale allowing to better observe possible consequences from the ion-beam sample preparation process (modified from Loucks et al., 2012).

Analyzing several SEM samples, multiple authors have postulated that the majority of the Eagle Ford microporosity is associated with kerogen (e.g. Walls et al, 2011, Curtis et al., 2012, and Loucks et al. 2012). This implies a strong influence of the maturation process on the Eagle Ford hydrocarbon storage capacity. However, in shale plays, and specifically in the Eagle Ford, this organic matter pore type is not the only source of porosity. In particular, Slatt and O'Brien (2011) discuss multiple sources for pores including porous floccules, porous fecal pellets, fossil fragments (e.g. sponge spicules, coccospheres and their spines, foraminifera with open chambers), mineral grains (e.g. pyrite framboids), microchannels within the shale matrix (e.g. micro burrows, scours, micro sedimentary structures) and fractures, each one contributing to the storage and flow capacity of the rocks. For instance, it is possible to observe porosity residing in floccule structures and various fossil fragments in SEM images of the Eagle Ford shale presented in Figure 1.4.21 and 1.4.22, respectively (Slatt and O’Brien, 2011). By properly characterizing pore-type it is possible to infer the proper relationships between porosity and permeability, and therefore to have a better estimate of flow performance. For example, Walls et al., 2011, postulates that Eagle Ford samples that show prominent intergranular porosity tent to be associated with lower natural permeability. Regardless of their type and origins, all these pores provide potential storage space for hydrocarbons accumulations such as the oil within the Eagle Ford’s coccolith chamber captured immediately after a pyrolysis test presented in Figure 1.4.23.

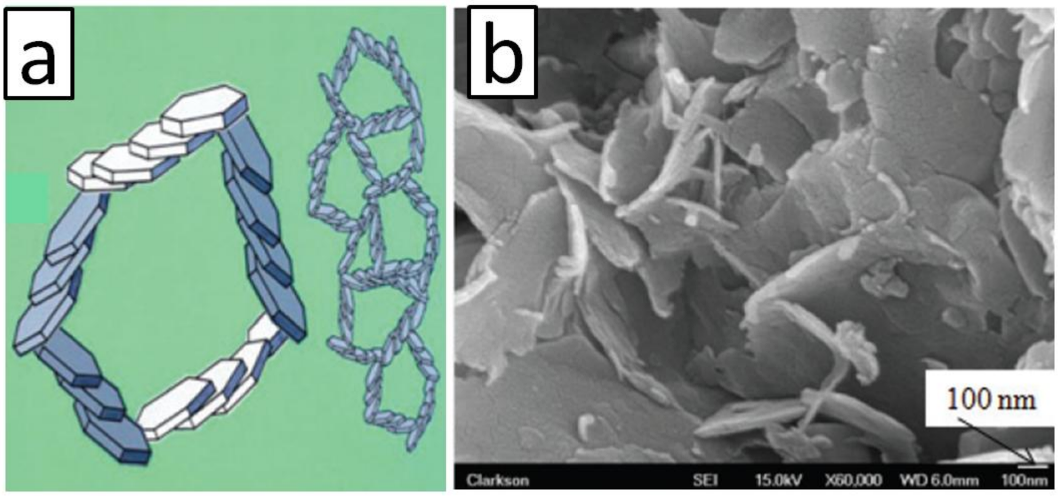

Figure 1.4.21. a) Cartoon representation of a flocculated clay particle and b) Eagle Ford shale SEM image distinctly presenting the same characteristic floccule pattern (modified from Slatt and O’Brien, 2011).

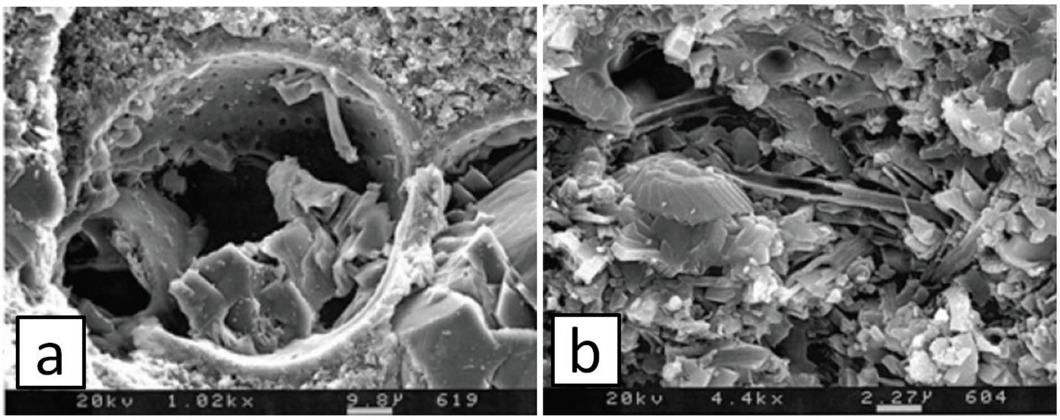

Figure 1.4.22. Eagle Ford shale SEM images clearly showing the contribution from fossil assemblages in the sample porous space. a) Interior of foraminifera partially filled with digenetic calcite. b) Hollow coccospheres and spines (modified from Slatt and O’Brien, 2011).

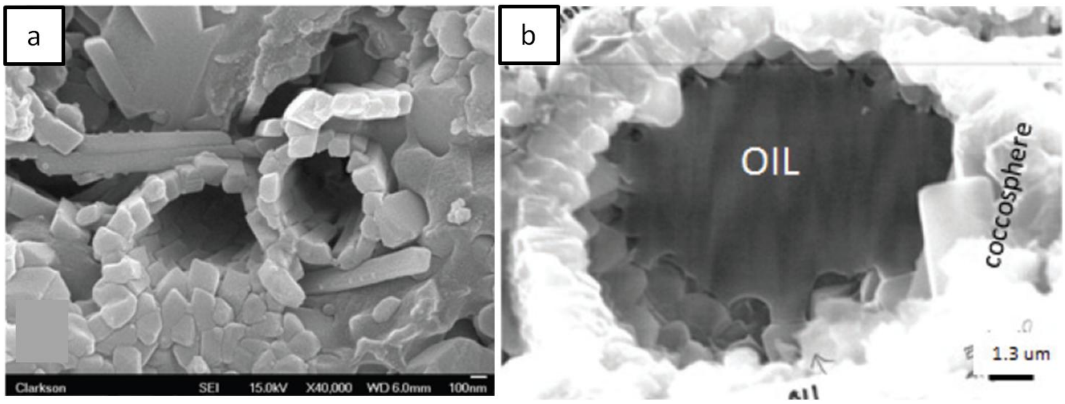

Figure 1.4.23. Eagle Ford shale SEM images clearly showing the contribution from fossil assemblages in the porous space. a) Hollow coccospheres and spines. b) Oil within coccolith chamber after hydrous pyrolysis (modified from Slatt, 2011).

1.4.5 Eagle Ford Sequence Stratigraphic Framework

This dissertation will use Donovan and Staerker's (2010) sequence stratigraphic framework of the Eagle Ford formation, which builds upon previous works by Freeman (1961), Pessagno (1969), Trevino (1988), and Lock and Peshier (2006), while it incorporates new insights from recent integrated subsurface and outcrop data analysis. Figure 1.4.12 summarizes the Eagle Ford sequence stratigraphic framework.

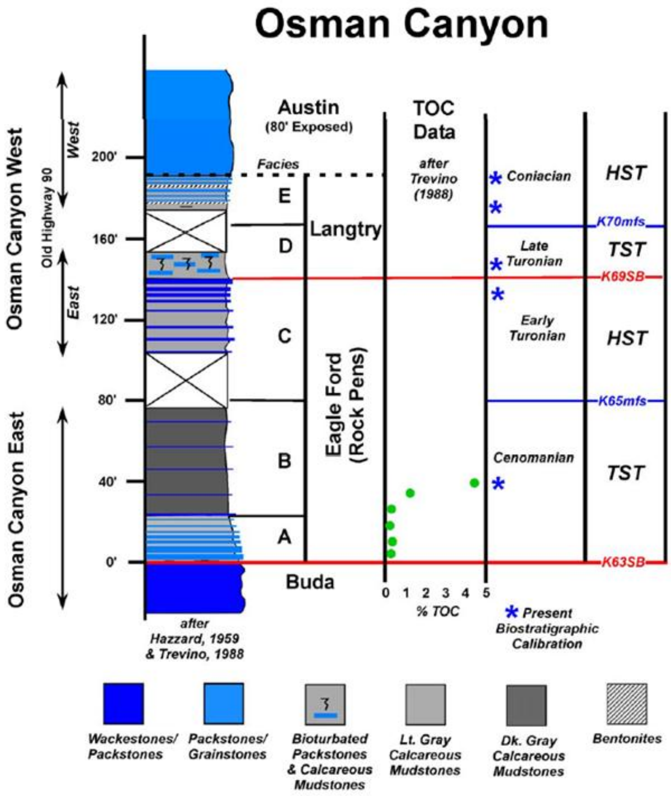

Figure 1.4.24. Eagle Ford sequence stratigraphic framework, Osman canyon fieldwork. Eagle Ford facies A and B are associated with a TST while facies C have typical HST characteristics. Facies A, B and C correspond with a second order sequence delimited by sequence boundaries K63SB and K69SB (authors' nomenclature). Observed lithologies, thickness, % TOC, and references to the canyon location and biostratigraphic geologic calibration are also shown. Notice that recognizing the K65mfs implies the presence of a condensed section on facies B and exhibits the highest TOC values and a significant carbonate content, making this unit very prospective for hydrocarbon exploration (after Donovan and Staerker, 2010).

Donovan and Staerker (2010) recognized multiple scales of regressive-transgressive cycles following sequence stratigraphic principles, and divided the Eagle Ford formation into five facies (A trough E) according with their observations. In particular, as seen in Figure 1.4.22, facies A and B are the Lower Eagle Ford member, which represent a TST, while facies C is associated with the Upper Eagle Ford member and has characteristics typical of a HST. For example, dark organic rich calcareous mudstones are ubiquitous in the TST, while distinctly prograding and lighter grey facies are associated with the HST. According with their work, the transgressive deposits formed by the Lower Eagle Ford (facies A and B) rests unconformable on top of the Buda formation. Following this interpretation, the contact between the Buda and Eagle Ford formations forms a regional combined sequence boundary/transgressive surface of erosion (SB/TSE) (Slatt and Rodriguez, 2012). This surface correlates with the Middle Cretaceous Unconformity at 96 ma described by Winkler and Buffler (1988), and recognized regionally in the Gulf of Mexico Basin (Haq et al., 1986). Following Donovan and Starker (2010) nomenclature, this major sequence boundary is labeled K63SB in Figure 1.4.22.

Based on the limited observed fauna (i.e. mainly planktonic organisms and bottom dwelling low oxygen adapted inoceramids), and the minimal presence of depositional structures and bioturbation indicators, sediments from the TST section are interpreted to have been deposited in a low energy, anoxic environment, capped by an mfs (labeled K65mfs in Figure 1.4.22). Donovan and Starker (2010) identify the organic-rich mudstones located immediately below the mfs as the most hydrocarbon rich section within the Eagle Ford. This is consistent with observations by Slatt and

Rodriguez (2012) for the Eagle Ford and other shale plays, and supports Lock and Pechier (2006) suggestions that this portion of the Eagle Ford has significant potential for hydrocarbon production. Indeed, this section represents a worldwide deposition of hydrocarbon-rich units.

On top of the mfs the typical Eagle Ford higher order limestone–marls cycles (parasequences dominated by the effect of *climate* and sea level fluctuation) serve as evidence of the characteristic depositional patterns, while carbonate content increases and limestone beds become more numerous in frequency and thickness (Donovan and Starker, (2010). Within these parasequences, it is also possible to recognize bioclastic and siliciclastic sediments probably supplied by southwestward prograding deltas, which represent proximal deltaic facies on the shallow shelf and distal deltaic facies basinward (Dawson and Almon, 2010). Lower TOC of this section corresponds with the more proximal facies and higher energy also supporting the interpretation of a regressive phase. Therefore, the sediment accumulation associated with Facies C could be interpreted as a HST, bounded at the top by a sequence boundary illustrated by the marker K69SB on Figure 1.4.22, which corresponds with the global unconformity at 89 ma (Haq et al., 1986).

The subsequent sedimentary accumulations are also properly described within a sequence stratigraphic framework as a TST and HST, respectively. Donovan and Starker (2010) recognize them as facies D and E of the Eagle Ford, and refer to these sections as the Langtry member. However, other authors (e.g., Dawson, 2000) prefer to associate the units above the Eagle Ford facies C with the basal members of the Austin Chalk, while others report that the whole Langrty member is missing in the subsurface as is the case in the Hawkville field, where this section is indistinguishable according to Hendershott (2012).

Major sequence stratigraphic surfaces and their associated system tracts can be identified easily in log records. Figure 1.4.25 shows a typical logging suite run on an Eagle Ford section and its sequence stratigraphic interpretation. The whole Eagle Ford is considered a second order sequence characterized by the general upward decrease in GR API that correlates with the coarsening upward stratigraphic section described in previous paragraphs and highlighted by the longest solid black arrow in Figure 1.4.25. Additionally, because high GR count readings may be interpreted as local flooding surfaces, the identification of these markers serve to identify GR parasequences (GRP) following Singh’s (2008) methodology. By implementing this approach, it is possible to identify GR upward-increasing and upward decreasing trends in Eagle Ford GR logs that serve to recognize multiple parasequences within the same section. These GRP are highlighted in Figure 1.4.25 by the use of dashed upward pointing arrows.

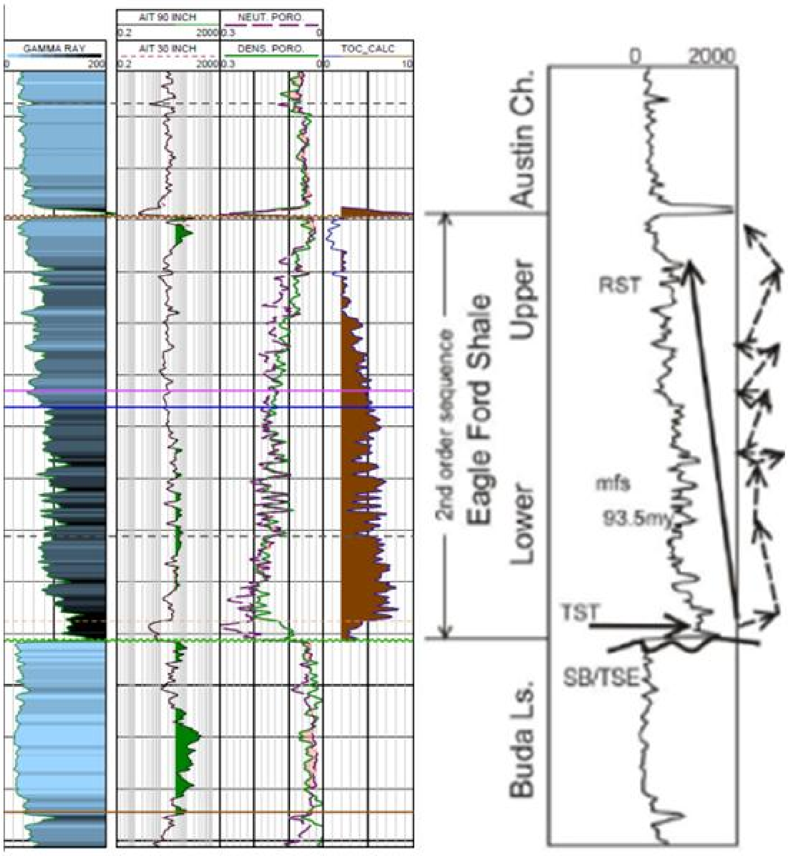

Figure 1.4.25. Typical open borehole logs responses from a vertical well penetrating the Eagle Ford shale play. Track one shows gamma ray curve. Track two displays medium (AIT30) and deep (AITC90) resistivity logs. Track three shows porosity measurements; density (green) and neutron (dashed purple); and Track 4 presents computed TOC. To the right, based on a GR curve interpretation, a solid arrow denotes a general upward decrease of API gamma ray counts at a second order scale while dashed arrows represents decreases and increases in API gamma ray counts associated with higher order variations (after Treadgold et al., 2010, and Slatt and Rodriguez, 2012)

Stacking patterns recognized by GRP are also very useful for development operations. For instance, they can be used to predict mechanical properties of lithologic sections because high GR readings are usually associated with ductile layers prone to shear failure, while low gamma ray measurements usually correlate with brittle zones and preferential tensile failure (Badra, 2011), thus having a direct impact in the design and analysis of hydraulic fracturing treatment. Additionally, staying away from clay rich zones, recognized by the high gamma ray readings, might help mitigate hazards associated with clay swelling induced by drilling fluids.

Logs associations such as those shown in Figure 1.4.25, also provide the basis to build regional sequence stratigraphic models, such as the cross section presented in Figure 1.4.26, where prograding patterns and abrupt truncations are easily recognized from the northwest to the south east in accordance with the depositional framework discussed in this chapter.

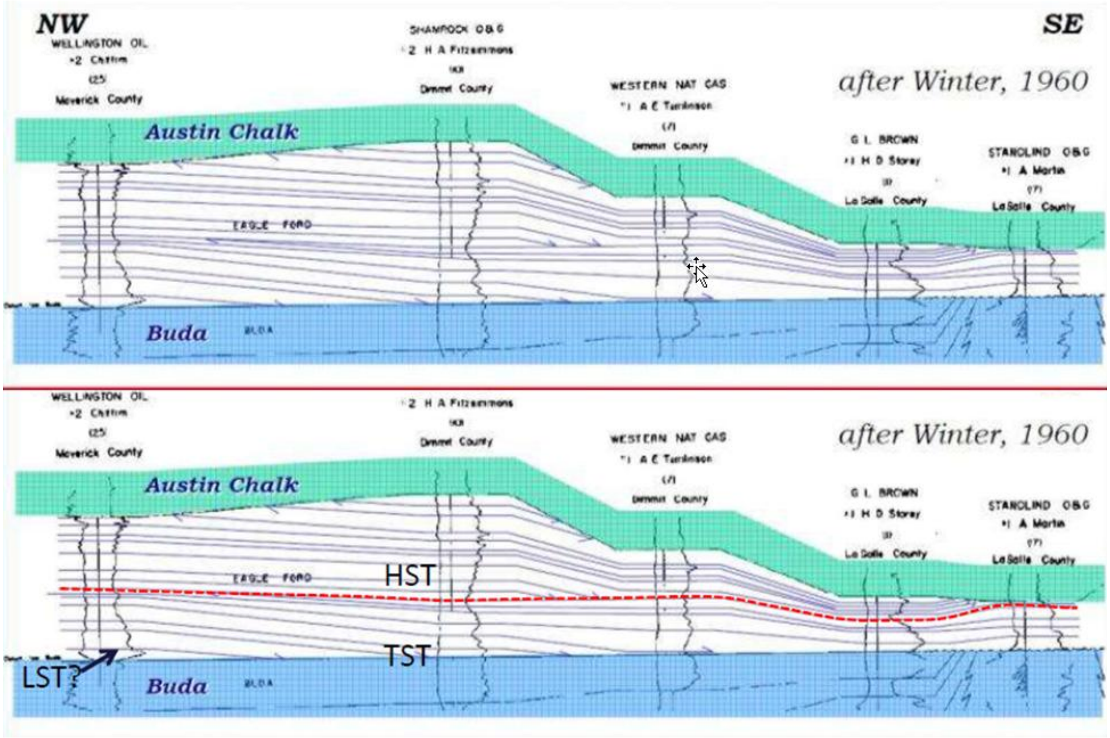

Figure 1.4.26. Regional cross-section showing major sequence stratigraphic characteristics of the Eagle Ford formation (after Bohacs and Lazar, 2010).

CHAPTER 2: Pitfalls locating microseismic events from borehole measurements – practical observations from field applications*

Cabarcas, C.

*Adapted from paper published in *Interpretation*, **Vol 1**. No 2 (November 2013); p. A11-A17. Copyright 2013, Society of Exploration Geophysicist and American Association of Petroleum Geologist.

2.1 Abstract

Borehole microseismic monitoring of hydraulic fracturing is among the best tools for reservoir stimulation evaluation. After decades of research and execution, the technique has gained a well-deserved place within the engineering toolbox. Moreover, in recent years, its popularity has increased exponentially, together with the development of unconventional resources. However, while involved with a significant number of borehole microseismic monitoring campaigns, I noticed that it is a common practice to overlook fundamental principles during the location of microseismic events. This may lead to potentially erroneous hydraulic fracturing assessments. Examples of microseismic results qualitatively illustrate this assertion showing poor recording, velocity models, processing constraints and display. They also underscore the interpreter's role in ensuring the most reasonable outcome from a microseismic hydraulic fracture evaluation. In this respect, any conclusion derived from a microseismic experiment should be fully supported by a thorough understanding of the impact that multiple acquisition and processing assumptions have on the

interpretation, as is the case for all other geophysical techniques. Ultimately, my intent is to raise awareness of some common pitfalls while also providing recommendations to increase the value of a microseismic monitoring exercise.

2.2 Introduction

In the oil and gas industry, borehole microseismic serves as an indirect diagnostic technique that uses low-magnitude seismic signals registered in a monitor well (or multiple wells) to study induced subsurface seismicity during hydraulic fracturing. In this particular application, seismic signals recorded throughout the stimulation treatment are later processed to obtain, at a minimum, their source location. The typical representation of the results of this processing step is a cloud of points interpreted as an envelope of activated fracture planes, thus providing an immediate first diagnostic of the stimulation work. For example, one common use of borehole microseismic is to estimate length, height, and azimuth of induced fractures to assess the performance of hydraulic fracturing treatments. The literature describing results and benefits from this approach is plentiful, and several decades of research on the topic support the case for borehole microseismic monitoring as a robust technology as discussed in the works of Warpinski (2009a); Maxwell et al. (2010a, b); and; Wuestefeld et al. (2012). However, geometric parameters obtained from borehole microseismic measurements may not always explain production records from the stimulated well. Based on my experience, most of these inconsistencies are a direct consequence of dislocated acquisition, processing, and interpretation phases, and are oftentimes not indicative of intrinsic microseismic technique limitations.

Previous publications have recognized pitfalls in the application of borehole microseismic technology as a diagnostic tool for hydraulic fracturing. Warpinski (2009a) advised the scientific community to ensure that event locations are real and not influenced by uncertainties and artifacts of the technology. Maxwell and Cipolla (2011) stated that due to location uncertainties, microseismic clouds usually tend to overestimate the area affected by the treatment. These authors also emphasized the impact that vector fidelity, sampling rate, sensors, array geometries, sensor placement (i.e. location bias) and anisotropy corrections have on the accuracy and precision of microseismic event locations (Warpinski et al., 2009; Maxwell et al. 2010a, b, c; Maxwell, 2010; and, Maxwell and Cipolla, 2011). Le Calvez et al. (2007) discussed similar issues and underscored the role of a proper geological framework on microseismic interpretation. Other authors such as Fehler et al. (2001), Drew and Le Calvez (2007), House and Shemeta (2008), and, Kurosawa (2011) provided examples of how picking methodologies could significantly impact the proper location of microseismic events, resulting in drastically different interpretations of stimulated reservoir volume. Mechanical limitations of the measuring tools (Pavlis, 1986), and, other errors such as the use of inaccurate well deviation surveys, surface location and depth controls, also contribute to a low quality microseismic evaluation. Personnel involved with microseismic operations devote a great deal of effort to address these pitfalls; however, they are still common today. This publication provides specific field examples of other common pitfalls and offers recommended best practices to avoid them in the future, while highlighting the role of the microseismic interpreter in addressing the technical challenges of the microseismic evaluation.

Following a brief series of comments describing the benefits of interpreter involvement on acquisition activities and modeling in advance of field operations, I discuss the influence of velocity models and location algorithms on the placement of microseismic events, while also making the case in favor of embracing reprocessing efforts. By documenting my experiences, I seek to raise the awareness of other interpreters about potential pitfalls that could influence their analysis. Additionally, this work may support a better implementation of future microseismic experiments, and consequently, the growth of borehole microseismic analysis as the preferred diagnostic tool for hydraulic fracture monitoring.

2.3 A note on data acquisition and modeling

Before I elaborate on the effects that event positioning have on hydraulic fracturing evaluations, I would like to share a few comments regarding the acquisition phase of microseismic data. Figure 2.1 illustrates inferior data quality recording during acquisition operations that cascaded to the processing and interpretation steps. In this particular example, only seven out of twelve multicomponent sensors registered data with enough signal-to-noise ratio to properly locate microseismic events acquired during twenty stages of hydraulic fracturing. That means 42% of the data registered during this project had no material use.

As equipment failure and operational issues can always happen during the acquisition of microseismic data, and indeed are very common (Rich, 2012), the key lesson from this experience is the need for constant interaction between the service company personnel and the operator. By doing so, all acquisition irregularities can be properly identified, documented and addressed. For instance, as a best practice, standard reporting documents should contain event statistics (e.g. number of discarded triggers) and detailed descriptions of all data manipulation steps. The quality control report presented in the work of Zimmer et al. (2007), which includes error bars along with the location of events, is a good reference for the type of information a final report should include. In this respect, it is important to ensure that error bars are associated not only with arrival times and ray path polarization, but also with the ultimate location of a given event. Good recordkeeping of field acquisition operations, usually known as “observer reports” on reflection seismic acquisitions, will also benefit the interpreter and processing team, especially if the recorded data is to be reutilized in the future.

A practical way to quantify the significance of missing information on properly located microseismic events is by analyzing synthetic models built during the planning stage of the experiment. In addition to supporting the acquisition design, these models could become a great aid during acquisition operations, processing, and real-time decision-making. For instance, a synthetic model may help in properly placing the recording instruments within a monitor well, and in understanding the characteristics of the zones of interest (e.g. the influence of high velocity layers). It can also aid the quantitative evaluation of missing information from one or more sensors and new array configurations if field deployment differs from the tool arrangement originally planned. The array configuration in Figure 2.1 shows an example of this situation in which some sensors of the array were to be in the stimulated zone, but ultimately only sensors located above the zone of interest registered useful data from the treatment. In this respect, I recommend to compare the synthetic model and the actual results from the microseismic experiment to better understand the effect of tool positioning and background noise on the acquired data, and the overall evaluation of the stimulation program.

Tool placement may also be associated with event location errors, as is illustrated in Figure 2.2. A map view of high magnitude microseismic events from a single stage hydraulic fracturing treatment on a vertical well is shown in this figure, along with the multi-component sensor arrays used to monitor the treatment from two adjacent horizontal wells. Sensor arrays and their associated microseismic events are shown in red and blue squares and diamonds, respectively. The figure highlights two different locations of the same event. This is obviously an artifact. There are multiple reasons why this could happen. For example, the differences in move-out observed by each array may result in slightly different positioning of the same event. Low signal-to-noise ratio for events in close proximity to the sensors may also interfere with the sensors ability to register such events. To minimize the chance of this pitfall, I recommend using multiple sensor arrays strategically placed surrounding the treatment well, coupled with an analysis that simultaneously considers all wave forms registered during the fracturing treatment.

2.4 Velocity model, location algorithms, and their implications

Since microseismic monitoring is intrinsically a geophysical method, symbiotic relationships exist between time, velocities, and distances while using this tool. In particular, velocities are key to properly placing the source of microseismic events in the subsurface, but it is rare to have an excellent estimation of such velocities. Multiple authors have already emphasized this fact and described typical pitfalls associated with the velocity model (e.g. Warpinski et al., 2005a,b; Wilson et al., 2008; Maxwell et al., 2010a; Mizuno et al. 2010, Eisner et al., 2011, and, Cabarcas et al., 2012). In this section I show specific examples that illustrate the significance of the velocity model and location algorithm on the final placement and interpretation of microseismic event sets.

A common practice in the microseismic event location workflow is to build an initial velocity model using compressional (Vp) and shear (Vs) velocities derived from dipole sonic logs. Then, a calibration is performed incorporating into the velocity model information obtained from the hydraulic fracturing operation. One such calibration method is described in the work of Warpinski et al. (2005a) and consists of recording the precise time of perforation (or string shot) firing in addition to its seismic signal to optimize the initial velocity model. The calibration phase is required because, in general, vertical velocities measured by the sonic tool are different from the horizontal velocities of a layered subsurface. Moreover, seismic signals propagate in radial patterns, thus requiring more than a horizontal and vertical component of the velocity to completely describe the microseismic signal travel path. Therefore, none of the calibration approaches currently in use fully compensate for the intrinsic anisotropic characteristic of the stimulated zone of interest in resource plays (Eisner et al., 2011).

The use of sonic logs to build the velocity model carries significant upscaling uncertainties as pointed out by Chesnokov et al. (2011). Similar issues arise when the velocity model is built using data from surface seismic experiments because velocities obtained from the surface, as well as from log measurements, suffer from well-known and difficult-to-compensate dispersion issues (Liner, 2012).

To illustrate the significance that the upscaling methodology has in the location of microseismic events, Figure 2.3 shows vertical cross sections representing possible scenarios for the localization of induced seismic activity (red dots) associated with a single hydraulic fracturing stage. As shown in this example, two substantially different assessments of the fracture geometry and the mechanical properties of the subsurface are implied by blocking the velocity logs using geological boundaries (Figure 2.3a), or by implementing a constant 5 m (15 ft) averaging upscaling approach (Figure 2.3b). The detailed blocking methodology used to generate Figure 2.3b -a common approach preferred by some contractors- it is usually not appropriate for most event location workflows. Consequently, the set of points displayed in Figure 2.3b forms lineaments that imply the stimulation of simple fractures with limited vertical growth as inferred by the flatness of these groups of events. These characteristics are most likely processing artifacts. In contrast, sequence stratigraphic principles provide viable boundaries during the upscaling process of the velocity model used to locate the events presented in Figure 2.3a. Implementing such an upscaling approach, the induced seismic activity plots as a cloud around the perforation points on the vertical cross section, in accordance with the expected response from this formation. The location of these microseismic events also confirms the anticipated relationship between rock type / stratification and microseismic events within the vertical (stratigraphic) dimension suggested by Slatt and Abousleiman (2011). These results underscore the importance of using a proper geological framework in microseismic interpretation. The need to adopt geologically-consistent and mathematically robust methodologies to properly upscale sonic log data becomes obvious, such as the one presented here or those described by Tiwary et al. (2009), and Liner (2012). Adopting a fit-for-all upscaling methodology and neglecting fundamental geological principles is a common industry pitfall.

Other geological assumptions made during the building of the velocity model also affect significant variations in the microseismic event location. For instance, Figure 2.4 shows an example where a 5-degree dip change suggested two completely different hydraulic fracture heights. In this example, the use of a tilted velocity model resulted in height differences half of those obtained from the original interpretation which did not account for geological dip. It is important to point out that both, the original velocity model and the subsequent velocity model that honored geological dip, were calibrated using data extracted from perforation shot records. This demonstrates that although velocity model calibration is a necessary step in the processing sequence, it is not sufficient to provide an acceptable velocity field. Therefore, additional steps must be taken to ensure geological characteristics of the subsurface are considered when building the velocity model. An earlier publication by Cabarcas et al. (2012) discusses in more detail the impact of a dipping velocity model on microseismic event locations.

The location algorithm chosen to place the events in the subsurface may also introduce artifacts during microseismic event positioning. As an example, Figure 2.5 illustrates discrete boundaries among microseismic events associated with a series of thirteen hydraulic fracturing treatments on a map view. In this figure, each hydraulic fracturing stage is denoted by a color, and thick red lines have been added to emphasize how the processing software arbitrarily assigned event locations to the confinement of a predetermined stimulated volume, such that overlapping of microseismic events between subsequent stages would be minimized. In this particular case, a series of constraints were imposed on the processing results because poor height estimates were expected from using only an array of detectors placed horizontally inside an adjacent borehole. Unfortunately, as depicted in Figure 2.5, constraints were also seen on the horizontal plane as the restrictions imposed were excessive. Needless to say, this approach lends itself to potentially erroneous interpretations of the stimulated volume and the preferential fracture orientation (maximum horizontal stress), as these were all arbitrarily preset at the processing stage.

Once the interpreter is comfortable with the event locations obtained, careful choice of a visualization approach should follow to enhance the stimulation evaluation. Special attention must be paid to not introducing a negative bias. It is important to use all properly located events after efforts were geared toward the generation of the most reasonable data set. Figure 2.6 shows a common interpretation practice; i.e. to associate the size and color of the symbol representing the event to its properties (in this particular case relative recording time and magnitude of the event). To minimize any negative impact this type of representation might generate, I recommend using more than one visual approach to analyze the available data, as well as a thorough understanding of the meaning of each property used to filter the event set. Concepts, such as magnitude, which may be considered universal because of their widespread use in the industry, often have different definitions among different contractors, as indicated in the work of Shemeta and Anderson (2010), and may lead to different interpretations.

Improper use of microseismic attributes may introduce bias as some events could be interpreted as more relevant than others based solely on their relative size or color, leading to interpretations that fail to recognize other scenarios. For instance, smaller events in Figure 2.6 may be associated with potential fracture containment issues and increased health, environmental, and, safety risks (e.g. the unintentional stimulation of an adjacent H_2S rich formation). In this case, out-of-zone fracture growth could also connect the well to an underlying aquifer, negatively impacting the well productivity. All these possible outcomes are minimized by the type of display chosen, which only implies a small stimulated reservoir volume surrounding the treatment well borehole and therefore mistakenly reassuring the interpreter low risk perception.

2.5 In support of reprocessing efforts

Reprocessing efforts are highly encouraged because, while the technology—as well as interpretation awareness—improves, the same data set could provide a completely different perspective of the stimulated volume. Also, as time elapses, more production records are available and a second look at legacy microseismic projects, in conjunction with the additional information, could provide a more accurate interpretation of the treatment results, possibly affecting future completion strategies or asset development plans.

Even the first time a data set is acquired, it is advantageous to involve multiple service companies as it minimizes the bias associated with a particular contractor's approach. As demonstrated in the case study presented by Hayles et al. (2011), differences from one contractor to another could be substantial, leading to completely different hydraulic fracture assessments. Moreover, in order to minimize a potential pitfall, the interpreter should supervise and impose specific guidelines during the reprocessing efforts. A good practice is to provide all contractors with the same calibrated velocity model, properly evaluate their processing output, and (as is the case in depth imaging) keep a significant level of engagement between processors and interpreters to ensure the most acceptable outcome from the microseismic experiment. Moreover, when the job is finished, the interpreter should request the raw data from the contractor (including all "real time" and any preliminary data sets instead of just the final results). Ensure that trace headers contain all the information associated with each seismic trace, and that ancillary information is properly archived because several years may go by before the reprocessing work takes place. These steps would also minimize the likelihood of missing relevant data and would better support future data trades and/or acquisition and divestiture efforts.

2.6 Final thoughts

This publication does not provide a solution for the myriad of issues that can be found in a typical microseismic job, but rather represents a call for awareness from the interpreter's point of view. I recommend paying special attention to the acquisition and processing steps before engaging in the interpretation phase. As discussed in this publication, the microseismic interpreter should be intimately familiar with all aspects of the acquisition, the building of the velocity model, and the location algorithm used on microseismic event location. In addition, the interpreter should test multiple scenarios based on fundamental geological principles and weigh the cost and benefit from reprocessing opportunities.

In the same way that the interpretation of surface reflection seismic is left to an experienced seismic interpreter, microseismic data should be manipulated by a professional who has developed familiarity with all aspects of this geophysical method, or better yet, an integrated multifunctional team that can assess the validity of all the assumptions and final interpretation of a microseismic experiment.

2.7 Acknowledgement

The figures presented in this publication had been modified from internal Hilcorp Energy Company (HEC) reports provided by multiple service companies. I would like to thank HEC management not only for permission to publish them, but also for their support and encouragement to innovate through the use, and challenge, of new technologies. In the same respect, my appreciation goes to all those microseismic subject matter experts involved in some of the projects here discussed. Their work contributed not only to answering key questions, but it eventually resulted in the implementation of a significant set of best practices in subsequent projects. Finally, I would like to appreciate and recognize my gratitude to Dawn Henderson for

proofreading numerous drafts of this manuscript as well as the reviewers and editors of Interpretation who also provided excellent feedback on the content of this publication.

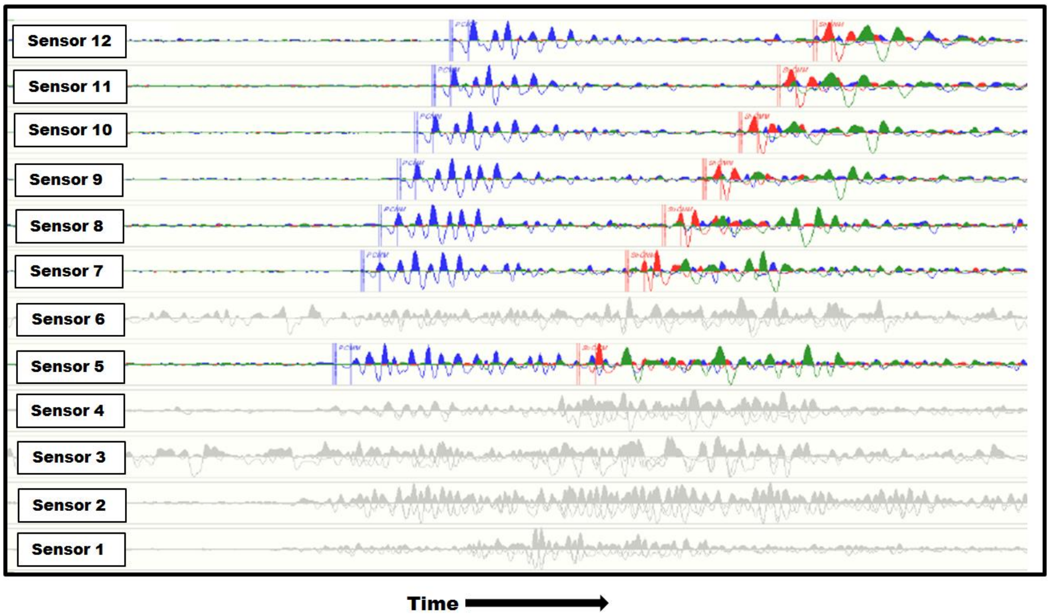

Figure 2.1. Raw traces from twelve borehole tri-component sensors used in the acquisition of a microseismic experiment. The detection of a microseismic event is inferred from the response of seven sensors as traces from the other sensors (grayed-out) only displayed unacceptable noise levels. Microseismic data from each component is plotted on top of each other. Blue traces display the information from the vertical component geophones, while red and green traces present the data from the two horizontal components. For each sensor display, the horizontal axis represents recording time increasing in the arrow direction while the vertical axis displays negative and positive values with respect to a horizontal zero base line. A vertical wellbore contains all sensors, sensor 1 being the deepest and sensor 12 the shallowest. This experiment ended up only having sensors above the treatment zone, though modeling supported placing some sensors within the zone of interest.

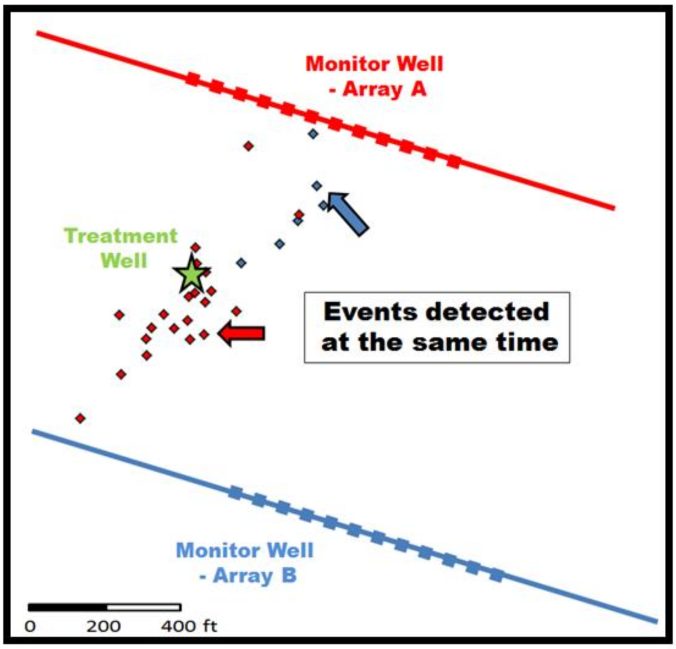

Figure 2.2. Map view of high magnitude microseismic events associated with a single stage hydraulic fracturing treatment on a vertical well. The treatment was monitored by two arrays (12 sensors each) shown in blue and red squares. Microseismic event locations determined by each array are shown in red and blue diamonds, respectively. The figure highlights two different locations for the same event.

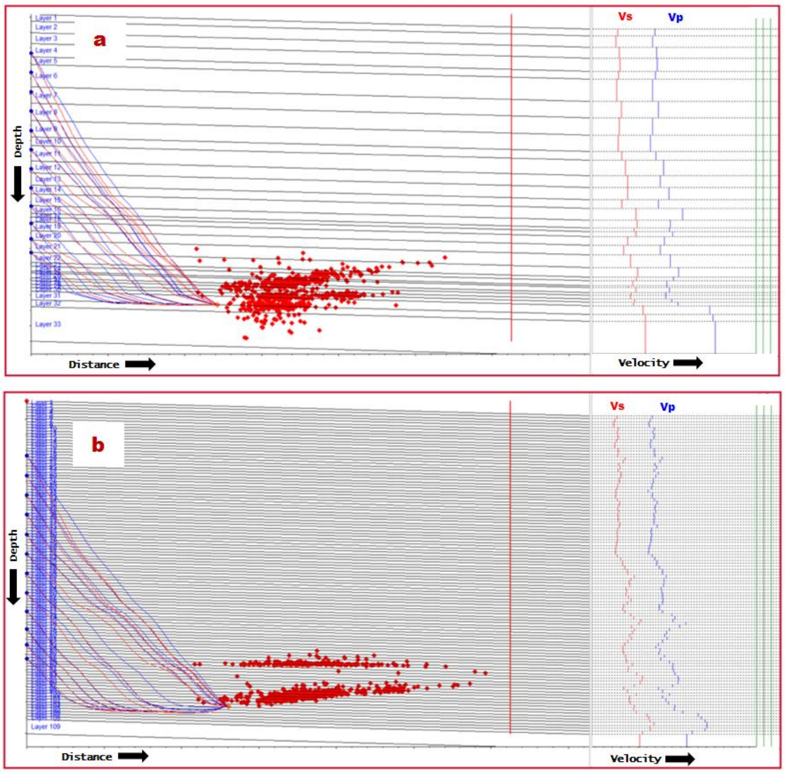

Figure 2.3. Vertical displays of microseismic events (red dots) associated with one hydraulic fracturing stage. The upscaling approach applied to compressional (Vp) and shear (Vs) logs in order to construct a calibrated velocity model have significant consequences on final event locations; a) follows an upscaling methodology that favors geological boundaries, and, b) shows the results of applying a constant 5 m (15 ft) blocking scheme. Notice how the number of layers surges from a to b. For illustration purposes, the figure also shows schematic ray paths from one source location to twelve borehole sensors located within a vertical wellbore. Depth, distance and velocities increase in the arrow's direction.

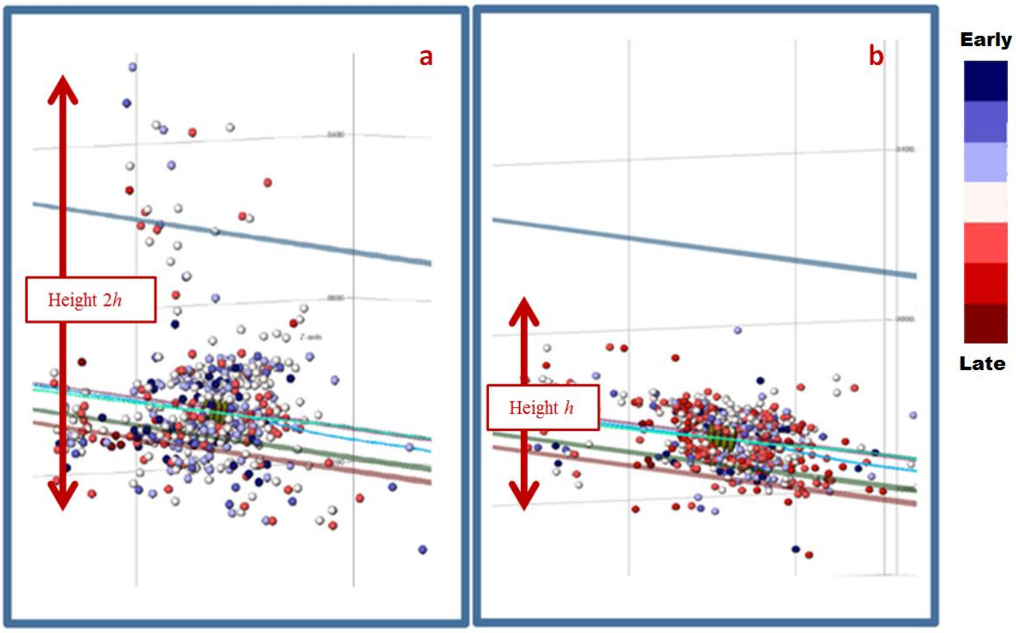

Figure 2.4. Microseismic events locations within a hydraulically stimulated zone of interest according to two different velocity models: (a) a flat layer velocity model, and (b) a model with minor dip (5 degrees) based on the geological characteristics of the subsurface. Inclined lines represent geologic horizons related to the zone of interest. Dots representing microseismic events are color-coded from those recorded earlier (blue) to those recorded later (red) following the displayed color scale.

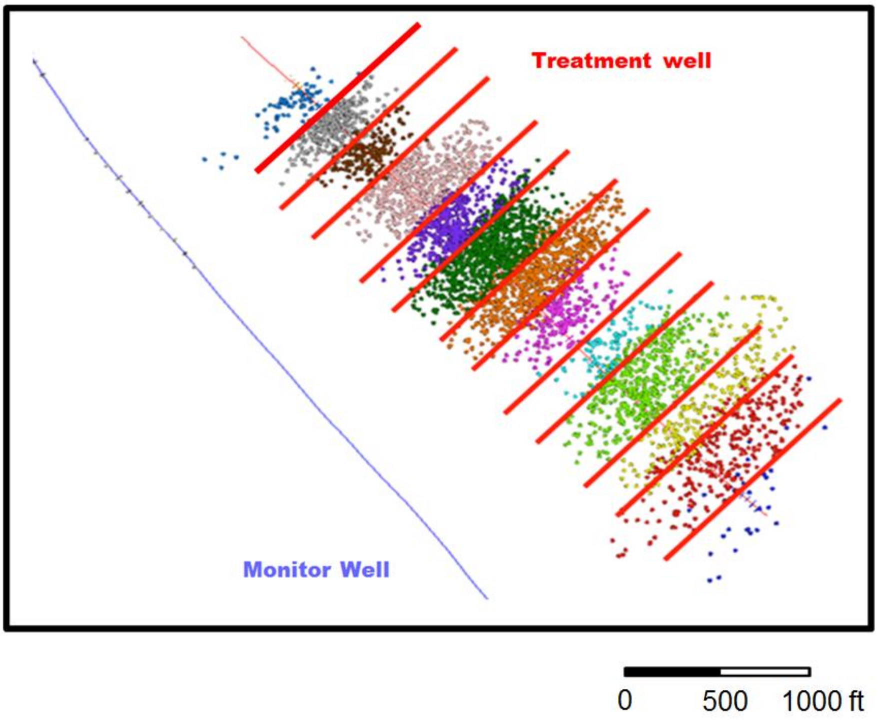

Figure 2.5. Map view of a treatment well (thin red line) and its associated monitor well (blue thin line), together with the final location of microseismic events from 13 hydraulic fracturing stages. Each hydraulic fracturing treatment is color-coded to differentiate them. Thick red lines perpendicular to the borehole azimuth highlight artificially generated boundaries caused by the location algorithm and probably unrelated to the stimulation procedure or its response from the formation.

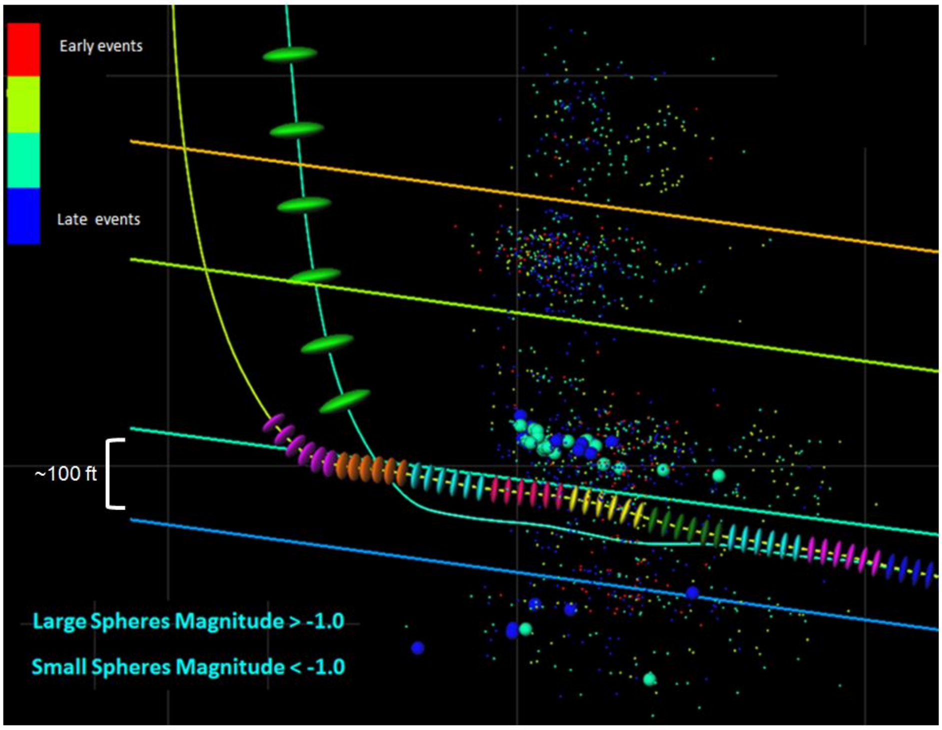

Figure 2.6. A typical illustration of microseismic events associated with a hydraulic fracturing stimulation treatment. Dots representing the microseismic events are colored based on their recorded time from early events to late events following the label in the figure. The sizes of the events are indicative of the events' magnitude. For reference purposes, the figure also displays schematic representation of the treatment well, perforation locations for each stage, monitor well, recording sensor locations, and horizons of interest. This type of representation relies heavily on the interpretation of high magnitude events recorded towards the end of one fracturing stage and discards most of the associated activity also available to the interpreter.

CHAPTER 3: The impact of dipping velocity models on microseismic events locations*

Cabarcas, C., L. Saugier, G Haas, J. Le Calvez, and J.C. Woerpel.

*Adapted from paper published in the proceedings of the Society of Petroleum Engineers Hydraulic Fracturing Technology Conference held in the Woodlands, Texas, USA, 6-8 February 2012. Paper 152600-PP. Copyright 2012, Society of Petroleum Engineers.

3.1 Abstract

Once a microseism is detected, its source location can relatively easily be identified if the velocity characteristic of the medium traversed by the recorded waveforms is known. Unfortunately, this is rarely the case. Velocity models are used to estimate, with some degree of confidence, microseismic event locations. This work shows how a simple modification to the velocity model, accounting for a 4.5-degree dip supported by geological data, significantly impacts the event final locations during a borehole-based hydraulic fracturing monitoring job. Overall geometry of the hydraulically-induced fracture system interpreted (e.g. height) is the most affected. For instance, when a preliminary event location is selected without introducing the observed structural component of the beds, these measurements could change by as much as fifty percent. For the reservoir engineer, sometimes unaware of the assumptions made at the microseismic processing level, these differences could imply major changes to the field development plans. These results underscore the

importance of integrating all available data and implementing well known quality controls before using microseismic monitoring data for reservoir analysis.

3.2 Introduction

Microseismic monitoring of hydraulic fracturing treatments is a powerful stimulation diagnostic technique when properly implemented. This paper describes one of the many parameters having a significant impact on the location of each microseismic event, the subsurface velocity model, which ultimately shapes the microseismic analysis. Despite its relevance, the importance of using accurate velocity models is sometimes underestimated. Several authors have already emphasized the significance of choosing an appropriate subsurface velocity model, and its impact on microseismic event location and subsequent interpretation. For instance, Warpinski (2009a) points out the velocity model as “the most important element in the whole process of microseismic mapping”, and describes how differences between vertical velocities (measured by logs) and horizontal velocities (used for ray path modeling), could originate event misplacements in the order of hundreds of feet. Wilson et al. (2008) also presented a case study on the variability originated by modified velocity structures in the presence of high velocity layers, thus underscoring the importance of the velocity model on any microseismic interpretation. Maxwell (2009) and Maxwell et al. (2010a, b), on the other hand, recognized that the velocity model, often built following calibration procedures such as the one described by Warpinski et al. (2005a), can result in oversimplified versions of the subsurface structure, which may carry significant uncertainty into the final event mapping. None of these previous studies, however, have addressed the effect of dipping velocity models in the event location and subsequence interpretation. This work highlights how geometric differences of velocity models, associated with known geological characteristics of the subsurface, may significantly affect the location of microseismic events and the overall stimulation diagnostic.

3.3 Geologic Framework

The main objective of the microseismic monitoring experiment described on this publication was to diagnose the performance of a multistage hydraulic fracturing treatment designed to stimulate a hydrocarbon bearing, low permeability reservoir. Surface reflection seismic and open hole logs across the area of interest suggest an image of the subsurface that is structurally and stratigraphycally simple. No major faults are believed to cut through the zone of interest. Moreover, the target zone consists of a predictable succession of thinly laminated beds dipping at a relatively constant angle of 4.5 degrees.

3.4 Layout of the Monitoring System

The treatment and monitor wells were both drilled parallel to one another with an 85.5 degree inclination, 300m (1000ft) apart, as shown in Figure 3.1. Microseismic events were registered in the monitor well via a receiver array consisting of eight multi-component seismic sensors, each separated by 30m (100ft). This array of seismic sensors was sequentially positioned along three different locations within the observation well during the job execution, in order to keep a reasonable separation distance between the monitoring tool and the stimulated zones. For the first nine fracturing stages the sensor array was positioned along two different sections of the horizontal portion of the monitor well, while the last four stages were monitored with the sensor array positioned in the vertical section.

Figure 3.1 illustrates schematically one of the positions of the sensor array, represented by green triangles, as well as the perforation clusters planned, each one color-coded relative to its associated fracturing stage. Different treatment designs and perforation clusters were also evaluated during this multistage hydraulic fracturing job, but their details are beyond the scope of this paper.

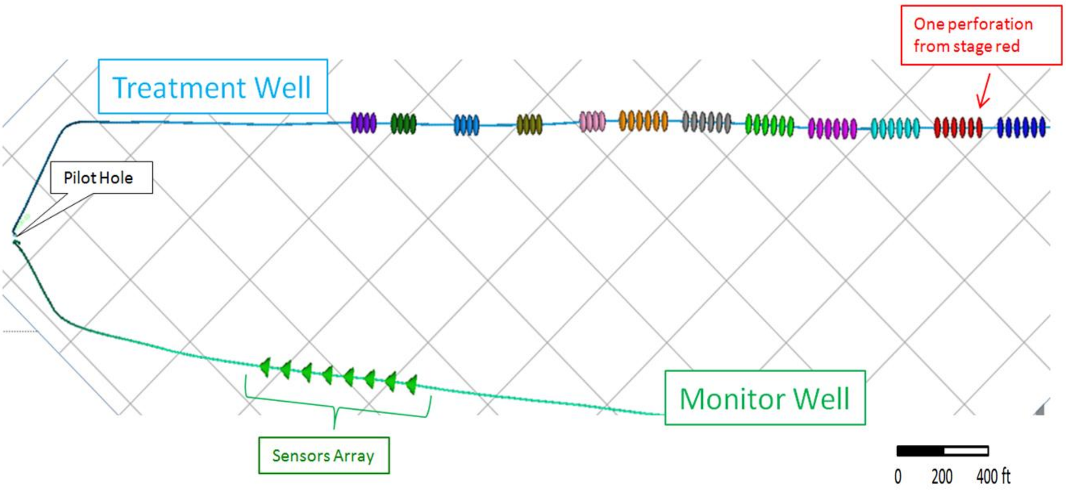

Figure 3.1. Schematic map view showing the relative location of treatment and monitor wells. Green triangles represent receivers on the monitor well while colored disks represent the planned perforations on the treatment well. Different disc groups are color-coded relative to their associated fracturing stage. Background grid spacing is 400 ft. (Only one of the three different locations of the receiver array is shown in this figure).

3.5 Velocity Model

Time signals (i.e. seismograms) registered in the monitor well are associated with a specific microseismic event in the subsurface via the use of an appropriate velocity model, which must be properly scaled in vertical and horizontal directions. The detection range of the sensor array determines the maximum length at which a signal can be registered, typically 600 to 1500m (2000-5000ft). Horizontal scaling of the velocity model is then achieved by means of an anisotropic analysis. There are a number of ways in which an anisotropy analysis can be performed. In this study I chose to manipulate Thomsen (1986) parameters to account for known differences between horizontal and vertical velocities. The vertical component of the velocity model, on the other hand, is impacted by the subsurface dip angle and therefore, it must be considered. Although in this case the dip angle of the formation is fairly constant, showing relatively small values within the target zone, it is taken into account in the velocity model. Thus, in this study, an anisotropy calibrated velocity model consisting of a constant dip layered velocity sequence, based on a 1D sonic log, is used. This may be called a 1.5D anisotropic model.

3.5.1 Velocity Model Building

The first step in the velocity model creation is smoothing and upscaling P-wave and S-wave sonic logs acquired in a vertical well (pilot hole). These sonic logs provide a good representation of the subsurface surrounding the zone of interest.

The pilot hole was drilled to support the design of directional plans and for geological control. The bottom section of this borehole was later plugged and abandoned. The treatment well was drilled from the same surface location as the pilot hole, as illustrated in Figure 3.1.

Since 15m (50ft) is a typical sonic log wavelength, a smoothing of 15 to 30m (50-100ft) is commonly used to work with a simplified data set. Original sonic logs (black), and a series of color-coded upscaled versions, generated by averaging across different length intervals, are shown in Figure 3.2. The selected 1D model (green), resulting from the use of an 80 ft smoothing window, is also shown in this figure.

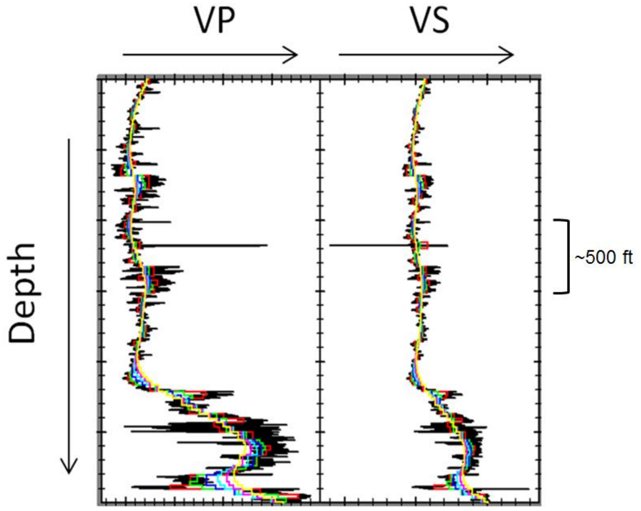

Figure 3.2. Schematic representation of smoothing and upscaling of sonic logs. Depth, Vp and Vs increase in the arrow direction. The selected 1D model resulting from the use of an 80 ft smoothing window is shown in green.

The horizontally layered model generated by using the selected upscaled sonic logs is shown in Figure 3.3. True well paths are overlaid in Figure 3.3a. For this particular study, 1500m (5000ft) laterals are drilled parallel to bedding along the zone of interest and both the zone of interest and the treatment lateral well dip 4.5 degree. This implies a velocity model depth error of at least 120m (400ft) from landing point to bottom hole location (almost twice the thickness of the zone of interest) if the model shown in Figure 3.3a is used. A tilted velocity model with a 4.5 degrees dip is required to keep the entire borehole in the correct layer as shown in Figure 3.3b.

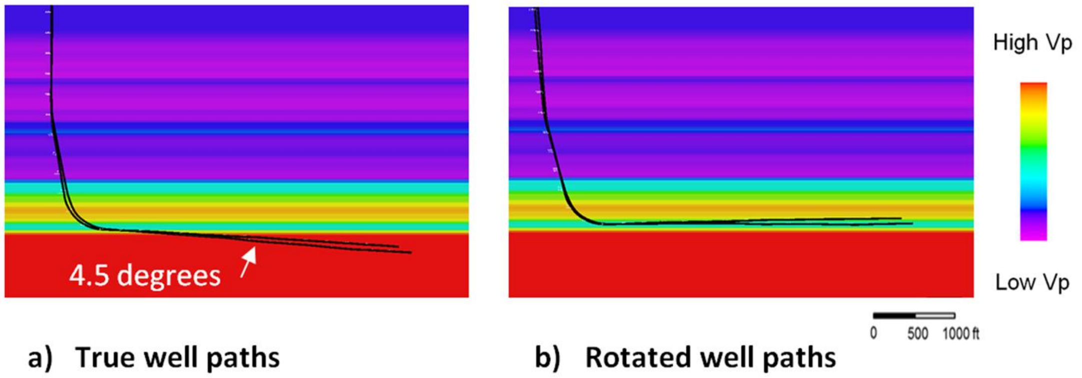

Figure 3.3. Schematic representation of the P-wave velocity model and coordinate rotations. a) True well paths. b) Well paths rotated by 4.5 degrees lay in correct relation to horizontal layers. Layers are thinner in the rotated model by cos (4.5) = 0.997. A Similar velocity model was built using S-wave velocities.

3.5.2 Anisotropy Corrections

Anisotropic calibration of the velocity model was accomplished by recording perforation shots from the treatment well. Modeled times were obtained by ray-tracing with a strong anisotropy vertical transverse isotropy ray tracer engine in one dimension. Mismatch between the observed arrival onsets and model times (residual times) is minimized by interactive adjustment of anisotropy parameters defined by Thomsen (1986). The P-wave moveout observed from the receiver arrays determines Thomsen-epsilon, while the SH-wave moveout and S-P time determines Thomsen-gamma. When SV-wave information is present, it constrains Thomsen-delta; otherwise it is left as zero. This is a good approximation in most hydrocarbon bearing shales. Figure 3.4a shows the mismatch of isotropic model times with the perforation shot waveforms. After adjustment for Thomsen epsilon and gamma, the arrivals are well matched by the selected anisotropic model, as observed in Figure 3.4b.

Anisotropic travel times for P-, SH- and SV-waves are calculated for all the grid points of a subsurface space to all receivers and stored in a lookup-table utilized to automatically locate the microseismic events in the subsurface.

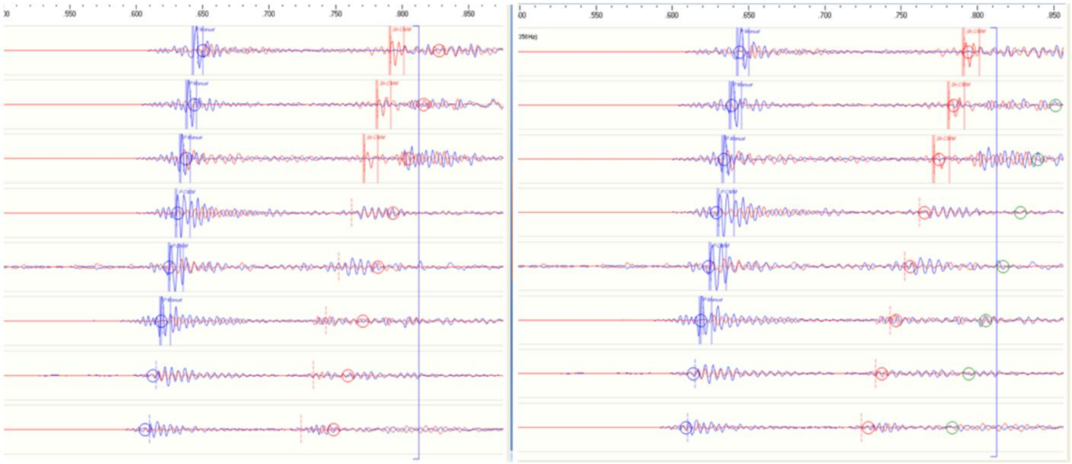

a) Isotropic model **b) Anisotropic model**

Figure 3.4. Anisotropy calibration from a perforation shot. The bottom shuttle P-wave model time is set to the picked time, so all other model times are relative. a) Isotropic model times for P-waves (blue circles) and SH-waves (red circles). P-wave moveout is too large and SH-wave time is too late. b) Anisotropic model times with Thomsen-epsilon 0.26 and Thomsen-gamma 0.21 provide a good fit to the arrivals.

3.6 Event Location

I determined event locations following the Coalescent Microseismic Mapping technique described by Woerpel et al. (2010). This automated picking methodology follows the conventional Geiger method, requiring many iterations of ray-tracing for each event to be located in real time. This means a simplified velocity model with only two or three layers must be used to reduce the calculation time. Implementing a look-up-table, however, becomes very practical in a way that all ray-tracing is done before the treatment starts, allowing for an anisotropic velocity model with more than 100 layers, without reduction in processing speed as the job is being executed.

Travel times are calculated by a 1D anisotropic ray-tracer, which assumes horizontal layers. Therefore, a mathematically equivalent method of rotating the coordinate system by 4.5 degrees is used, following the wells azimuth direction. All wellhead locations and deviation logs are first rotated to a flattened coordinate system (Figure 3.3b) before loading them into the ray-tracer. At the end of the location process, located hypocenters, the positions from where the microseism is believed to be originated, are rotated back to the true coordinate system.

3.7 Real-time Editing and Geiger Relocation

As each event is auto-located, its hypocenter is displayed in a 3D visualization software. From here, it is easy to retrieve waveforms associated with a given hypocenter with modeled times plotted for quality control as shown in Figure 3.4. Outlier events are then reviewed following this step. If modeled times do not fit the arrival onsets, the arrival times are then re-picked by hand, and the event may be relocated by a conventional Geiger least squares inversion method of arrival times. The waveforms associated with outlier events are then revised, and if the model times fit valid arrivals, the hypocenter location is retained. This process increases the level of confidence associated with each event location, resulting in higher quality processing of the data and all subsequent analyses.

3.8 Results and Discussion

The results from the microseismic monitoring job are presented in Figures 3.5 and 3.6. Figure 3.5, shows the hypocenters plotted relative to a cross-section view of the wells path. A horizontally layered velocity model with zero dip was used to generate this data set in real time, as the fracturing treatment was being executed. Figure 3.6, on the other hand, shows the results obtained a few weeks after the treatment was completed and the data reprocessed using an anisotropic velocity model with a 4.5 dip as previously explained in this work.

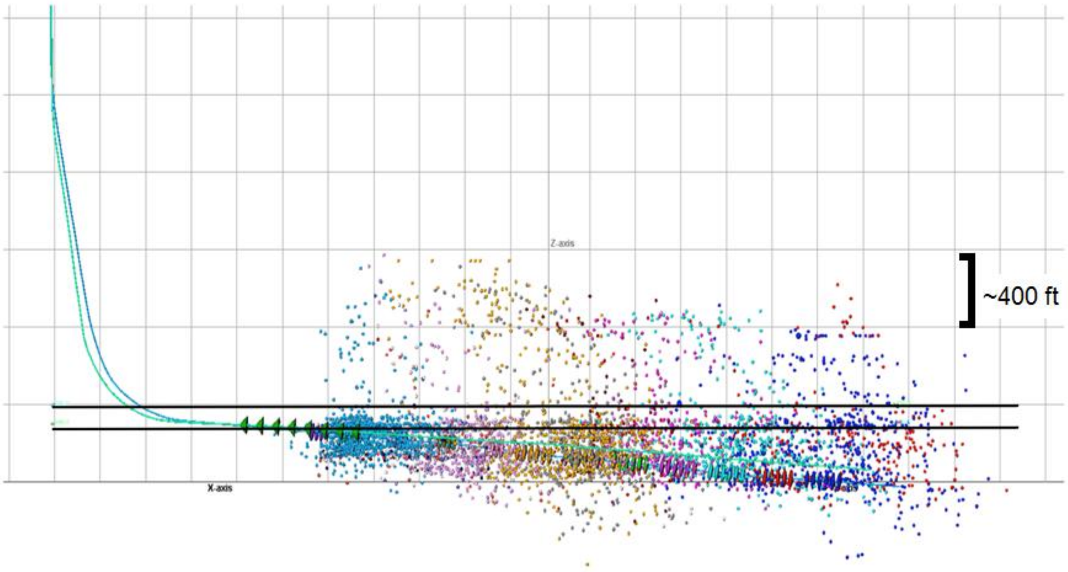

Figure 3.5. Schematic representation of the monitor and treatment well paths (blue and green lines), and the location of microseismic events (color dots) associated to each hydraulic fracturing stage obtained using a horizontally layered velocity model with zero dip. The top and bottom of the velocity model layer associated to the target zone is illustrated by black solid lines. Placement of the sensor array during one of the treatment stages is depicted by green triangles for reference purposes.

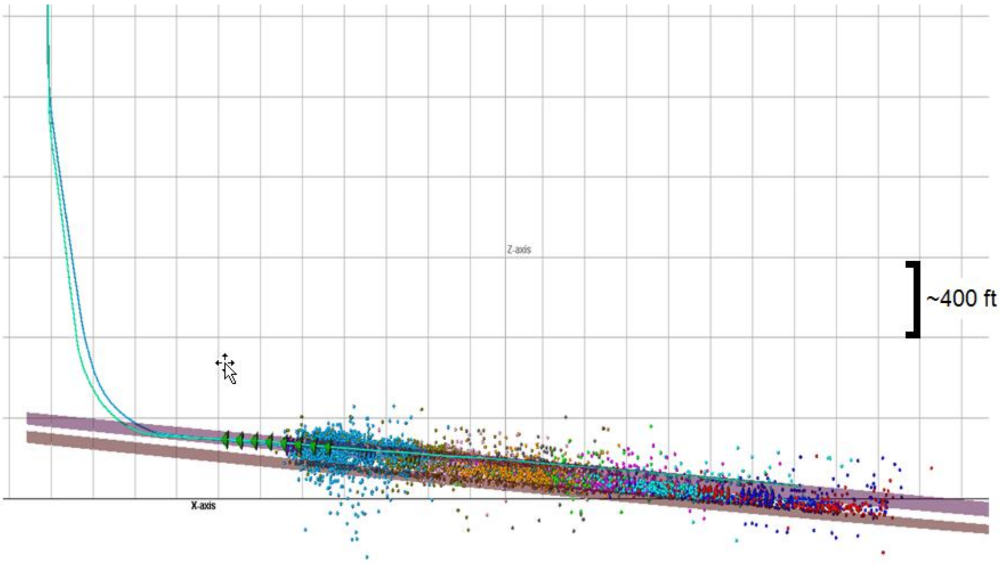

Figure 3.6. Schematic representation of the monitor and treatment well paths (blue and green lines), and the location of microseismic events (color dots) associated to each hydraulic fracturing stage obtained using an anisotropic velocity model with a 4.5 degree dip. The top and bottom of the velocity-model-layer associated to the target zone, showing good agreement with the well trajectory, is illustrated by purple and brown planes. Placement of the sensor array during one of the treatment stages is depicted by green triangles for reference purposes.

Direct comparison of Figures 3.5 and 3.6 shows that the location of microseismic events is significantly affected by the velocity model used, which then impacts the interpretation of the estimated stimulated volume (ESV). This is particularly evident in the spread of hypocenters along the vertical direction, with the majority of the events lying across the target horizon when a 4.5 dip is taken into account in the velocity model (Figure 3.6). In contrast, a much larger spread in the vertical location of microseismic events is observed in Figure 3.5, which can potentially lead to misleading conclusions regarding fracture containment.

In general, layered subsurface velocity models cause the microseismic events to preferentially align along the interface between velocity layers with significant velocity contrast. This is observed in Figure 3.7 (detailed view of Figure 3.5), where a sequence of horizontally aligned dots (hypocenters) line up along the layer boundaries due to this processing artifact. The presence of these well-aligned dots could potentially be misinterpreted as a consequence of the hydraulic treatment, instead of a layer within the velocity model.

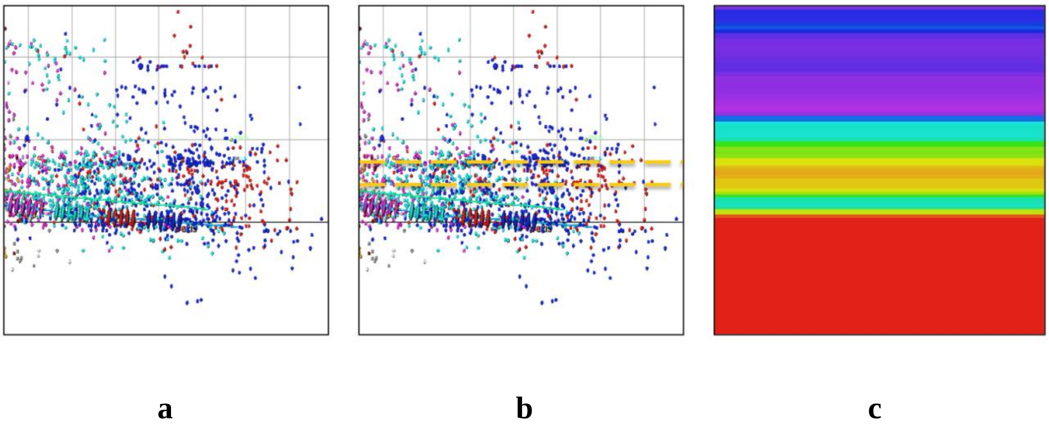

Figure 3.7. Example of location artifacts associated with the velocity model. a) Detailed view of Figure 3.5. b) Yellow dashed lines highlighting processing artifacts. c) Velocity model used to locate the events. Color scale same as Figure 3.3.

It is important to note that the artifacts originated by the implementation of an incorrect velocity model were observed throughout the job execution, independently of the placement of the sensor array within the wellbore. Nonetheless, as expected, the impact of the artifact was less noticeable when the sensor array is placed in the vertical section of the monitor well, due to its location relative to the source of hypocenters.

The workflow followed to generate the results shown in this paper required additional time to re-process the data gathered during the fracturing treatment. Nowadays, however, tilted velocity models can be implemented in real time, thus allowing for more accurate placement of microseismic events and better decisions regarding fracturing diagnostics and overall field development strategies.

3.9 Conclusions and Recommendations

This work showed how implementing a tilted velocity model, based on a simple coordinate rotation during processing steps, made significant changes to previously estimated microseismic event locations. When targeted hydrocarbon bearing beds have even a relatively small dipping angle, this observed subsurface characteristic should be accounted for during the event location process, particularly in the vicinity of significant velocity contrasts.

Given these results, it is my recommendation that the microseismic interpreter fully understands the assumptions made to locate microseismic events so that subsequent treatment analyses are supported by robust data.

3.10 Acknowledgments

The authors would like to thank the management of Hilcorp Energy Company and Schlumberger for giving permission to publish this paper. I would also like to recognize valuable contributions provided by Mike Craven during the acquisition and processing of the data presented in this publication.

CHAPTER 4: The Magnitude vs. Distance Plot, a tool for fault reactivation identification*

Cabarcas, C., and O. Davogustto.

*Adapted from extended abstract prepared in conjunction with oral presentation at AAPG Annual Convention and Exhibition, Pittsburg, Pennsylvania, May 19-22, 2013. Search and Discovery article #41185 (2013). Copyright 2013, American Association of Petroleum Geologist.

4.1 Abstract

On a multistage fracturing job monitored from a borehole for microseismic activity, high magnitude microseismic events are characteristic of reactivated faults. When plotted against their distance from the monitor-well and compared to events from other hydraulic stimulation stages, it becomes apparent that these microseismic events are associated with fault reactivation. Here, I present an example Magnitude vs. Distance Plot used to discriminate between fault reactivation (i.e. stimulation failure) and other successfully completed stages. Plot analysis and treatment records suggested reactivation of a fault during the hydraulic fracturing, but no other subsurface data supported this interpretation. As soon as a 3D reflection seismic volume was available, it was clear that microseismic events aligned with a fault plane interpreted on seismic profiles, corroborating the hypothesis of a preexisting fault reactivation. This work shows that in the absence of other subsurface data (or integrated with all the available

information), Magnitude vs. Distance Plots provide a useful tool to analyze stimulation results and support decisions regarding completion strategies in real time.

4.2 Introduction

Sheriff (1999) defines a fault as a displacement of rocks along a shear surface. Most of this movement releases energy that propagates as elastic waves (i.e. seismic information). Magnitude is a measure of this energy. The works of Shemeta and Anderson (2010), and Baig and Urbancic (2010) review in detail the magnitude concept within the context of the microseismic technology. Maxwell and Cipolla (2011) describe the fundamentals of fault mechanics as pertinent to microseismic exploration. For the purposes of this publication, I rely on the aforementioned publications simply stating that magnitude values of the recorded microseismic events are proportional to the size of the surface and the displacement involved in faulting. Therefore, assuming that surfaces and displacements associated with preexisting faults are bigger than those of hydraulically induced fractures, then, during hydraulic stimulation, registered higher magnitudes should characterize fault reactivation.

Borehole microseismic is a diagnostic tool used to monitor seismic activity generated during hydraulic fracturing. Magnitude is usually one of the parameters derived from borehole microseismic measurements. In practice, microseismic recording sensors only detect microseismic events occurring within a certain radius from them, usually no more than a few thousand feet. One way to quantify this phenomenon is with a Magnitude vs. Distance Plot (MDP). This plot shows the relationship between the energy associated with a particular event and its distance from the monitor well.

The MDP is a useful analysis tool in microseismic interpretation for all the information it summarizes on a simple graphic display, as demonstrated in the schematic diagram presented in Figure 4.1 (Zimmer, 2011). For instance, events with a combination of highest magnitude and greatest distance away from the monitor well define the maximum detection distance, which can be used to plan the maximum distance for monitor well placement in future jobs. The rest of the recorded events populate the middle upper left portion of the MDP graph, forming a quasi-triangular pattern. Notice that closer to the monitor well it is possible to detect relatively lower magnitudes and therefore more events than farther away from it. The curved base of this triangular shape also identifies the minimum detection limit due to ambient noise (Ambient or background noise refers to all other signals registered by the microseismic sensors, commonly not associated with the stimulation job). Finally, an upper boundary depicted by the constant high magnitude value associated with all the stages of a particular treatment-well also delimits the events set.

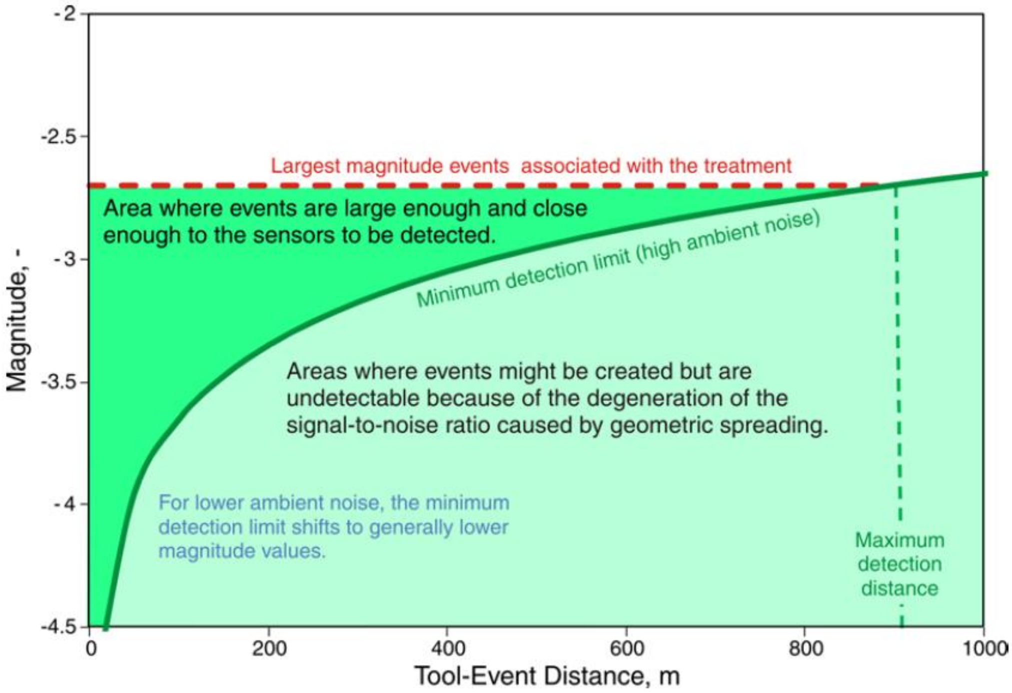

Figure 4.1. Schematic Magnitude vs. Distance Plot (Zimmer, 2011). During a hydraulic stimulation treatment monitored from a borehole for microseismic activity most detected microseismic events fall within the quasi-triangular area with concave downward base colored dark green. Copyright 2011, SPE. Reproduced with permission of SPE. Further reproduction prohibited without permission.

The presence of faults in the subsurface and their reactivation during hydraulic stimulation thus becomes noticeable on MDP’s, because magnitudes of events associated with fault reactivation are usually higher than the rest. Figure 4.2 shows a MDP example from a Barnett shale stimulation (Warpinski, 2009a). In this particular example, the typical maximum magnitude of microseismic events associated with the stimulation treatment is -2.5, and the group of events with significantly higher magnitudes (as high as -0.5) could be detected in response to fault reactivation.

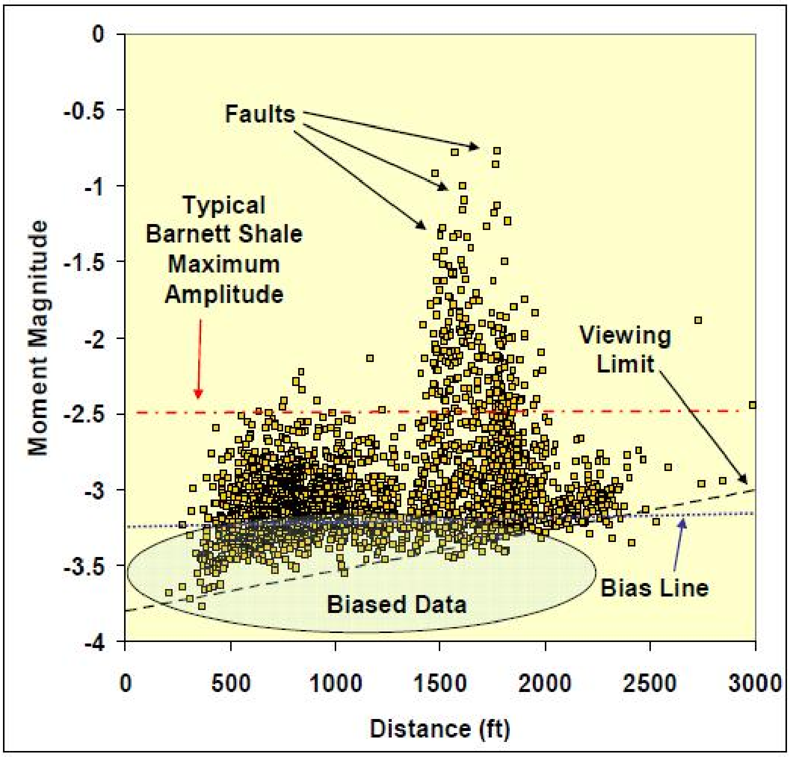

Figure 4.2. Magnitude vs. Distance Plot from a multistage horizontal hydraulic stimulation job in the Barnett shale (Warpinski, 2009a). As highlighted, high magnitude events are interpreted as the result of fault reactivation. Copyright 2009, SPE. Reproduced with permission of SPE. Further reproduction prohibited without permission.

Also highlighted in Figure 4.2 is the biased data. This area of the graph represents the low magnitude events identified only because of their proximity to the monitor well. For some interpretation purposes, it is common to discard these events during the analysis phase in order to compare events without the bias associated with the location of the sensors. In that sense, the MDP also results to be a very useful tool for filter parameters selection. However, I do not favor totally discarding these low magnitudes microseismic events, as in my opinion, they contain most of the information from the hydraulic fracturing stimulation. For example, Figure 4.3 shows differences between a data set of events and a filtered version of it based on a particular magnitude threshold. By eliminating these data points, it is difficult to convey a robust interpretation for parameters such as stimulated fracture azimuth based solely on filtered microseismic events. Indeed, it seems that this portion of the well has not been stimulated at all while production records prove otherwise.

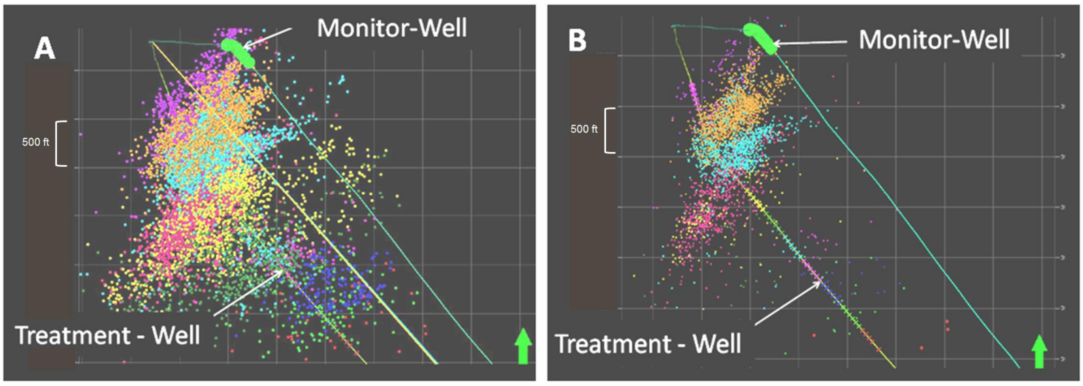

Figure 4.3. Map view of all events from a multistage hydraulic fracturing stimulation (A) and its associated filtered version based on an arbitrary magnitude value (B). (Internal Hilcorp's report) Each colored-dots set aggregates all microseismic events associated with an individual fracturing stage. By evaluating only the filtered version, it is very difficult to come up with a stimulation evaluation.

As an additional example illustrating the use of MDPs, Figure 4.4, from Warpinski et al. (2008), shows the MDP associated expression of fault reactivation for hydraulic fracture stimulation from multiple geographical regions.

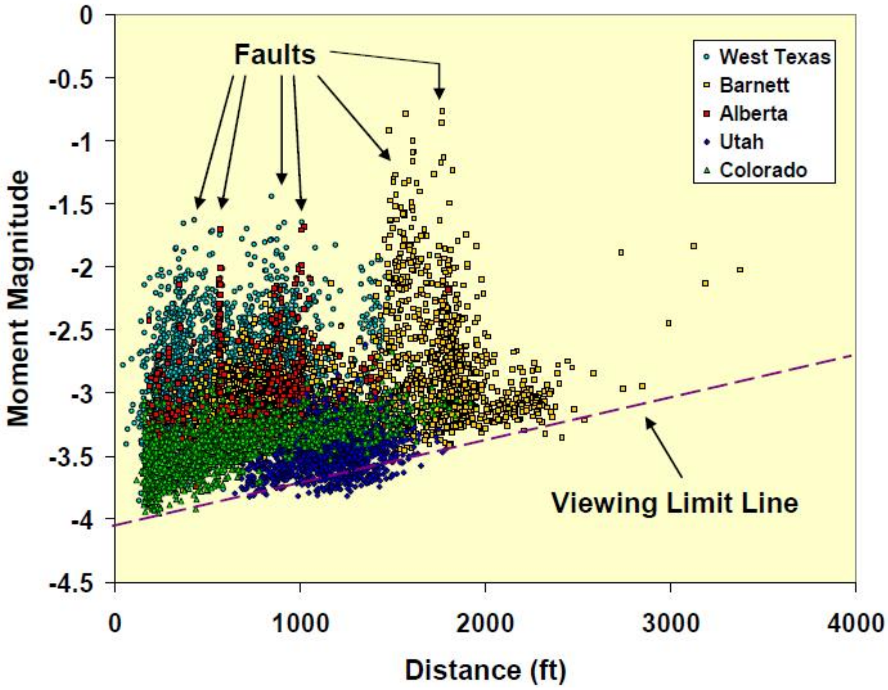

Figure 4.4. Magnitude vs. Distance Plot of microseismic events detected during a variety of treatments monitored at multiple geographical regions (Warpinski et al., 2008). Different multistage hydraulic fracturing stimulation treatments are each represented by a single color, based on the legend shown in the figure. Copyright 2008, SPE. Reproduced with permission of SPE. Further reproduction prohibited without permission.

A few other examples of Magnitude vs. Distance Plots suggesting the reactivation of faults are available in the literature (e.g., Wolhart et al., 2006; Downie et al., 2010 and; Maxwell and Cipolla, 2011). Nevertheless, to the best of my knowledge, no publication has presented multiple independent data in support of the fault reactivation interpretation. This work illustrates an integrated case study in which fault reactivation is interpreted based on independent data sets, including microseismic MDP, 3D reflection seismic sections, and pressure plots in order to build confidence in the use of MDP's as a robust interpretation tool.

4.3 Fault reactivation identification – an integrated case study

I used the Magnitude vs. Distance Plot evaluation technique described in the previous section to discern fault reactivation in a microseismic monitoring exercise performed real-time during hydraulic fracturing operations. The results are shown in Figure 4.5. In this figure, the higher magnitudes events associated with possible reactivated faults are highlighted by a dotted blue oval.

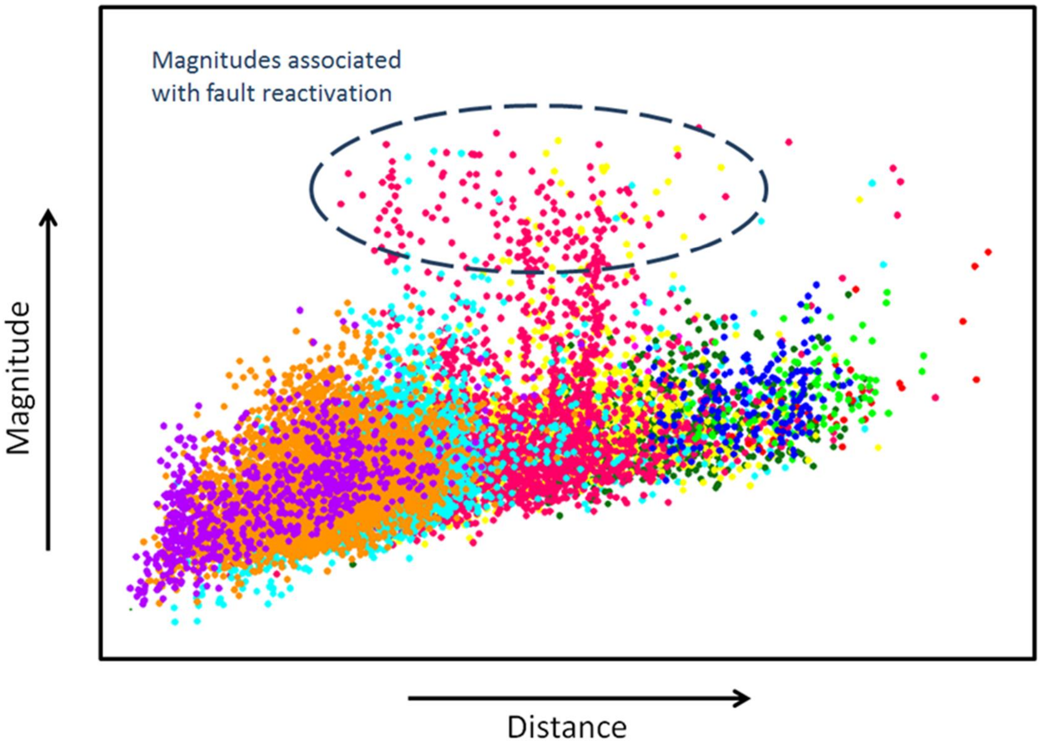

Figure 4.5. Magnitude vs. Distance Plot from a multi stage hydraulic stimulation job monitored from a borehole for microseismic activity. Different colors represent event sets from different stages. Most of the stages generate microseismic event that predictably populate the graph (i.e. lower magnitude events can be detected near to the monitor well while farther away from the monitor well only relatively higher magnitudes event can be detected). Stages yellow, cyan, and especially stage red, suggest fault reactivation due to their higher magnitude, as compared to magnitudes from other stages. Magnitude and distance increase respectively in the direction pointed by the arrows.

When implementing the hydraulic stimulation no surface seismic data was available and subsurface geologic maps, built solely on sparse wells information, did not foresee the possibility of a fault in the area. This encouraging geologic model also supported the drilling and stimulation of the treatment well.

More than a year after the stimulation of the well associated with Figure 4.5, newly available 3D reflection seismic data provided a better image of the subsurface near the well. Unfortunately, due to resolution limitations, the broadband frequency data from this 3D reflection seismic survey does not provide unequivocal evidence for the presence of a fault. However, coupling the 3D seismic data with the microseismic events interpreted as the response of fault reactivation it is possible to infer the presence of a fault in the seismic image. This is clearly illustrated in Figure 4.6 by showing sections with and without the microseismic events. The simple image of the microseismic events overlaid on the 3D seismic vertical section suggests the presence of an antithetic fault in the subsurface and its possible reactivation due to hydraulic fracture stimulation. The microseismic event set aligned very well in the direction of the interpreted fault plane.

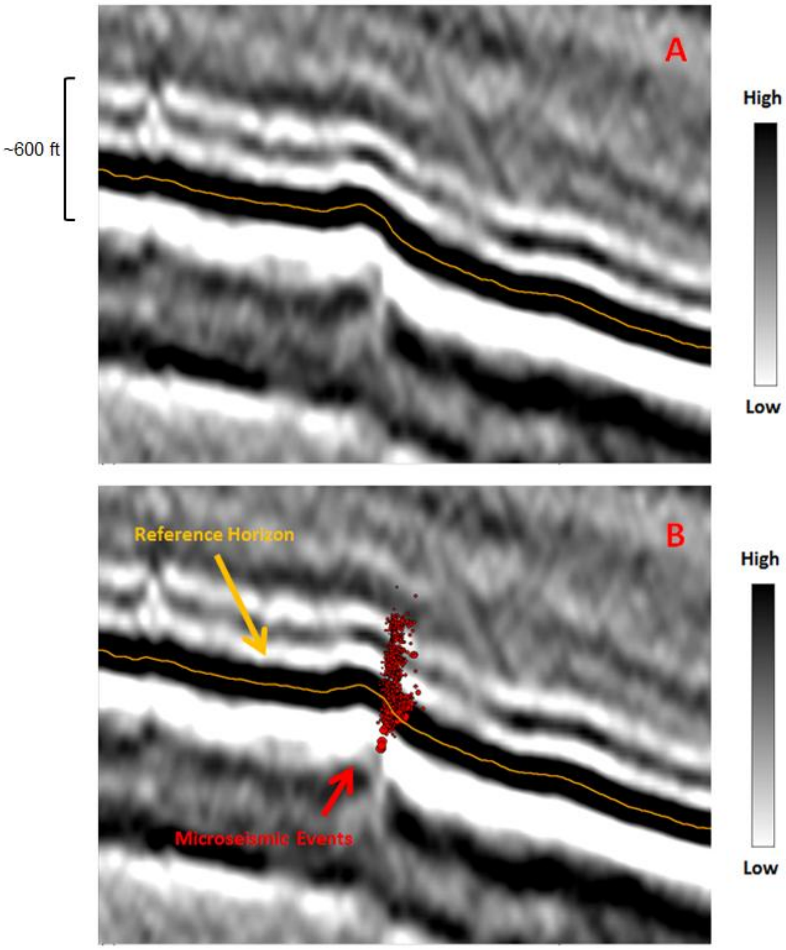

Figure 4.6. (A) Vertical seismic section parallel to the azimuth of a treatment well monitored for microseismic activity (courtesy of Seitel, Inc.) (B) Same seismic line overlaid by microseismic events from a stage interpreted as associated with a fault reactivation. Microseismic events align very well depicting the trace for an antithetic normal fault verging opposite to the inclination of the reflectors, and, beds.

Further analyses implementing the use of simple seismic attributes also enhance and support this interpretation. For example, after computing Similarity on the 3D seismic volume and extracting a surface slice from this volume at the zone of interest, it is possible to interpret the presence of a fault crossing the path of the treatment well. The good correlation between microseismic events lineation and the extrapolation of Similarity trends provides further evidence for the hypothesis of fault reactivation due to the hydraulic fracturing treatment. This is illustrated in the map view presented on Figure 4.7.

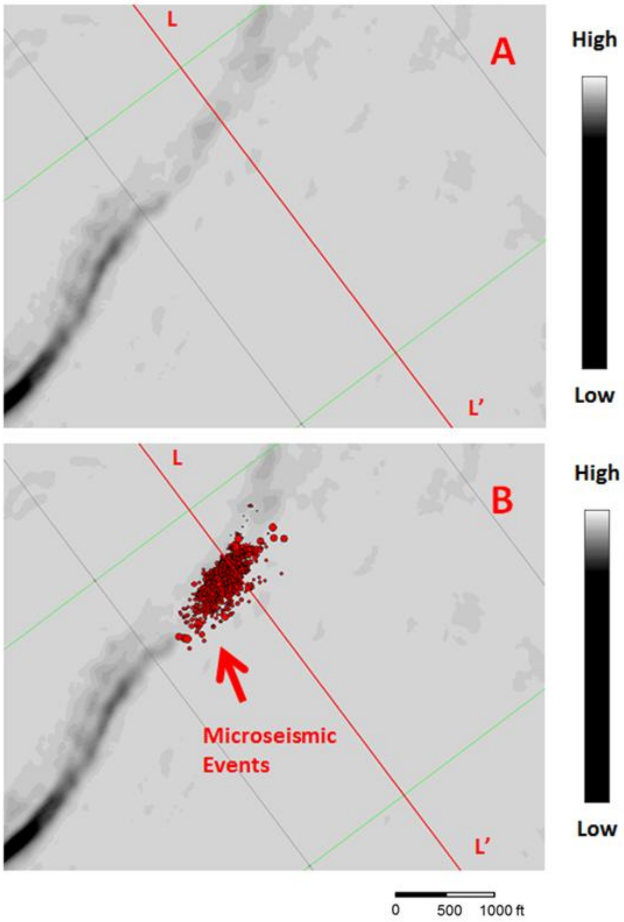

Figure 4.7. Similarity horizon slice extracted along the stimulated zone of interest monitored for microseismic activity. The original seismic data used as input into the similarity algorithm is the property of Seitel Inc. Highly similar data is colored in grey shades while areas with low similarity values are tinted black as shown in the figure label. Microseismic events from the hydraulic stimulation stage believed to have reactivated a fault are aligned very well with a Similarity anomaly that also represents a fault system trace. The treatment well is shown for reference purposes. The red line labeled L-L' represents the direction and length of the line shown in Figure 4.6.

As an additional support for the fault reactivation interpretation, Figure 4.8 displays the microseismic events associated with a later hydraulic fracturing stage. A zoom-in over the area presented in Figure 4.7 makes clear an azimuth change observed between a regular stimulation and a fault reactivation. This characteristic, solely based on microseismic event location, provides another tool to derive subsurface geological information not emphasized in previous publications. It is thus my claim that in the absence of additional supporting data (e.g. 3D seismic coverage) an azimuth change observed from microseismic sets coupled with anomalously high magnitudes for the same events, could create enough evidence for interpreting a fault reactivation. Moreover, when integrated with treatment pressure information, these microseismic observations could be used in the decision-making process of changing a predesigned treatment job and could significantly reduce completion costs.

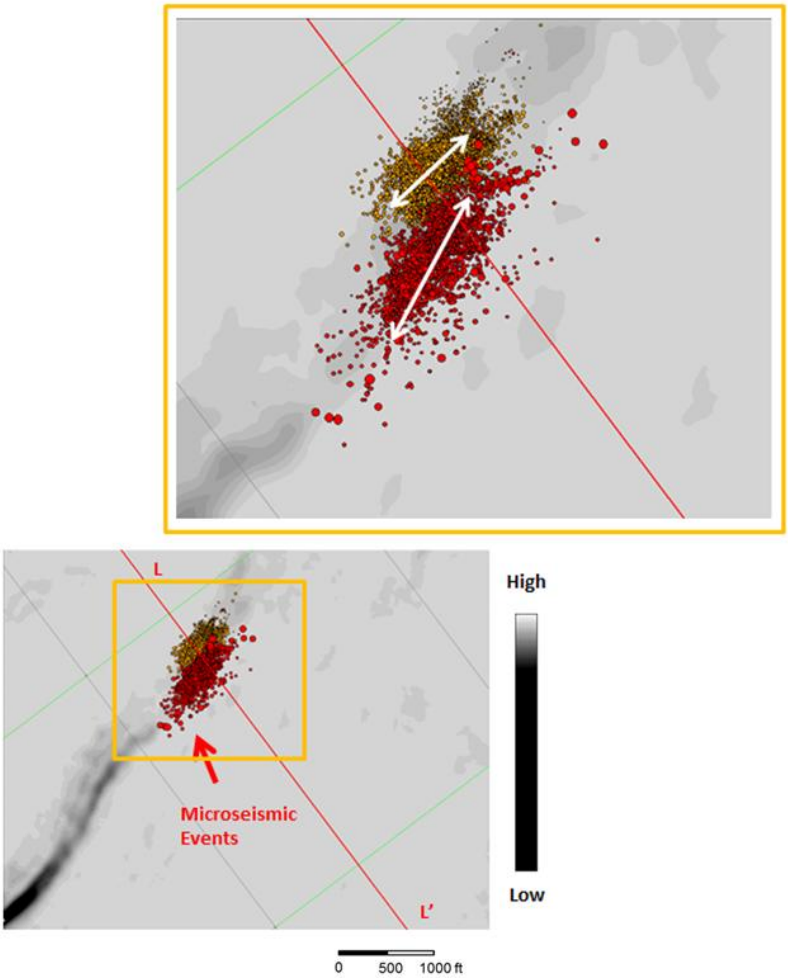

Figure 4.8. Close-up view of Figure 4.7 together with the addition of the microseismic events recorded during a subsequent hydraulic fracturing stage. White arrows highlight the associated azimuth interpreted from the microseismic events set associated with each stage.

4.4 Conclusions

The example presented in this publication serves to validate and support the use of microseismic- derived Magnitude vs. Distance Plots as a tool to identify fault reactivation in the absence of additional subsurface data. Moreover, as shown in this case study, when combined with other independent measurements (e.g. 2D or 3D reflection seismic sections) MDP's could unequivocally characterize the reactivation of a fault based on higher amplitudes and possible azimuth changes. This work also shows that 3D seismic is a powerful tool to mitigate drilling and completion risks as those encountered when faults are not anticipated along the well path. Availability of 3D seismic data beforehand could have improved well placement and possibly resulted in lower completion costs and better well performance.

4.5 Acknowledgement

I would like to thank the management of Hilcorp Energy Company for permission to publish this work, as well as its support on the application of new technologies. In addition, I would like to thank Seitel Inc. for permission to publish their seismic profiles and Dawn Henderson for her help editing this document.

CHAPTER 5: Sequence stratigraphic principles applied to the analysis of borehole microseismic data*

Cabarcas, C., and R. Slatt.

*Adapted from paper accepted for publication in *Interpretation*, manuscript ID INT-2013-0151R1. Copyright 2014, Society of Exploration Geophysicist and American Association of Petroleum Geologist.

5.1 Abstract

Based on a sequence stratigraphic framework developed using gamma ray stacking patterns, I identified brittle-ductile couplets, which allowed me to better interpret the microseismic response recorded during a single-stage hydraulic fracture stimulation treatment monitored from three strategically-located observation wells. I analyzed and compared hydraulic fracturing results inferred by individual processing of microseismic data acquired from horizontal and vertical sensor arrays, as well as the results from simultaneously processing the signals recorded by all three sensors. Ultimately, I decided in favor of the triple array simultaneous solution as the most useful data set to interpret the stimulation treatment due to the location of the microseismic events coupled with the theoretical expectation from my sequence stratigraphic framework. The final data set not only allowed me to better interpret the hydraulic fracturing results, but it also helped me improve recommendations in support of the field development campaign.

5.2 Introduction

This publication integrates concepts from hydraulic fracturing, earthquake seismology and sequence stratigraphy. Principles of hydraulic fracturing can be found in multiple monographs such as Economides and Nolte (2000), while the theory behind the use of earthquake seismology methods to monitor hydraulic fracturing-induced microseismicity from downhole boreholes is discussed in various publications, as in the works of House and Shemeta (2008), Warpinski (2009), and Maxwell, (2010). Nevertheless, because of the recent exponential growth of hydraulic fracturing and microseismic monitoring associated with the vast exploitation of resource plays, new and innovative applications of these tools are continuously evolving, making it necessary to be attentive of the latest literature.

Regarding the topic of sequence stratigraphy, the works of Payton (1977), Van Wagoner et al. (1990), Emery and Myers (1996), Posamentier and Allen (1999), and Catuneanu et al. (2011), among others, provide detailed information on the subject. For more than four decades, sequence stratigraphy has proven to be a key tool for the exploration and production geoscientist, providing the basis to predict and characterize spatial and temporal relationships between the different rock units of the petroleum system (i.e., source, seal and reservoir rocks).

Sequence stratigraphy refers to the study of genetically-related sedimentary packages within a chronostratigraphic context (Van Wagoner et al., 1990). Based on a sequence stratigraphic framework, subsurface data may be analyzed in a much more informative manner rather than simply following lithologic rock typing.

The depositional model implied by sequence stratigraphy is observed at multiple scales, from basin analysis to exploration plays and prospects, going beyond reservoir studies and interpretations at higher scales. In general, several orders of eustatic sea level cyclicity act simultaneously (Slatt, 2013), resulting in a complex interaction of stratigraphic patterns. The superposition of multiple orders of eustatic sea level cyclicity is a key characteristic revealed when analyzing log responses within a sequence stratigraphy framework. In particular, because high gamma ray (GR) API readings may be interpreted as associated with flooding surfaces (fs), the identification of these markers serve to recognize gamma ray parasequences (GRP) such as presented in the work of Singh (2008), and Abouelresh and Slatt (2012). For instance, Figure 5.1 presents three GRP identified by upward-decreasing, upward-increasing, and constant GR API units on log signatures, also supported by associated grain size and other characteristic geological changes observed in core samples from three different sections of the Barnett Shale.

Sequence stratigraphic analysis extends beyond log analysis and is applicable to data of multiple scales; from basin-long seismic profiles, to outcrop, to core (Van Wagoner et al., 1990). The use of sequence stratigraphic principles in the analysis of surface reflection seismic has proven to be an excellent exploration and development tool for the Oil and Gas industry. In the analysis of surface seismic reflection data, a key principle provided by sequence stratigraphy is that seismic reflections are time-significant stratal surfaces (Vail et al., 1977). Therefore, a surface seismic reflection data set interpretation based on a sequence stratigraphic framework carries a wealth of information and provides a unique perspective of the subsurface. In this context, the power of sequence stratigraphy, among other things, relies on using the seismic data to predict the presence of certain lithologies away from known control points.

Sequence stratigraphic principles also improve the analysis of information from core samples and its integration with thin sections, log analysis, hydrocarbon systems records, and basin history, leading to a more coherent geological interpretation. In exploration of conventional hydrocarbon accumulations, this integration is very useful, as it helps to recognize and predict the presence, among other elements, of well-sorted grains of relatively high particle size that are typically associated with high porosity and permeability reservoirs. Moreover, during the analysis of unconventional shale plays, where source, reservoir, and seal are essentially the same rock unit, sequence stratigraphy also has a key role. For example, based on sequence stratigraphic principles, Slatt and Rodriguez (2012) recognized several characteristics of currently productive organic-rich shale plays that serve as the basis to propose a predictive model where condensed sections represent the most prolific candidates for hydrocarbon resource rocks.

In the development stage of a resource play, a sequence stratigraphic framework also provides opportunities to better identify geomechanical characteristics of target zones. For instance, Slatt and Abousleiman (2011) merged concepts from sequence stratigraphy and geomechanics to recognize typical fabric characteristics, which supports the hypothesis that laminae/bedding contacts represent planes of weakness for hydraulic fracturing; the lack of significant authigenic cement along bed/lamination contacts weakens the rock at those contacts, and geomechanical properties are highly dependent on bedding direction (perpendicular vs. parallel), as well as the presence of layers with fractures perpendicular to the bedding intermixed with non-fractured layers. Additionally, the authors recognized layers of similar geomechanical characteristics that represent brittle-ductile couplets at the parasequence and sequence scale. Brittle–ductile couplets correlate well with distinctive hydraulic fracture propagation lengths. As shown in Figure 5.2, longer lengths are associated with thicker and perhaps more brittle sections as compared to ductile sections and fracture length also diminishes for higher order couplets.

To build the brittle-ductile couplets model illustrated in Figure 5.2, Slatt and Abousleiman (2011) relied on lithofacies stacking patterns to identify cyclic units associated with eustatic changes in sea level as presented in Figure 5.3. This methodology, validated via core and outcrop observations, provides a practical workflow that combines principles of sequence stratigraphy and geomechanics to properly map and develop the most prospective sections of a resource play. The robustness of this technique allows its extrapolation to other resource plays even in the absence of whole core data.

This present publication builds upon prior knowledge, extending and emphasizing the use of sequence stratigraphic principles to provide an appropriate framework to analyze borehole microseismic data recorded during hydraulic fracturing operations. In a similar manner as sequence stratigraphy is used to interpret stratigraphic architecture, and the likelihood of finding hydrocarbon–bearing rock units, it is also possible to use the same principles to predict the sedimentary column response to hydraulic fracturing stimulation and their associated microseismic records.

5.3 Monitoring equipment layout and hydraulic fracturing operations

The results presented in this publication deal with microseismic data acquired to assess the near wellbore stress distribution of a zone of interest in support of a subsequent development campaign. Monitoring a single-stage hydraulic fracturing treatment on a vertical well was a key element of this project. The monitoring equipment layout is illustrated schematically in Figure 5.4. To ensure high quality measurements, three sensor arrays were strategically placed in three observation wells, spaced approximately 120 degrees around a vertical borehole, which was subjected to a fracture stimulation treatment. The average distance between the stimulated well and the center of the arrays in the observation wells was circa 180 m (600ft). The observation wells included two horizontal wells and a vertical monitor well explicitly drilled for the microseismic experiment and the acquisition of multiple modalities of vertical seismic profiles (VSP); the latter experiment, however, is beyond the scope of this publication.

An 8-level multicomponent receiver array measuring 210m (700ft), which was located inside the vertical observation well, was partially straddled on the zone perforated in the treatment well – i.e., two multicomponent sensors positioned across the zone of interest. Two 12-level multicomponent sensor arrays were also strategically positioned horizontally inside the two horizontal observation wells, covering a longitudinal distance of 170m (550ft). The separation between sensors was 15m (50ft) for the horizontal arrays and 30m (100ft) for the vertical array. The sensors were geophones with a 3Hz to 1600Hz dynamic response.

Since the perforation job preceded a diagnostic fracture injection test (DFIT) performed weeks in advance of the monitored hydraulic stimulation, a string shot was used to properly calibrate the microseismic experiment (i.e. sensors rotations and velocity model optimization). In particular, an initial velocity model constructed by blocking acoustic logs registered at the vertical treatment well, using sequence stratigraphic relevant surfaces as the boundaries of interval velocity blocks, was optimized based on best fitting string shot locations. Moreover, the final velocity model also included time-distance relationships computed from properly recording the string shot firing time. This additional information provided more confidence in the velocity model and the estimated position of microseismic events. However, the validity of this velocity structure decreases as the distance between the microseismic event location and the perforated interval increases. Additionally, a very detailed quality control workflow was implemented during the acquisition and processing of the data, following the recommendations presented by Cabarcas (2013).

At an average rate of 24 bpm, the treatment introduced in the subsurface 909 bbl of slickwater, 765 bbl of YF-120ST crosslinked gel, and 302 bbl of WF-120ST linear gel, with 6280 lb of 100-mesh white sand and 110,840 lb of 40/70-mesh premium white sand. Note: The fracture treatment was preceded by a 25 bbl (15% HCl) acid treatment and, during sweeps and flushes, linear gel followed the 5 ppg 40/70-mesh sand concentrations. Treatment parameters and monitoring data are presented in Table 4 and Figure 5.5, respectively. Notice the temporary drop in pressure following pump failure at approximately 1 hour after the start of the job. Pumpability was good overall, except for this incident, which was quickly resolved with minor impact to the operations.

Table 4. Treatment design parameters

Rate (bpm)	24
Pressure (psi)	5,921
Slickwater (bbl)	909
YF-120ST Crosslinked Gel (bbl)	765
WF-120 Linear Gel (bbl)	302
15% HCl Acid (bbl)	25
100 - Mesh White sand (lb)	6,280
40/70 - Mesh Premium White Sand (lb)	110,840
Total Proppant (lb)	117,120

5.4 Data quality and initial results

Moderate moment magnitudes (Mw) computed from the seismic signals averaged -3.5 and -3.3 Newton meters (Nm) for the horizontal arrays and -3.2 Nm for the vertical array. The farthest imaged event locations included an event 270m (880ft) away from the horizontal arrays, and an event 375m (1,230ft) from the vertical array. To estimate these and all microseismic event locations, P-wave and S-wave arrival times selected automatically, together with the optimized velocity model, served as input to a location algorithm based on the principles proposed by Nelson and Vidale (1990), where a grid search over a pre-computed space of possible locations provides quick estimates to event positioning. Nevertheless, an analyst reviews each selection and manually adjusts automatic choices when necessary, for instance in the presence of dubious picks associated with traces having low signal-to-noise ratio (S/N).

Moreover, additional adjustments of the velocity structure also occur during the location process, such as a best fitting based on location residual minimizations according to predetermined velocity and location thresholds.

Microseismic events uncertainties for the events located from the horizontal array averaged +/- 20m (70ft) in the Z direction (i.e. elevation or depth), +/- 10m (32ft) in the azimuthal position and +/- 13m (43ft) in the radial direction (the shortest distance between the tool and the event, also simply referred as distance). For the events located from the vertical sensor array the uncertainties averaged +/- 9m (28ft) in elevation, +/- 13m (43ft) in azimuthal position and +/-12m (41ft) in distance. It is important to note that these error estimations are theoretical computation based on the assumption of good quality data and a valid velocity model. The error calculations refer to the results from a Monte Carlo simulation and not to direct uncertainty measurements associated, for example, with instrument errors or the actual microseismic source location, which remains unknown for all signals except the string shot. Therefore, the location measurements error can be higher than the values reported. Nevertheless, the overall data quality for this project is high due to the high S/N observed on waveforms and the use of receivers forming a triple array configuration. Additionally, low anisotropy values computed independently by VSP inversion and microseismic data analysis make little to no difference to the microseismic event locations when incorporated in event positioning (i.e., by the use of anisotropic velocity models), providing more confidence in the final results.

Figure 5.6 presents initial microseismic results on a vertical view of the subsurface. The GR from the vertical section is included for reference. GR counts and specific depth values were intentionally omitted to protect the confidentiality of the data, but a 24m (80ft) mark is included as a vertical scale and to highlight the perforated interval on the GR curve. API units increase from left to right, while depth increases from top to bottom in the directions pointed by the arrows. The treatment well and a horizontal scale are also included for reference. The figure displays microseismic event locations obtained from individual processing of signals recorded by a vertical (Figure 5.6a) and a horizontal (Figure 5.6b) sensor array. Note: the response from the horizontal arrays used in this study are very similar, therefore, only one of them is shown in Figure 5.6b. Microseismic events are shown as pink circles sized by magnitude; with larger magnitude events depicted as larger circles.

On a first look interpretation, the lack of microseismic activity below the perforated interval in Figures 5.6a and 5.6b suggests that the underlying formation serves as a good seal, which is expected, for this is mainly composed of a high-strength limestone, but it is difficult to support any other meaningful conclusion from the data at hand. Fundamentally different stimulated volume estimates can be inferred from the results shown in Figure 5.6. Microseismic events recorded from the vertical sensor array (Figure 5.6a) suggest that not only the perforated zone was stimulated, but also an asymmetric fracture zone, approximately 410m (1350ft) long, was created 150m (500ft) above the perforated interval. It is important to note that very few events were registered by the vertical array in the zone between the perforated interval and the large cloud of events above it. In comparison, Figure 5.6b shows a single cloud of events, approximately 210m (700ft) long and 90m (300ft) high, registered by the horizontal array. These contrasting results illustrate how challenging the interpretation of a borehole microseismic job can be.

5.5 Data analysis and interpretation

Many interpretations could explain the ambiguity of the preliminary results presented in Figure 5.6. For example, the results presented in Figure 5.6 could simply be the expression of artifacts associated with acquisition and processing steps. The vertical array solution may suffer from high velocity layers “trapping” the rays that approximate signal propagation and support event location estimations. Similarly, the horizontal array solution, commonly known to have elevation estimation deficiencies, relies on take-off or arrival angles assumptions that impose significant constraints in results obtained from this geometry, possibly increasing the gap between horizontal and vertical array solutions. Additionally, notice that the difference in the position of the events located using the horizontal array compared to the events located using the vertical array is greater than the sum of the reported vertical uncertainties, which corroborates my concerns regarding current uncertainties reporting practices as discussed in the previous section and also reviewed by Cabarcas (2013). However, I minimized these constraints through detailed quality control during all phases of the acquisition and processing of this project and assumed that the main reason for the observed discrepancies relies in the sensor arrays not always identifying the same events (i.e. not all the microseismic events located by the vertical array are included in the horizontal array solution and vice versa).

Ultimately, recognizing acquisition and processing limitations, I recommend to first estimate the microseismic event locations via simultaneous processing of the microseismic signals gathered from all observation wells and then to rely on an appropriate sequence stratigraphic framework to interpret the results.

During the acquisition and analysis stages of a microseismic monitoring job, a multiple array configuration is preferred because it minimizes the bias and constraints associated with a single observation well (Warpinski et al., 2005; Johnston and Shrallow, 2011; Seibel et al., 2011; Lim et al., 2012; and, Murer et al., 2012). Furthermore, as pointed out by Maxwell and Le Calvez (2010), significantly different results are expected from the use of vertical and horizontal sensor arrays, and not a single configuration is completely better than another. In this work, both vertical and horizontal layouts were used simultaneously in data processing, which compensates for those differences. Figure 5.7 shows waveforms associated with a microseismic event recorded simultaneously by the three sensor arrays. Note that events clearly registered simultaneously by the three sensor arrays represent a smaller sample from the total number of recorded events, creating a more representative event set from the monitoring job. Additionally, processing a three dimensional network of sensors all together enriches data output, as this allows the estimation of other microseismic source characteristics based on seismic moment tensor inversion (Baig and Urbancic, 2010, and Warpinski and Du, 2010). A discussion of such analysis is beyond the scope of this paper.

Once the triple array solution is obtained, it is necessary to analyze GR stacking patterns and build a model of brittle-ductile couplets for the stratigraphic column of interest, as shown in Figure 5.8, to apply my proposed workflow. I selected the stacking patterns boundaries presented in Figure 5.8 based on high GR readings interpreted as fs (flooding surfaces) and their associated SB (sequence boundaries) at two different scales. It is important to note that the maximum flooding surface (mfs), interpreted from the highest GR reading, constitutes the boundary between the brittle and ductile sections at a first order interpretation and that I interpret the sharp GR readings contrast, inside the first order ductile section, as an erosive base representing a combined sequence boundary/transgressive surface of erosion (SB/TSE). This gamma-ray vertical stratigraphy is common to many unconventional resource shales (Slatt and Rodriguez, 2012; Slatt, in press).

Solid upward-pointing arrows depict the first order of analysis in Figure 5.8, while dashed upward-pointing arrows illustrate a higher order of detail, resulting in my GRP interpretation. The green rectangles and red ovals in Figure 8 depict schematically brittle-ductile couplets. In this regard, I emphasize that the selection of fs and SB based on gamma ray log observations is a non-unique solution, i.e. other interpretations may be possible in the absence of additional and independent support information (e.g. whole core, biostratigraphic data, etc.). Moreover, notice how the number of fs and SB increases for higher order analyses, and while the mfs selection is fairly simple, the designation of fs and SB for second and higher orders becomes more subtle. For that reason, to supplement our interpretation, I included a lithostratigraphic column built from mud-logging records, and an acoustic impedance log (i.e., the product of velocity and density logs) in Figure 8. They represent an example of independent information that also could help the interpreter to discern small differences in ductile vs. brittle behavior of the subsurface.

It is important to note that in this work the term brittle is not rigorously defined, it rather applies to rocks easily damaged as compared to ductile rocks. I refer the reader to the work by Handin and Hager (1957), Hetenyi (1966) and Perez (2013), among other publications presenting full-length discussions regarding the brittleness term. Moreover, I recognize that other properties such as the strength of the formation or the stress regime acting upon it, which are not discussed in my model, do have a significant impact on the formation's response to hydraulic fracturing treatment. Therefore, I recommend combining geological and geomechanical principles for a more quantitative interpretation of hydraulic fracturing stimulation results.

Figure 5.9 presents the results obtained when microseismic signals recorded using a triple array configuration were simultaneously processed to estimate the subsurface location of their source. I interpret these results in the context of the sequence stratigraphic framework presented in Figure 5.8, expecting (within the same order) longer fracture lengths for brittle sections as compared to ductile sections. I observed more microseismic activity in the first order brittle layer, which could be associated with induced hydraulic fractures of longer lengths in accordance with my sequence stratigraphic model, also included in Figure 5.9 for reference. This observation holds true at a second order interpretation scale; notice how most of the events encircled by the big ellipse line up with brittle regions (green rectangles in first and second order interpretations), while ductile sections, which may act as seals and/or hydrocarbon source (storage) rocks, show minimal microseismic activity (i.e. the region between ellipses, which lines up almost perfectly with red ovals depicting ductile sections of the stratigraphic column). It is important to note that the microseismic activity associated with the out-of-zone fracture growth does not necessary imply that this upward zone is propped or even hydraulically connected.

The small ellipse in Figure 5.9 encircles microseismic events located in the target zone around the perforated interval. This event cloud is approximately 50m (160ft) high and 90m (300ft) long and it corresponds to the most likely stimulated area, according to my interpretation. Moreover, these microseismic events fall within a ductile region (red oval) on a first order interpretation, which explains its small dimensions compared to the events cloud above it. Nonetheless, when analyzed at a higher level of detail, the small events cloud (small ellipse) occurs at the boundary of a brittle-ductile transition, which maximizes the probability of achieving an effective stimulation treatment, despite its location within a first order ductile region. It is my recommendation to align the perforations as much as possible with relatively more brittle sections of the stratigraphic column, as it was the case in this particular example.

In summary, the results from the triple array configuration in Figure 5.8 not only resemble the results in Figure 5.6a (vertical array), but also honor the expected behavior from the brittle-ductile couplets model presented in Figure 5.8, allowing us to confidently discard, the conflicting response from the horizontal array in Figure 5.6b, which also showed the largest measurement error as discussed in the experimental section.

Ultimately, this stratigraphic approach to microseismic data interpretation provided a higher level of confidence in the evaluation of the hydraulic fracturing treatment. Moreover, based on these observations, I conclude that the use of less viscous fracturing fluids and lower proppant concentrations could aid fracture containment for this particular stress regime. These results underscore, once again, the value of microseismic information to explain stimulation results and to provide the necessary data to support changes to the original fracturing design proposed for the development campaign.

5.6 Conclusions

For the first time, I demonstrate that in the presence of a sequence stratigraphic framework provided by gamma ray stacking patterns in conjunction with lithologic information, it is possible to identify brittle-ductile couplets to aid in the interpretation of the microseismic response from a single stage hydraulic fracturing treatment. Moreover, the simultaneous processing of microseismic data from a triple sensor array configuration coupled with a sequence stratigraphic based interpretation provided a high degree of confidence in the inferred results of the stimulation treatment and the decisions made upon it.

5.7 Acknowledgement

I would like to thank the management of Hilcorp Energy Company for permission to publish this work, as well as its support of the application of new technologies. Special thanks go to Sean Machovoe for processing all of the data presented in this work, Dawn Henderson for proofreading this manuscript, and the reviewers and editors of *Interpretation* who provided excellent feedback on the content of this manuscript.

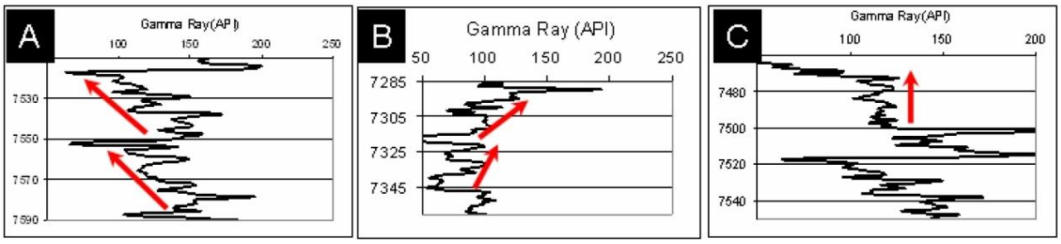

Figure 5.1. Barnett Shale example of A) upward-decreasing, B) upward-increasing, and C) constant GR API counts. These observations are fundamental to delimit parasequences from gamma-ray log patterns (after Singh, 2008).

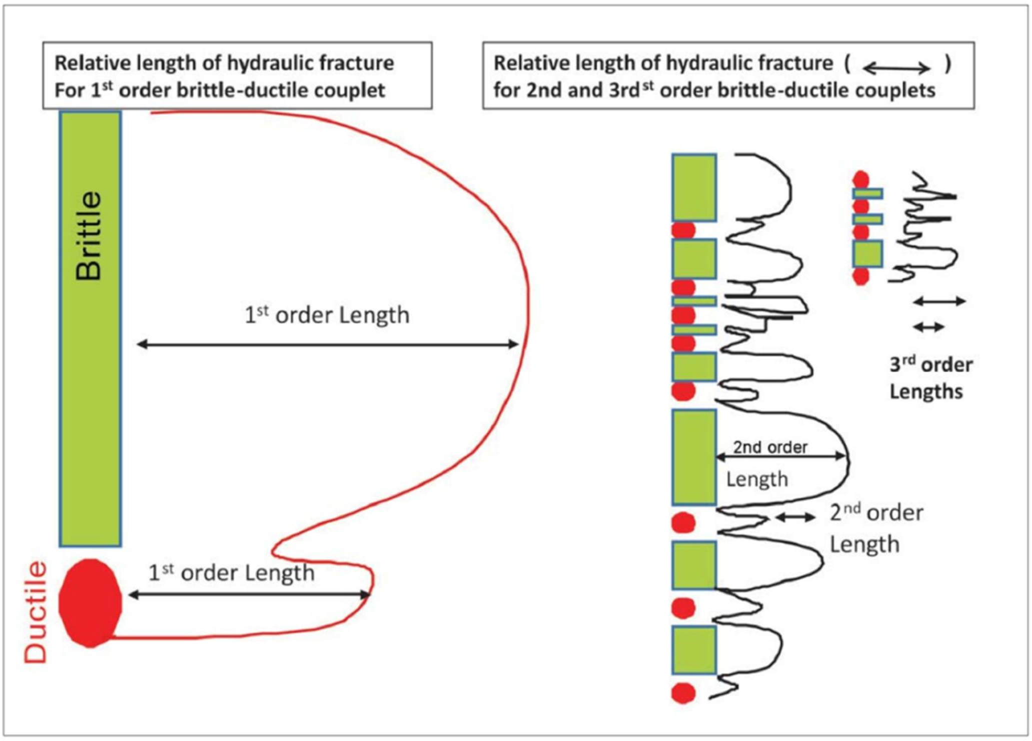

Figure 5.2. Schematic hydraulic fractures lengths variations within multiple scales of brittle-ductile couplets (after Slatt and Abousleiman, 2011).

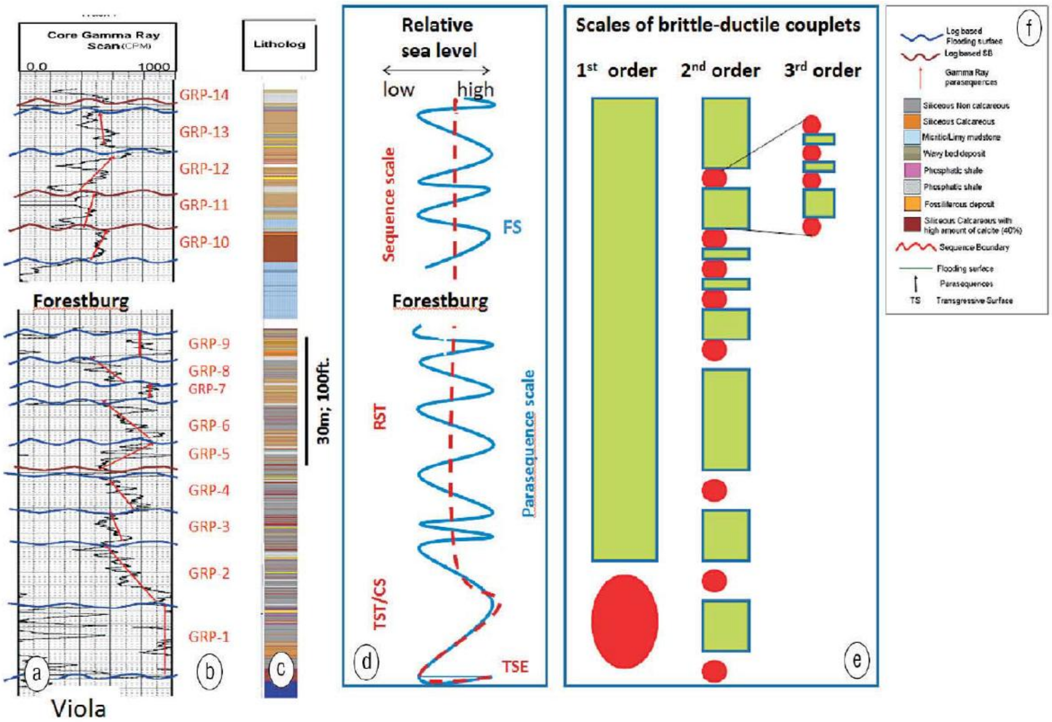

Figure 5.3. (a) Barnett Shale gamma-ray log showing parasequence boundaries (wavy blue lines) and parasequence patterns (red arrows). (b) 14 gamma-ray parasequences (GRP) for the well. (c) Core facies description and (f) explanation. (d) Relative sea-level curve for the complete Barnett Shale sequence (brown dashed line) and the 14 parasequences listed alongside the gamma-ray log (solid blue curve). (e) Three scales of ductile-brittle couplets. Sequence, parasequence and bedset refer to first, second and third order respectively. FS: flooding surface; RST: regressive system tract; and, TST/CS: transgressive system track / condensed section (after Singh, 2008, and Slatt and Abousleiman, 2011).

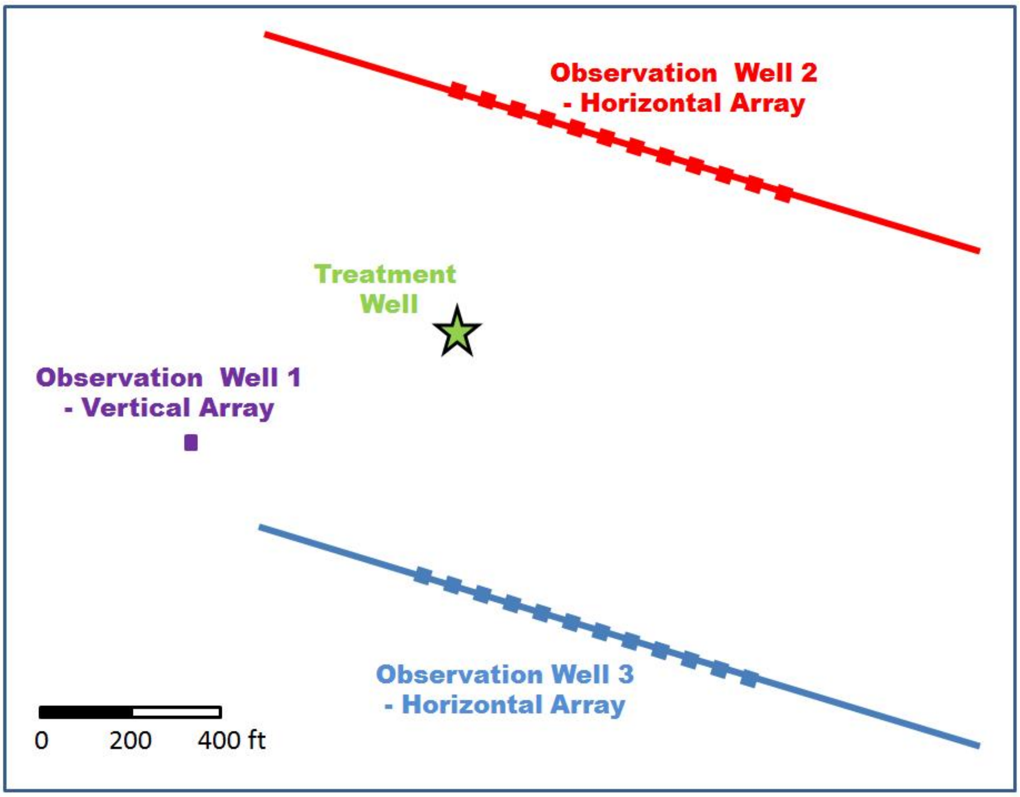

Figure 5.4. Map view of borehole layouts and sensor locations associated with a single stage hydraulic fracturing treatment on a vertical well (green star). The stimulation was monitored by three arrays, two horizontal arrays of twelve multicomponent sensors each, and a vertical array of eight multicomponent sensors shown as red, blue, and purple squares respectively.

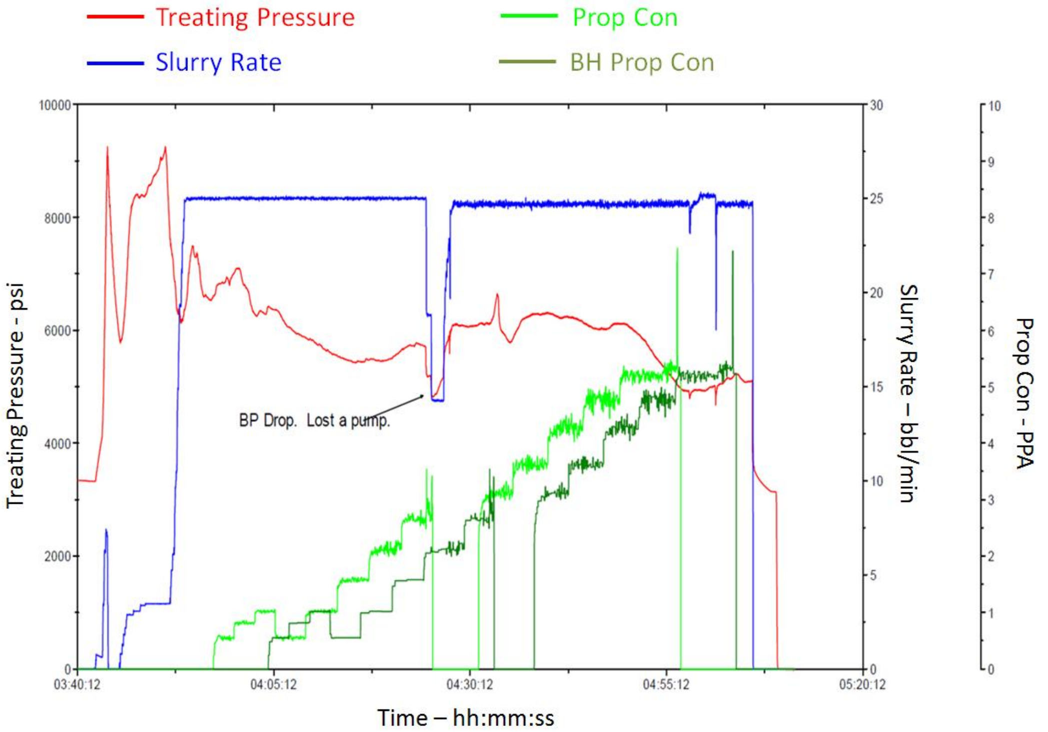

Figure 5.5. Treatment summary plot describing how treating pressure, slurry rate, proppant and bottom hole proppant concentrations changed during the stimulation treatment (time increases to the right on the horizontal axis).

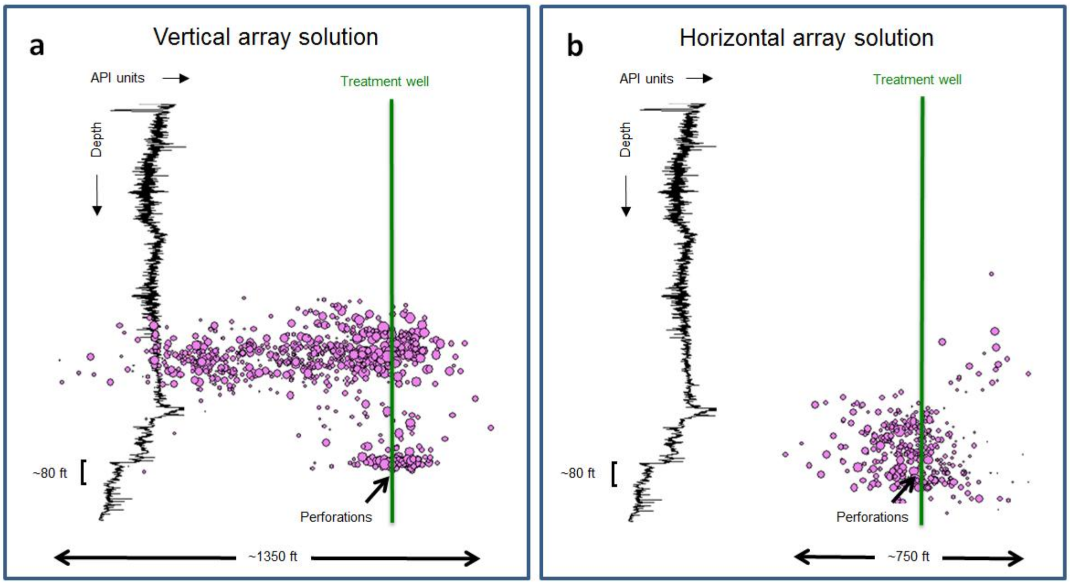

Figure 5.6. Vertical section representation of the subsurface illustrating the relative position of microseismic events (pink circles sized by magnitude) associated with a single stage hydraulic fracturing treatment. Locations were estimated independently from microseismic signals recorded from a) a vertical and b) a horizontal array. GR profile (in API units) is also included for reference. Note: GR counts and depth were intentionally omitted to protect the confidentiality of the data. API counts increase from left to right, while depth increases from top to bottom. The perforated interval and the target zone, approximately 24m (80ft), are also depicted.

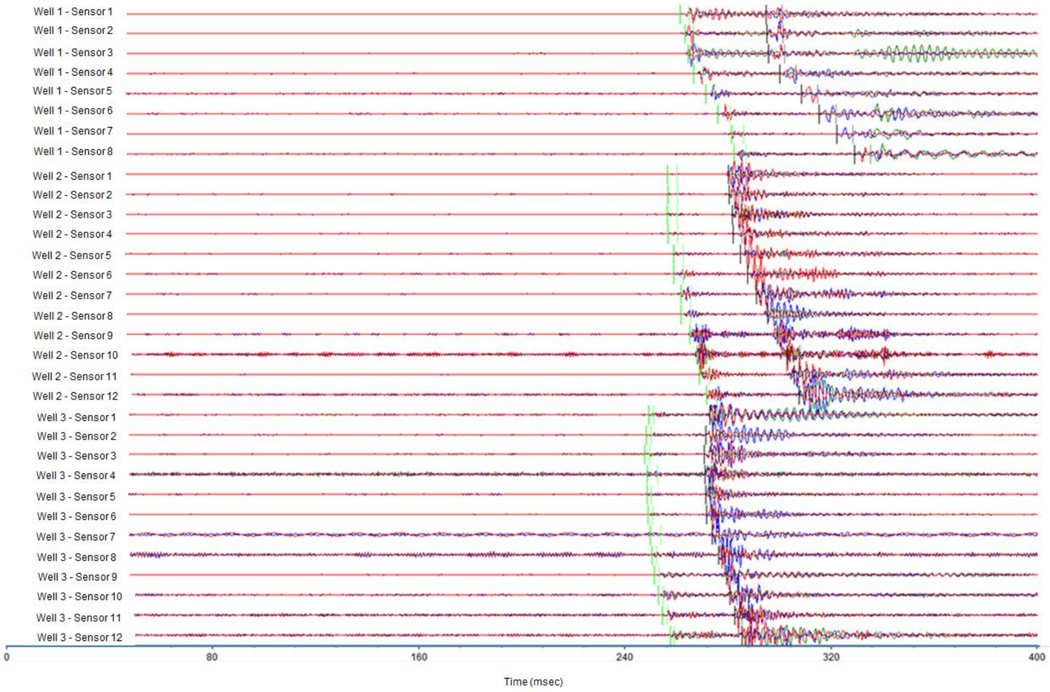

Figure 5.7. Microseismic waveforms associated with a single microseismic event as recorded by thirty two borehole tri-component sensors. Microseismic data from each component is plotted on top of each other. Green traces display the information from the vertical component geophones, while red and blue traces present the data from the two horizontal components. For each sensor display, the horizontal axis represents recording time while the vertical axis displays negative and positive amplitude values with respect to a horizontal zero base line.

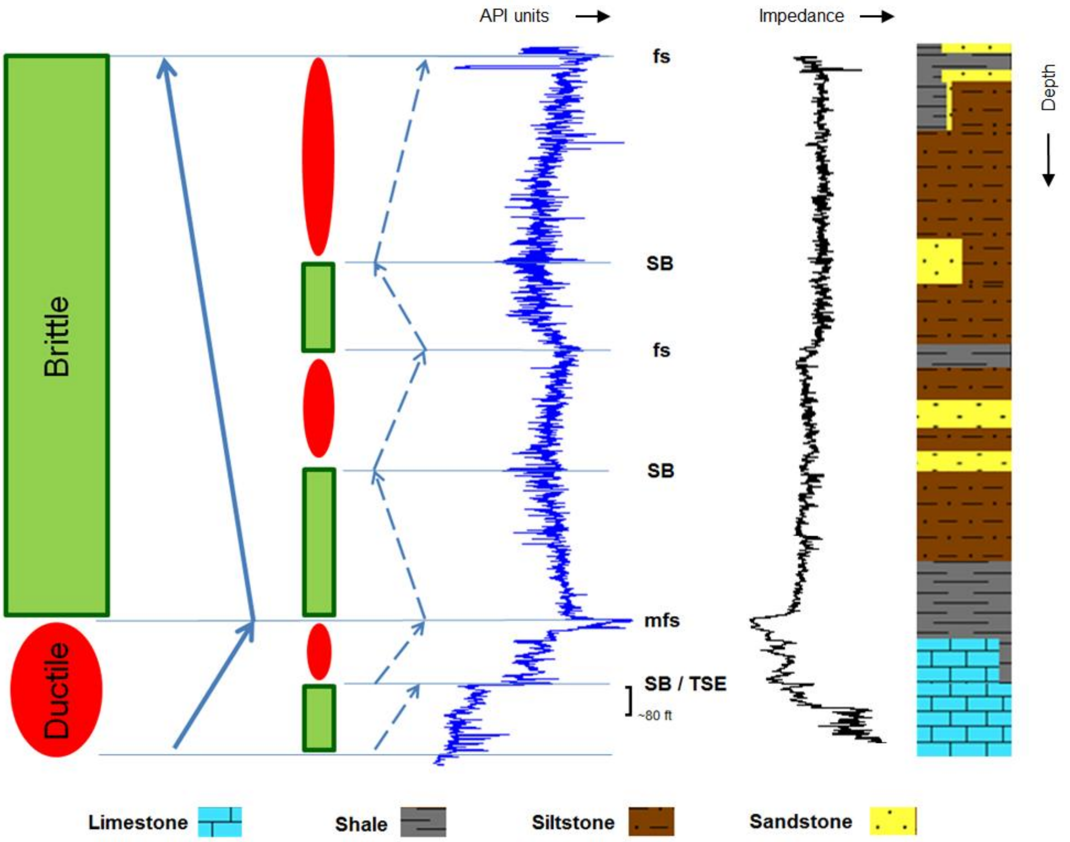

Figure 5.8. Two orders of brittle-ductile couplets (green rectangles and red ovals) interpreted from the identification of gamma-ray log parasequence stacking pattern and subsurface lithologic information. Gamma-ray (GR) and impedance logs, together with a schematic geologic column depicted from mud-logging records, are also included. According with this interpretation, different orders of hydraulic fracturing are expected from the brittle and ductile zones as shown schematically in Figure 2. Note: logs units and specific depth measurements intentionally omitted to protect the confidentiality of the data. GR and impedance units increase from left to right, whereas depth increases from top to bottom as implied by the small black pointing arrows. A mark, approximately 24m (80 ft) long, highlights the target zone.

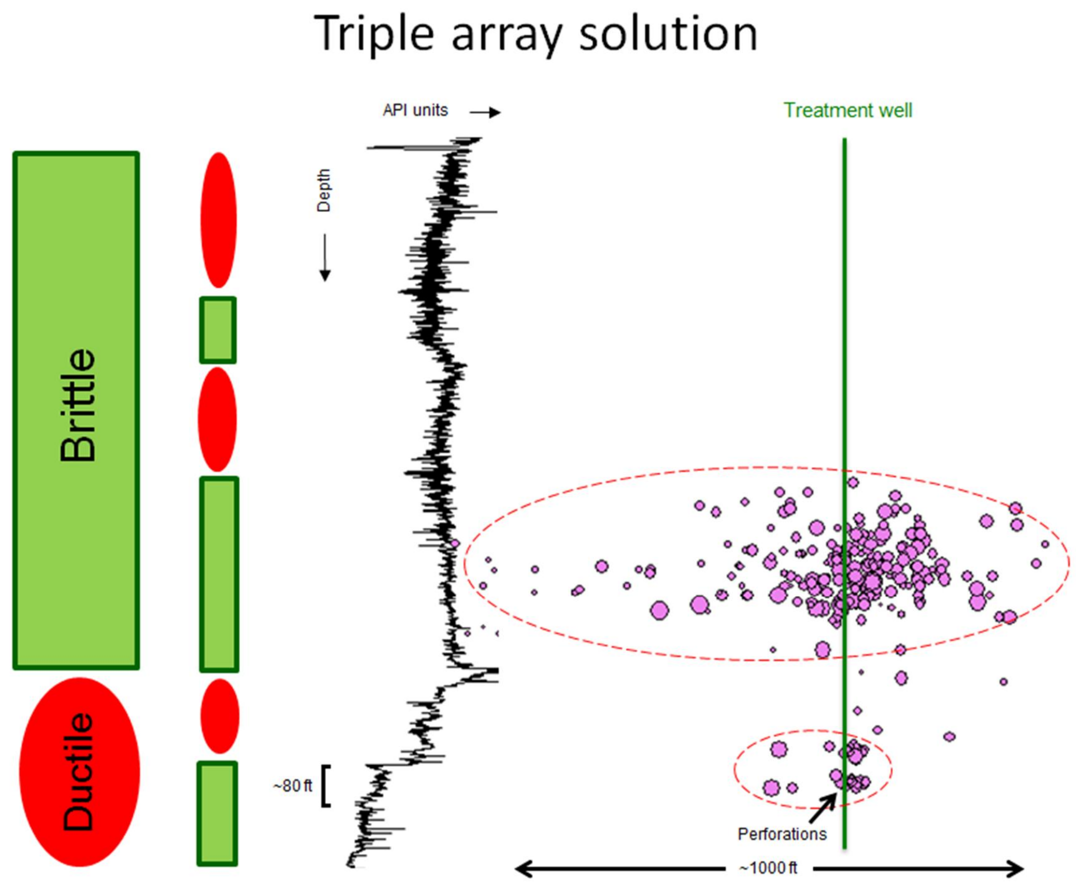

Figure 5.9. Vertical section representation of the subsurface illustrating the relative position of microseismic events (pink circles sized by magnitude) associated with a single-stage hydraulic fracturing treatment. Microseismic events locations are estimated following a simultaneous triple array processing, as opposed to the individual sensor arrays solutions previously illustrated in Figure 6. Notice how most of the event clouds coincide with the brittle sections identified from the stacking pattern interpretation shown in Figure 8 (green rectangles and red ovals). GR profile is also included for reference. Note: GR counts and depth are intentionally omitted to protect the confidentiality of the data. API counts increase from left to right, whereas depth increases from top to bottom. A mark, approximately 24m (80 ft) long, highlights the perforated target zone.

CHAPTER 6: Conclusions

I demonstrated that brittle-ductile couplets identified using gamma ray stacking patterns provide a robust framework to interpret the microseismic response from a single stage hydraulic fracturing treatment. Moreover, the simultaneous processing of microseismic data from a triple sensor array configuration, coupled with a sequence stratigraphic based interpretation, provided a high degree of confidence in the inferred results from the stimulation treatment, and the decisions made from it to support future development campaigns. It is my opinion that these statements holds true in other geological regions provided that the microseismic data used to evaluate the hydraulic fracturing treatment follows simple, but meaningful acquisition and processing quality control procedures. In particular, the microseismic interpreter should be intimately familiar with all aspects of the acquisition, the building of the velocity model, and the location algorithm used to locate microseismic events in the subsurface.

After all efforts have been made to obtain a proper microseismic data set, an integrated analysis also provides significant insights about the subsurface. For instance, in this dissertation I validated the use of microseismic-derived Magnitude vs. Distance Plots (MDP) as a tool to identify fault reactivation, and showed that when combined with other independent measurements such as 3D reflection seismic sections, MDP could unequivocally characterize the reactivation of a fault based on higher amplitudes and azimuth changes.

In closing, just as an experienced seismic interpreter often performs the interpretation of surface reflection seismic, a professional who has developed familiarity with all aspects of borehole microseismicity, in addition to the engineering basis of the stimulation treatment and the geological principles governing the subsurface, should carry the analysis of data from microseismic experiments. A best practice will be to have a multifunctional team evaluating the validity of all assumptions made at every step of the project, collaborating together in order to generate a proper integrated interpretation of borehole microseismic data from hydraulic fracturing stimulation treatments.

References

Abouelresh, M. O., and R. M. Slatt, 2012, Lithofacies and sequence stratigraphy of the Barnett Shale in east-central Fort Worth Basin, Texas. AAPG Bulletin, **v. 96**, no. 1, pp. 1–221.

Badra, H., 2011, Field Characterization and analog modeling of natural fractures in the Woodford shale, southeast Oklahoma: M.S. thesis, The University of Oklahoma.

Baig, A. and T. Urbanicic, 2010, Magnitude determination, event detectability, and assessing the effectiveness of microseismic monitoring programs in petroleum applications: CSEG Recorder, 2, 22-26.

Bazan, L., S. Larkin, M. Lattibeaudiere, and T. Palisch, 2010, Improving production in the Eagle Ford shale with fracture modeling, increased conductivity and optimized stage and cluster spacing along the horizontal wellbore: Proceedings, Society of Petroleum Engineers Tight Gas Completions Conference, paper 138425.

Bohacs, K. M., and Lazar, O. R., 2010, Sequence Stratigraphy in Fine-Grained Rocks at the Field to Flow-unit Scale: Insights for Correlation, Mapping, and Genetic Controls, presented at Houston Geological Society, Applied Geoscience Conference, February 8-9, 2010, Houston.

Borstmayer, R., N. Stegent, A. Wagner and J. Mullen, 2011, Approach optimizes completion design: The American oil and gas reporter, **8**,172-179.

Catuneanu, O., W. Galloway, C. Kendall, A. Miall, H. Posamentier, A. Strasser, and M. Tucker, 2011, Sequence Stratigraphy: Methodology and Nomenclature. Newsletters on Stratigraphy, Vol. 44/3, 173–245.

Cabarcas, C., L. Saugier, G. Haas, C. Woerpel and, J. Le Calvez, 2012, The impact of dipping velocity models on microseismic event locations: Proceedings, Society of Petroleum Engineers Hydraulic Fracturing Technology Conference, paper 152600.

Cabarcas, C., and Davogustto, O., 2013a, Micro MDPs can be a big tool in fault finding: AAPG Explorer, Geophysical Corner, **3**, 36-37.

Cabarcas, C., and Davogustto, O., 2013b, The Magnitude vs. Distance Plot, a tool for fault reactivation identification: Proceedings, American Association of Petroleum Geologist Annual Conference and Exhibition, expanded abstract 1556622.

Cabarcas, C., and Davogustto, O., in press, Monitoring the unexpected; understanding hydraulic fracturing issues using microseismic data: AAPG Explorer, Geophysical Corner.

Cabarcas, C., 2013, Pitfalls locating microseismic events from borehole measurements – practical observations from field applications: Interpretation, **1,** no. 2, pp. A11-A17.

Cabarcas, C., and Slatt, R, in press, Sequence stratigraphic principles applied to the analysis of borehole microseismic data: Interpretation, **2**, no. 3.

Chesnokov, E., I. Bayuk, and M. Ammerman, 2010, Determination of shale stiffness tensor from standard logs. Geophysical prospecting, 58, 1063-1082.

Cipolla, C.L., Warpinski, N.R., Mayerhofer, M.J., and Lolon, E. P., 2008, The Relationship between Fracture Complexity, Reservoir Properties, and Fracture Treatment Design: Proceedings, Society of Petroleum Engineers Annual Technical Conference and Exhibition. Paper 115769.

Cipolla, C., S. Maxwell, M. Mack, and R. Downie, 2011, A practical guide to Interpreting microseismic measurements: Proceedings, Society of Petroleum Engineers North American Unconventional Gas Conference, paper 144067.

Cohen, C., C. Abad, X. Weng, K. England, A. Phatak, O. KResse, O. Nevvonen, V. Lafitte and P. Abivin, 2013, Analysis on the impact of fracturing treatment design and reservoir properties on production from shale gas reservoirs. Proceedings, International Petroleum Technology Conference, paper IPTC-16400-MS-P.

Curtis, M., C. Sondergeld, R., Ambrose, and R. Chandra, 2012, Microstructural investigation of gas shales in two and three dimensions using nanometer-scale resolution imaging. AAPG Bulleting, V96, No 3 (April 2012) PP. 665-677.

Daneshy, A., 2013, Horizontal well fracturing: A state-of-the-art report. World Oil Magazine, July.

Dawson, W. C., 2000, Shale microfacies: Eagle Ford group (Cenomanian-Turonian) North-Central Texas outcrops and subsurface equivalents: Gulf coast association of geological transactions, 50, 607- 621.

Dawson, W. C., and W. R. Almon, 2010, Eagle Ford Shale variability: Sedimentologic influences on source and reservoir character in an unconventional resource unit: Gulf Coast Association of Geological Societies Transactions, v. 60, p. 181- 190.

Drew, J., and J. Le Calvez, 2007, Complexities in the quick analysis and interpretation of microseismic data: 77st Annual meeting, SEG, Expanded Abstract, 1347-1348.

Donovan, A. D., and T. S. Staerker, 2010, Sequence stratigraphy of the Eagle Ford (Boquillas) Formation in the subsurface of South Texas and outcrops of West Texas: Gulf Coast Association of Geological Societies Transactions, **60**, 861-899.

Downie, R.C., E. Kronenberger, and S. Maxwell, 2010, Using microseismic source parameters to evaluate the influence of faults on fracture treatments – a geophysical approach to interpretation: Proceedings, Society of Petroleum Engineers Annual Technical Conference and Exhibition, paper 134772.

Economides, M.J., and K.G. Nolte, (eds.), 2000, Reservoir Stimulation (3rd ed.): John Wiley & Sons Ltd.

Eisner, L., M. Thornton, and J. Griffin, 2011, Challenges for microseismic monitoring: 81st Annual meeting, SEG, Expanded Abstract, 1519-1523.

Emery, D., and K. J. Myers, 1996, Sequence Stratigraphy: Blackwell.

Energy Information Administration (EIA) http://www.eia.gov/oil_gas/rpd/shaleusa9.pdf accessed 10 January 2012.

Fan, L., R. Martin, J. Thompson, K. Atwood, J. Robinson, and G Lindsay, 2011, An integrated approach for understanding oil and gas reserves potential in Eagle Ford Shale Formation. Proceedings, Society of Petroleum Engineers Canadian Unconventional Resources Conference, paper 148751.

Fehler, M., A. Jupe, and H. Asanuma, 2001, More than cloud: New technique for characterizing reservoir structure using induced seismicity. Society of Exploration Geophysicist, The Leading Edge, March, 338-343.

Freeman, V. L., 1961, Contact of the Boquillas flags and Austin Chalk in Val Verde and Terrell counties, Texas: American Association of Petroleum Geologists Bulletin, v. 45, p. 105-107.

Goldhammer, R. K., and C. A. Johnson, 1998, Middle Jurassic-Upper Cretaceous paleogeographic evolution and sequence-stratigraphic framework of the northwest Gulf of Mexico rim, in C. Bartolini, R. T. Buffler, and A. Cantú-Chapa, eds., The western Gulf of Mexico Basin: Tectonics, sedimentary basins, and petroleum systems: AAPG Memoir 75, p. 45-81.

Guidry, F.K., D.L Luffel, and J.B. Curtis, 1996, Development of Laboratory and Petrophysical Techniques for Evaluating Shale Reservoirs, Gas Research Institute, GRI - 5/0496.

Haq, B. U., J. Hardenbol, and P. R. Vail, 1986, Chronology of fluctuating sea levels since the Triassic (250 million years ago to present): Science, v. 235, p. 1156-1167.

Handin, J., and R. V. Hager, 1957, Experimental deformation of sedimentary rocks under confining pressure: Tests at room temperature on dry samples: American Association of Petroleum Geologists Bulletin, 41, 50.

Hayles, K., R. Horine, S. Checkles, and J.P. Blangy, 2011, Comparison of microseismic results from the bakken formation processed by three different companies: Integration with surface seismic and pumping data: 81st Annual meeting, SEG, Expanded Abstract, 1468-1472.

Hendershott, Z., 2012, Evaluation of the depositional environment of the Eagle Ford formation using well log, seismic, and core data in the Hawkville Trough, La Salle and McMullen counties, South Texas. M.S. Thesis, Louisiana State University.

Hetenyi, M., 1966. Handbook of experimental stress analysis: Wiley.

House, N., and J. Shemeta, 2008, Understanding hydraulic fractures in tight-gas sands through the integration of borehole microseismic data, three-dimensional surface seismic data, and three-dimensional vertical seismic profile data: A Jonah field case study, in S. P. Cumella, K. W. Shanley, and W. K. Camp, eds., Understanding, exploring, and developing tight-gas sands: Vail Hedberg Conference: AAPG Hedberg Series, no. 3, 77 – 86.

Hubbert, M.K. and D.G. Willis, 1957, Mechanics of hydraulic fracturing: Trans. AIME., Vol. 210, 153-168.

Hunt, J. M., 1996, Petroleum geochemistry and geology, 2nd ed.: W. H. Freeman and Company, New York, 743 pp.

Inamdar, A., R., Malpani, K. Atwood, K. Brook, A. Erwemi, T. Ogundare, and D. Purcell, 2010, Evaluation of stimulation techniques using microseismic mapping in the Eagle Ford Shale: Proceedings, Society of Petroleum Engineers Tight Gas Completions Conference, paper 136873.

Jarvie, D. M., R. J. Hill, T. E. Ruble, and R. M. Pollastro, 2007, Unconventional shale-gas systems: the Mississippian Barnett Shale of North-Central Texas as one model for thermogenic shale-gas assessment: AAPG Bulletin, **91**, 475 - 499.

Johnston, R., and J. Shrallow, 2011, Ambiguity in microseismic monitoring: Proceedings, Society of Exploration Geophysicist Annual meeting.

King, G, 2012, Hydraulic fracturing 101: What every representative, environmentalist, regulator, reporter, investor, university researcher, neighbor and engineer should know about estimating frac risk and improving frac performing in unconventional gas and oil wells: Proceedings, Society of Petroleum Engineers Hydraulic Fracturing Technology Conference, paper 152596

Kurosawa, I, 2011, Microseismic Location Accuracy by using Double-Difference Earthquake Location Algorithm: Proceedings, CSPG, CSG, and, CWLS Convention.

LaFollette, R., 2010, Key considerations for Hydraulic fracturing of Gas shales: Presented at the Geosciences Technology Workshop, AAPG.

Le Calvez, J. H., R. Klem, K. V. Tanner, L. Bennett, and, M. Craven, 2007, Real-time microseismic monitoring of hydraulic fracture treatment: A tool to improve completion and reservoir management: Proceedings, Society of Petroleum Engineers Annual Technical Conference, paper 106159.

Liner, C., 2012, Elements of seismic dispersion: A somewhat practical guide to frequency-dependent phenomena. SEG DISC series, No 15.

Lim, T.K., Y. Li, and X.G. Yang, 2012, application of dual well micro-seismic monitoring in hydraulic fracturing stimulation in a tight oil reservoir: Proceedings, Petroleum Geosciences Conference and Exhibition.

Liro, L.M., W. Dawson, B. Katz, and V. Robinson, 1994, Sequence stratigraphic elements and geochemical variability within a “condense section”: Eagle Ford Group, East-Central Texas. Transactions of the Gulf Coast Association of Geological Societies, **vol.** XLIV.

Lyle, D., 2010, Eagle ford joins Shale Boom: Eagle Ford: The playbook, supplement to the EP magazine.

Lock B. E., and L. Peschier, 2006, Boquillas (Eagle Ford) upper slope sediments, West Texas: Outcrop analogs for potential shales reservoirs: Gulf Coast Association of Geological Societies Transactions, v. 56, p. 491-508.

Lock, B. E., L. Peschier, and N. Whitcomb, 2010, The Eagle Ford (Boquillas Formation) of Val Verde County, Texas – A window on the South Texas play: Gulf Coast Association of Geological Societies Transactions, v. 60, p. 419-434.

Loucks, R., R. Reed, S. Ruppel, and U. Hammer, 2012, Spectrum of pore types and networks in mudrocks and a descriptive classification for matrix-related mudrock pores: American Association of Petroleum Geologists Bulletin. V96, No 6. PP 1071-1098.

Martin, T., and P. Valko, 2007, Hydraulic fracture design for production enhancement. Chapter 4; in M., Economides and T. Martin Modern fracturing –enhancing natural gas production- ET Publishing Houston, Texas, 2007.

Martin, R., J. Baihly, R. Malpani, G. Lindsey, and W.K. Atwood, 2011, Understanding production from Eagle Ford – Austin chalk system: Proceedings, Society of Petroleum Engineers Annual Technical Conference, paper 145117.

Matsutsuyu, B., 2011, South Texas Eagle Frd shale geology – regional trends, recent learning's, future challenges: Hart Energy's Developing Unconventional Gas Conference.

Maxwell, S.C., 2009, Microseismic Location Uncertainty, in CSEG Recorder, April 2009.

Maxwell, S.C., B. Underhill, L. Bennett, and A. Martinez, 2010a, Key criteria for a successful microseismic project: Proceedings, Society of Petroleum Engineers Annual Technical Conference, paper 134695.

Maxwell, S.C., J. Rutledge, R. Jones, and, M. Fehler, 2010b, Petroleum reservoir characterization using downhole microseismic monitoring: Geophysics, 75, No 5, 75A129 - 75A137.

Maxwell, S.C., L. Bennett, M. Jones, and, J. Walsh, 2010c, Anisotropic velocity modeling for Microseismic processing: Part I – Impact of velocity model uncertainty. SEG Denver Annual Meeting.

Maxwell, S.C., 2010, Microseismic: Growth born from success. Society of Exploration Geophysicist, The Leading Edge, march 2010, 338-343.

Maxwell, S.C., and J. Le Calvez, 2010, Horizontal vs vertical borehole-based microseismic monitoring: Which is better?: Proceedings, Society of Petroleum Engineers Annual Technical Conference, paper 131780.

Maxwell S.C., and C. Cipolla, 2011, What does microseismic tell us about hydraulic fracturing?: Proceedings, Society of Petroleum Engineers Annual Technical Conference, paper 146932.

Minisini, D., S. Bergman, and C. Macaulay, 2011, Bed-scale facies variability of outer shelf deposits in a gas-shale reservoir analog: Cretaceous Eagle Ford formation, Del Rio, SW Texas: Proceedings, American Association of Petroleum Geologists International Conference and Exhibition.

Miskimins, J., 2008, Design and life cycle considerations for unconventional reservoir wells: Proceedings, Society of Petroleum Engineers Unconventional Reservoirs Conference, paper 114170.

Mizuno, T., S. Leaney, and G. Michaud, 2010, Anisotropic Velocity Model Inversion for Imaging the Microseismic Cloud: Proceedings, European Association of Geoscientists and Engineers, Expanded Abstract.

Mullen, J., 2010, Petrophysical characterization of the Eagle Ford shale in South Texas: Proceedings, Canadian Unconventional Resources & International Petroleum Conference, paper 138145.

Murer, A., G. McNeish, T. Urbancic, M. Prince, and A. Baig, 2012, Why monitoring with a single downhole microseismic array may not be enough: a case for multiwall monitoring of cyclic steam in diatomite. SPE Reservoir Evaluation & Engineering, 385-392.

Nelson, G.D. and Vidale, J.E., 1990, Earthquake Locations by 3D Finite Difference Travel Times: Bulletin of the Seismological Society of America, **80**, p. 395-410.

Paillet, F., 1985, Problems in fractured-reservoirs evaluation and possible routes to their solution. The log analyst, November-December, 12 p.

Passey, Q. R., S. Creaney, J. B. Kulla, F. J. Moretti, and J. D. Stroud, 1990, A practical model for organic richness from porosity and resistivity logs: AAPG Bulletin, **74**, 1777 - 1794.

Pavlis, G, 1986, Appraising Earthquake Hypocenter Location Errors: A Complete, Practical Approach for Single-Event Locations: Bulletin of Seismological Society of America, **94**, 1817-1830.

Payton, C. E. (ed.), 1977, Seismic stratigraphy – applications to hydrocarbon exploration: American Association of Petroleum Geologists Memoir 26.

Pearson, C., 1981, The relationship between microseismicity and high pore pressure during hydraulic stimulation experiments in low permeability granitic rock. Journal of Geophysical Research, **86**, pp. 7855-7864.

Perez, R., 2013, Brittleness estimation from seismic measurements in unconventional reservoirs: application to the Barnett shale: Ph.D. dissertation, The University of Oklahoma.

Pessagno, E. A., 1969, Upper Cretaceous stratigraphy of the western Gulf Coast area of Mexico, Texas, and Arkansas: Geological Society of America Memoir 111, Boulder, Colorado, 139 p.

Posamentier, H.W., and G. P. Allen, 1999. Siliciclastic sequence stratigraphy: concepts and applications. SEPM Concepts in Sedimentology and Paleontology no. 7, 210 pp.

Rich, J., 2012, Interpreting micro-seismic results in unconventional plays: Presented at the GSH June Microseismic Special Interest Group.

Scott, R. W., 2010, Cretaceous stratigraphy, depositional systems, and reservoir facies of the northern Gulf of Mexico: Gulf Coast Association of Geological Societies Transactions, v. 60, p. 597-609.

Shemeta, J., and P. Anderson, 2010, It's a matter of size: Magnitude and moment estimates for microseismic data. Society of Exploration Geophysicist, The Leading Edge, **3**, 296-302.

Sheriff, R.E., 1999, Encyclopedic dictionary of exploration geophysics, third ed.: Society of Exploration Geophysicists.

Singh, 2008, Lithofacies and sequence stratigraphic framework of the Barnett shale, northeast Texas: Ph.D. dissertation, The University of Oklahoma.

Slatt, R.M., 2006, Stratigraphic reservoir characterization for Petroleum Geologists, Geophysicists, and Engineers: Elsevier.

Slatt, R., 2011, Important Geological Properties of Unconventional Resource Shales. Oklahoma City Geological Society. Shale Shaker. November – December. page 224-

Slatt, R.M., and N.R. O'Brien, 2011, Pore types in the Barnett and Woodford gas shales: contribution to understanding gas storage and migration pathways in fine-grained rocks: American Association of Petroleum Geologists Bulletin.

Slatt, R.M. and Y. Abousleiman, 2011, Merging sequence stratigraphy and geomechanics for unconventional gas shales: The Leading Edge, 30, no. 3, 274-282.

Slatt, M., and N. D. Rodriguez, 2012, Comparative Sequence Stratigraphy and Organic Geochemistry Of Gas Shales: Commonality Or Coincidence? Journal of Natural Gas Science and Engineering, v. 8, p. 68-64.

Slatt, R. M., in press, 2013, Sequence stratigraphy of unconventional resource shales: *in* R. Rezaee, ed., Fundamentals of Gas Shale Reservoirs: John Wiley and Sons.

Smith, M.B., and J.W. Shlyapobersky, 2000, Basics of Hydraulic Fracturing, Reservoir Stimulation, *in* Economides, M.J., and K.G. Nolte, (eds.), 2000, Reservoir Stimulation (3rd ed.): John Wiley & Sons Ltd.

Smith, M.B., 2013, Hydraulic Fracturing – a concise overview. Society of Petroleum Engineers course notes.

Sondhi, N., 2011, Petrophysical characterization of Eagle Ford shale: M.S. thesis, The University of Oklahoma.

Stegent, N.A., A.L. Wagner, J. Mullen, R.E. Borstmayer, 2010, Engineering a successful fracture-stimulation treatment in the Eagle Ford shale: Proceedings, Society of Petroleum Engineers Annual Technical Conference and Exhibition, paper136183.

Stoneburner, D., 2012, The exploration, appraisal and development of unconventional reservoirs: A new approach to petroleum geology: AAPG Distinguish Lecture Tour.

Tiwary, D., I. Bayuk, A. Vickhorev, and, E. Chesnokov, 2009, Comparison of seismic upscaling methods: From sonic to seismic: Geophysics, **74**, No 2, WA3-WA14.
Thomsen, L., 1986, Weak elastic anisotropy: Geophysics, **51**, 1954-1966.

Treadgold, G., B. McLain, S. Sinclair, D. Nicklin, 2010, Eagle Ford Shale Prospecting with 3D Seismic Data within a Tectonic and Depositional System Framework – Part 1, in Critical Assessment of shale resource plays, AAPG Hedberg Research Conference, Dec., Austin, Tx.

Trevino, R. H., 1988, Facies and depositional environments of the Boquillas Formation, Upper Cretaceous of southwest Texas: M.S. Thesis, University of Texas at Arlington, 135 p.

University of California, Geology Labs online; www.sciencecourseware.org/glol/ accessed 20 April 2013.

Vail, P. R., R. M. Jr. Mitchum, and S. Thompson, 1977, Seismic stratigraphy and global changes of sea level. In: Payton, C. E. (ed.), Seismic Stratigraphy – Applications to Hydrocarbon Exploration. American Association of Petroleum Geologists Memoir 26.

Van Wagoner, J.C., R.M. Mitchum, K.M. Campion, and V.D. Rahmanian, 1990, Siliciclastic sequence stratigraphy in well logs, cores and outcrops: concepts for high resolution correlation of time and facies: AAPG Methods in Exploration Series, no.7, 53 p.

Walls, J., E. Diaz, N. Derzhi, A. Grader, J. Dvorkin, S. Arredondo, G. Carpio, and S. Sinclair, 2011, Eagle Ford Shale Reservoir Properties from Digital Rock Physics: HGS Applied Geoscience Mudrocks Conference.

Wang, F.P., and J. F. W. Gale, 2009, Screening criteria for shale-gas systems: GCAGS Transactions, **59**, 779 - 793.

Warpinski, N., R.B. Sullivan, J.E. Uhl, C.K. Waltman, and S.R. Machovoe, 2005a, Improved microseismic fracture mapping using perforation timing measurements for velocity calibration. SPE Journal, March. Paper 84488.

Warpinski, N.R., Kramm, R.C., Heinze, J.R., and Waltman, C.K, 2005b, Comparison of single- and dual-array microseismic mapping techniques in the Barnett shale: Proceedings, Society of Petroleum Engineers Annual Technical Conference, paper 95568.

Warpinski, N.R., M.J. Mayerhofer, M.C. Vicent, C.L. Cipolla, and E.P. Lolon, 2008, Stimulating Unconventional Reservoirs: maximizing network growth while optimizing fracture conductivity: Proceedings, Society of Petroleum Engineers Unconventional Reservoirs Conference, paper 114173.

Warpinski, N., 2009, Microseismic monitoring: Inside and out: Proceedings, Society of Petroleum Engineers Annual Technical Conference, paper 118537.

Warpinski, N.R., 2009, Integrating microseismic monitoring with well completions, reservoir behavior, and rock mechanics: Proceedings, Society of Petroleum Engineers Tight Gas Completions Conference, paper 125239.

Warpinski, N, C. Waltman, J. Du, and Q. Ma, 2009, Anisotropic Effects in Microseismic Mapping: Proceedings, Society of Petroleum Engineers Annual Technical Conference, paper 124208.

Warpinski, N., and J. Du, 2010, Source mechanism studies on microseismic induced by hydraulic fracturing: Proceedings, Society of Petroleum Engineers Annual Technical Conference, paper 135254.

Wilson, S., 2008, The effects of velocity structure on microseismic location estimates: a case study: 78th Annual meeting, SEG, Expanded Abstract.

Winkler, C. D., and R. T. Buffler, 1988, Paleogeographic evolution of early deep-water Gulf of Mexico and margins, Jurassic to Middle Cretaceous (Comanchean): American Association Petroleum Geologists Bulletin, v. 72, p. 318-346.

Wolhart, S.L., T.A. Harting, J.E. Dahlem, T.J. Young, M.J. Mayerhofer, and E.P. Lolon, 2006, Hydraulic fracture diagnostics used to optimize development in the Jonah field: Proceedings, Society of Petroleum Engineers Annual Technical Conference and Exhibition, paper 102528.

Woerpel, J.C., S. Maxwell, B. Underhill, and J. Wolfe, 2010, Automated Monitoring of Hydraulic Fracture by Coalescence Microseismic Mapping: Proceedings, Society of Petroleum Engineers Annual Technical Conference and Exhibition, paper 139043.

Wuestefeld, A., T. Urbancic, A. Baig, and, Marc Prince, 2012, After a Decade of Microseismic Monitoring: Can We Evaluate Stimulation Effectiveness and Design Better Stimulations: Proceedings, Society of Petroleum Engineers Annual Technical Conference, paper 152665.

Zimmer, U., S. Maxwell, C. Waltman, and, N. Warpinski, 2007, Microseismic monitoring quality-control (QC) reports as an interpretative tool for non-specialists. SPE Journal, December. Paper 110517.

Zimmer, U., 2011, Calculating stimulated reservoir volume (SRV) with consideration of uncertainties in microseismic-event locations. Proceedings, Canadian Unconventional Resources Conference, paper 148610.

Appendices

Appendix A: Micro MDPs can be a big tool in fault finding*

Cabarcas, C and O. Davogustto.

* Adapted from article published February 2013 in The Geophysical Corner, a regular column in the AAPG EXPLORER magazine, edited by Satinder Chopra. Copyright 2013, American Association of Petroleum Geologist.

Microseismic technology is crucial these days for understanding reservoirs and planning development programs:

- Borehole microseismic is used to monitor seismic activity generated during hydraulic fracturing.
- The displacement of a rock along a shear wave is referred to as a fault, and the energy released by such a movement propagates as a seismic wave; a measure of this energy within the domain of microseismic technology is referred to as magnitude.
- The magnitude values of the recorded microseismic events are proportional to the size of the surface and the displacement involved in faulting. Assuming that surfaces and displacements associated with preexisting faults are bigger than those of hydraulically induced fractures, during hydraulic stimulation, the registered higher magnitudes should characterize fault reactivation.

Magnitude is usually one of the parameters derived from borehole microseismic measurements. Additionally, microseismic recording sensors only detect microseismic events occurring within a certain radius from them – usually no more than a few thousand feet. One way to quantify this phenomenon is with a Magnitude vs. Distance Plot (MDP). This plot shows the relationship between the energy associated with a particular event and its distance from the monitor well.

The MDP is a useful analysis tool in microseismic interpretation for all the information it summarizes on a simple graphic display.

Events with a combination of highest magnitude and highest distance away from the monitor well define the maximum detection distance, which can be used to plan the maximum distance for monitor well placement in future jobs. The rest of the recorded events populate the middle upper left portion of the MDP graph, forming a quasi-triangular pattern.

The presence of faults in the subsurface – and their reactivation during hydraulic stimulation – thus becomes noticeable on MDPs, because magnitudes of events associated with fault reactivation are usually higher than the rest.

* * *

I use the MDP technique to discern fault reactivation in this microseismic monitoring exercise, performed real-time during hydraulic fracturing operations.

➢ In Figure 1, the higher magnitudes’ events associated with possible reactivated faults are highlighted by a dotted blue circle.

When implementing the hydraulic stimulation no surface seismic data was available – and subsurface geologic maps, built solely on sparse wells information, did not foresee the possibility of a fault in the area. This encouraging geologic model also supported the drilling and stimulation of the treatment well.

More than a year after the stimulation of the well associated with Figure 1, newly available 3-D reflection seismic data provided a better image of the subsurface near the well. Unfortunately, due to resolution limitations, the broadband frequency data from this 3-D reflection seismic survey does not provide unequivocal evidence for the presence of a fault. By coupling the 3-D seismic data with the microseismic events interpreted as the response of fault reactivation, however, I infer the presence of a fault in the seismic image.

- In Figure 2 I show sections with and without the microseismic events.

The overlay of microseismic events on the 3-D seismic vertical section suggests the presence of an antithetic fault in the subsurface and its possible reactivation due to hydraulic fracture stimulation. The microseismic event set aligned very well in the direction of the interpreted fault plane.

By computing similarity on the 3-D seismic volume and extracting a surface slice from seismic data at the zone of interest, I interpret the presence of a fault crossing the path of the treatment well.

The good correlation between microseismic event lineaments and the extrapolation of similarity trends provides further evidence supporting my hypothesis of fault reactivation due to the hydraulic fracturing treatment – which I illustrate in figure 3.

- Figure 3 also shows that the azimuth of the event cloud associated with the fault reactivation is different from the azimuth inferred from previous stimulation stages.

This characteristic, solely based on microseismic event location, provides another tool to derive subsurface geological information not generally emphasized.

I suggest that in the absence of additional supporting data, an azimuth change observed from microseismic sets – coupled with anomalously high magnitudes for the same events – could be interpreted as an indication of fault reactivation.

Moreover, when integrated with treatment pressure information, these microseismic observations could be used in the decision-making process of changing a predesign treatment job – and could significantly reduce completion costs.

The example presented here serves to validate and support the use of microseismic-derived MDPs as a tool to identify fault reactivation in the absence of additional subsurface data.

Moreover, when combined with other independent measurements, MDPs could unequivocally characterize the reactivation of a fault based on higher amplitudes and possible azimuth changes.

I also show that 3-D seismic is a powerful tool to mitigate drilling and completion risks as those encountered when faults are not anticipated along the well path. Availability of 3-D seismic data beforehand could have improved well placement and possibly resulted in lower completion costs and better well performance.

* * *

I would like to thank the management of Hilcorp Energy Company for permission to publish this work, as well as its support on the application of new technologies. In addition, I would like to thank Seitel Inc. for permission to publish their seismic profiles, and Dawn Henderson for her help editing this document.

(Editor's note: Cabarcas is a geophysicist at Hilcorp and Ph.D. candidate at University of Oklahoma; Davogustto is a Ph.D. candidate at University of Oklahoma, working with Kurt J. Marfurt. All are AAPG members.)

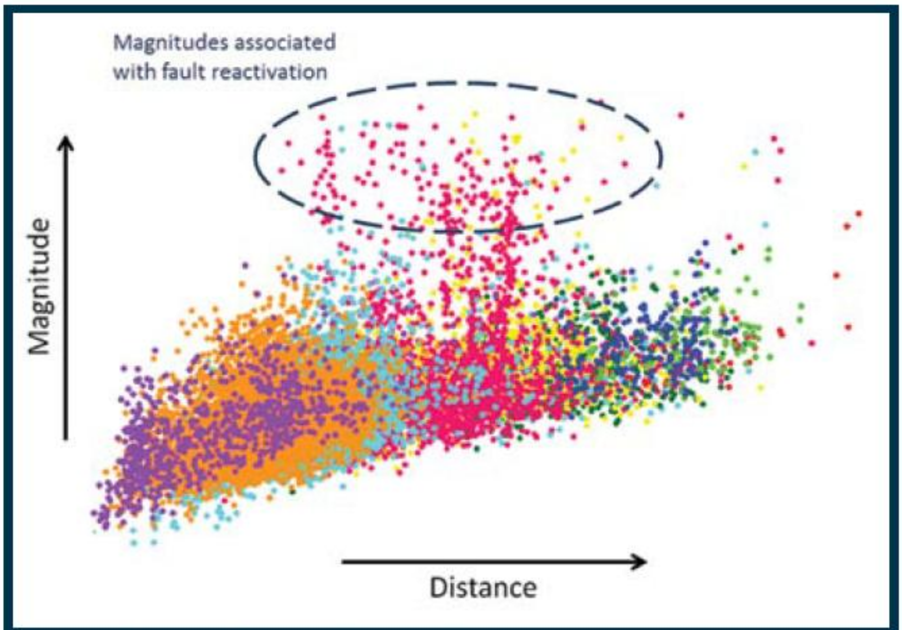

Figure1 – Magnitude vs. distance plot from a multi-stage hydraulic stimulation job monitored from a borehole for microseismic activity. Different colors represent event sets from different stages. Most of the stages generate microseismic event that predictably populate the graph (i.e. lower magnitude events can be detected near to the monitor well while farther away from the monitor well only relatively higher magnitudes event can be detected). Stages yellow, cyan and, especially, stage red suggest fault reactivation due to their higher magnitude, as compared to magnitudes from other stages. Magnitude and distance increase respectively in the direction pointed by the arrows.

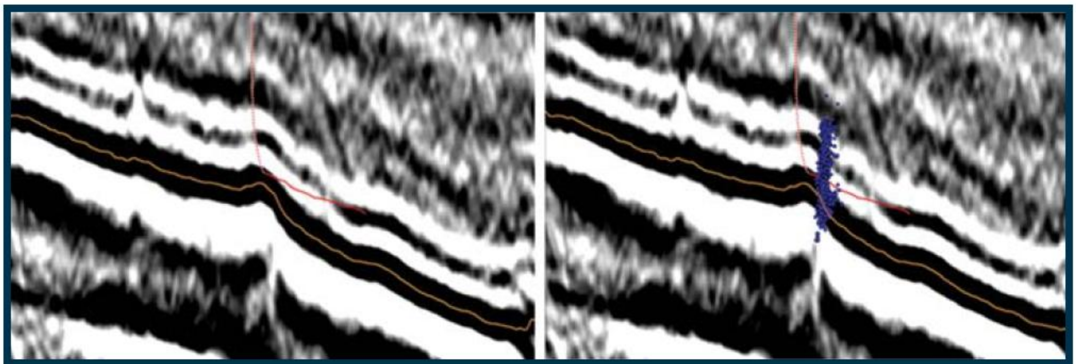

Figure 2 – (a) Vertical seismic section parallel to the azimuth of a treatment well monitored for microseismic activity (courtesy of Seitel Inc.); (b) Same seismic line overlaid by microseismic events from a stage interpreted as associated with a fault reactivation. Microseismic events align very well depicting the trace for an antithetic normal fault verging opposite to the inclination of the reflectors, beds and horizontal well.

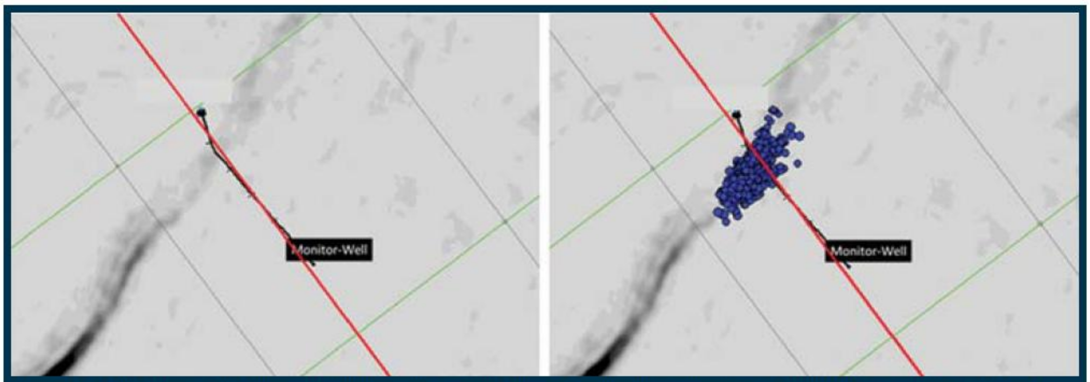

Figure 3 – Similarity horizon slice extracted along the stimulated zone of interest monitored for microseismic activity. (The original seismic data used as input into the similarity algorithm is the property of Seitel Inc.) Highly similar data is colored in grey shades while areas with low similarity values are tinted black as shown in the figure label. Microseismic events from the hydraulic stimulation stage believed to have reactivated a fault are aligned very well with a similarity anomaly that also represents a fault system trace. The treatment well is shown for reference purposes. The red line labeled A-A' represents the direction and length of the line shown in figure 2.

Appendix B: Monitoring the unexpected; understanding hydraulic fracturing issues using microseismic data*

Cabarcas, C and O. Davogustto.

* Adapted from article submitted to The Geophysical Corner, a regular column in the AAPG EXPLORER magazine, edited by Satinder Chopra. Copyright 2013, American Association of Petroleum Geologist.

There are many examples in the literature that illustrate the use of microseismic information to monitor hydraulic fracturing treatments in resource plays. Most of these examples describe typical benefits from analyzing microseismic data, for instance, estimating the stimulated volume and fracture geometry associated with newly created flow paths. Here, using two specific examples, I discuss a less popular approach; the use of microseismic data to recognize unexpected out of zone fracture growth.

***

Figure 1 shows the first example, a three dimensional perspective of the subsurface depicting both a treatment and a monitor well, along with colored spheres which represent microseismic events associated with three hydraulic fracturing stages. The lateral sections of both wells are parallel and approximately 245m (800ft) apart. As seen in this Figure, the microseismic events for the red and green stages gather as clouds around the perforations in the zone of interest. However, this is not the case for the subsequent stage (represented by pink spheres), as much of the fracture growth takes place vertically and horizontally away from the target zone. This is not uncommon; throughout multiple fracturing treatments I have observed microseismic activity near the heel of the well, which is not part of the original stimulation design.

It is important to point out that different contractors processed this data, and the results were very similar. This minimizes the possibility of a processing artifact. Indeed, the waveform characteristics; the travel time between the P and S waves, the array response move-out, and the azimuth calculated from the particle motion of the event waveforms, all indicate that the events generated in the last stage occurred in a location far from the target zone. There may be different reasons for these unexpected results. For instance, fracturing fluids leakage due to poor casing integrity or along an open fault are both plausible explanations. Stress concentration near the heel of the well as the result of the drilling process together with high pressures generated during fracturing, could also explain the out of zone fracture growth seen in Figure 1.

Coupling microseismic and pressure data along with production records has proved valuable in root cause analyses for unexpected results. In this particular example, real-time processing of the microseismic data interpreted in the context of a sudden decrease in the tubing pressure shortly after the start of pumping supported the hypothesis of out of zone fracture growth. This integrated analysis allowed the on-site crew to quickly make changes to the original fracture design in an effort to arrest the fracture containment issue.

***

The second example deals with microseismic data acquired as part of an experiment designed to assess the near wellbore stress distribution of a zone of interest, in support of a future development campaign. Monitoring a single stage hydraulic fracturing treatment on a vertical well was a key element of this project. To ensure high quality measurements, multiple sensor arrays, strategically placed in three monitor wells surrounding the vertical treatment well, captured all the microseismic signals from this experiment. Figure 2 shows a vertical section of the subsurface with the treatment well and the microseismic events locations (blue dots) obtained from simultaneous processing of the signals from all arrays. For simplicity, the Figure shows only one of those sensors arrays (green squares). From this Figure, it is clear that the vast majority of events originated outside of the formation of interest, approximately 150m (500ft) above the perforated interval depicted by a blue arrow.

It is worth noting that the subsurface location of a string shot as estimated by its seismic signal correlated well with its known location, nearby the perforated interval. This provided enough information to build a calibrated velocity model giving a high degree of confidence in the output of the microseismic experiment.

The post treatment stress profile inferred from the microseismic activity in Figure 2 suggests an out of zone fracture growth episode. Based on these observations, I concluded that the use of less viscose fracturing fluids and lower proppant concentrations could aid fracture containment for this particular stress regime. These results underscore, once again, the value of microseismic information to explain unexpected results and to provide the necessary data to support changes to the original fracturing design.

***

A final thought - Fracture containment issues have been the subject of much discussion and debate in recent years, partly because of environmental concerns related to groundwater pollution with fracturing fluids during stimulation operations. In this respect, microseismic data has proved to be a valuable tool to quantify any potential risk. Microseismic surveys from thousands of hydraulic fracturing treatments demonstrate that all recorded instances of out of zone fracture growth are limited to a few hundred feet around the stimulated zone, as shown in Figure 2, much deeper than common sources of underground water typically used for human activities.

Acknowledgment

I acknowledge the service companies involved in these projects, and express my gratitude to the management of Hilcorp Energy Company for their permission to publish the results presented in this article, and its support of innovative ideas.

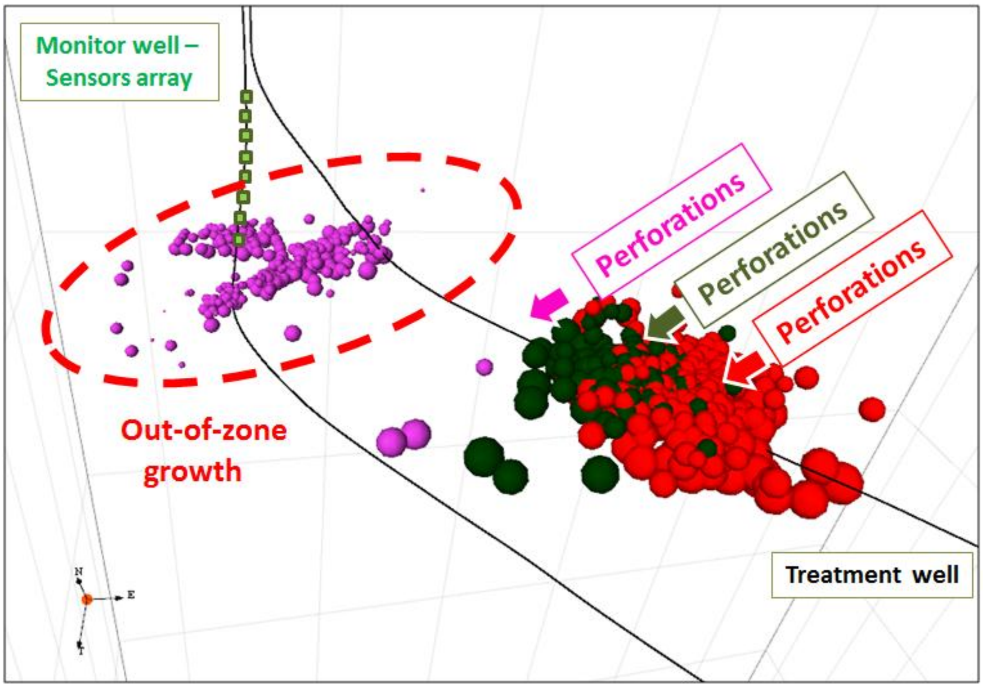

Figure 1. Three-dimensional perspective of the subsurface showing microseismic events (red, green, and pink spheres) associated with three hydraulic fracturing stages on a horizontal treatment well. The figure also shows a sensor array in green. The distance between the lateral sections of the wells is approximately 245m (800ft). Microseismic events for the red and green stages occur near the perforations in the zone of interest, whereas those for the pink stage lie out of the target zone, suggesting out of zone fracture growth.

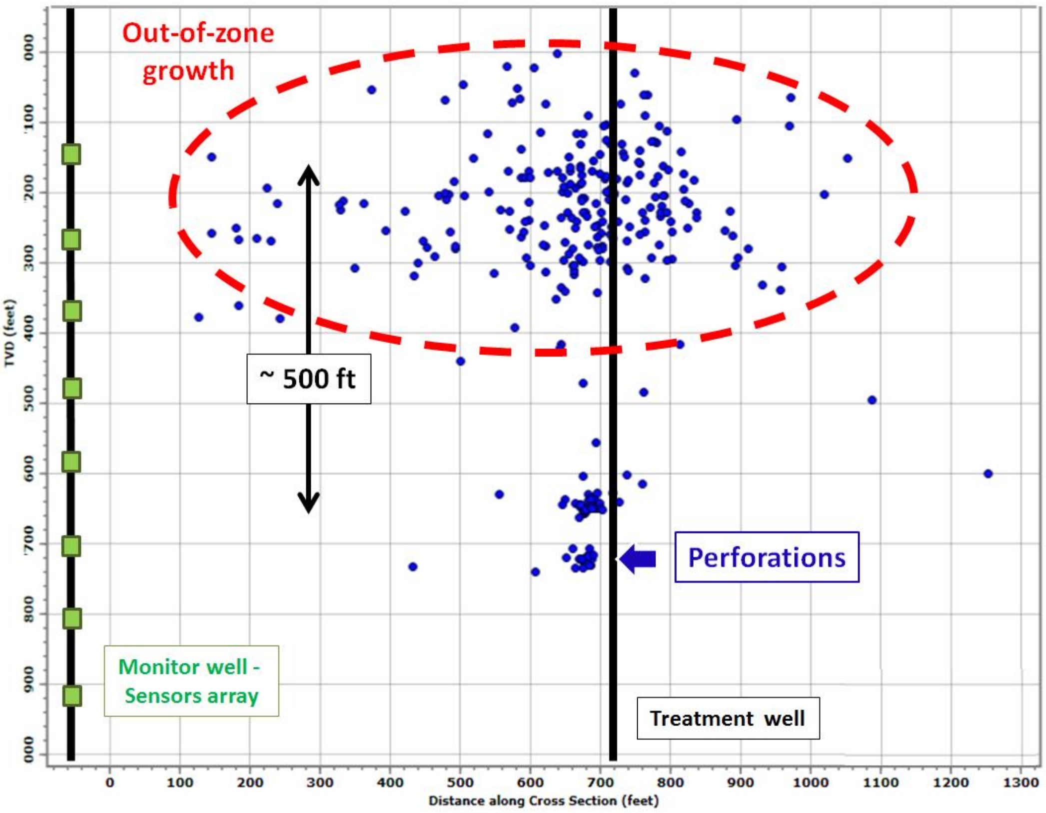

Figure 2. Microseismic events (blue dots) associated with a single stage hydraulic fracturing treatment on a vertical well. The figure shows the perforated interval (blue arrow), and a sensor array within the vertical monitor well in green for reference. Significant microseismic activity approximately 150m (500ft) above the perforated interval suggests out of zone fracture growth.

Appendix C: List of acronyms and abbreviations

%Ro	Vitrinite reflectance
3-D	Three dimensional
$\sigma_{min,}$ Sh	Minimum horizontal principal stress
$\sigma_{max,}$ SH	Maximum horizontal principal stress
ν, PR	Poisson’s ratio
μ	Viscosity
API	American Petroleum Institute
BH prop con	Bottom hole proppant concentration
BHTP	Bottom hole pressure
Cal	Calcite
CALI	Caliper
Chl	Chlorite
CS	Condensed Section
CT	Computed Tomography
DFIT	Diagnostic Fracture Injection Test
Dol	Dolomite
DTC	Compressional transit time
DTS	Shear transit time
E	Young’s modulus
E’	Plane strain modulus
ESV	Estimated Stimulated Volume
GAPI	Gravity API
GR	Gamma Ray
GRI	Gas Research Institute
GRP	Gamma Ray Parasequences
H/C	Atomic ratio of hydrogen to carbon
HCL	Hydrochloric acid
HEC	Hilcorp Energy Company
HER	Hilcorp Energy Resources
H_f	Fracture height
HI	Hydrogen Index
HST	Highstand System Tract
I/M	Illite/Mica
I/S	Illite /Smectite
Kao	Kaolinite
Ker	Kerogen
KGD	Khristianovich and Zeltov and Geertsma and de-Klerk
$K_{Ic\text{-}app}$	Fracture toughness (tip effects)
LST	Lowstand System Tract
Mar	Marcasite
MDP	Magnitude vs Distance Plot

mfs	maximum flooding surface
Mw	Moment magnitude
NPHI	Neutron porosity
O/C	Atomic ratio of oxygen to carbon
OI	Oxygen Index
PI	Production Index
Plg	Plagioclase
P_{net}	Net pressure
Prop Con	Proppant Concentration
P-waves, Vp	Primary (Compressional) wave velocity
PKN	Perkins and Kern–Nordgren
Pyr	Pyrite
Q	Fluid injection rate
Qtz	Quartz
RHOB	Bulk density
RM	Medium Resistivity
RST	Regressive System Tract
RT	Deep Resistivity
RXO	Shallow Resistivity
S/N	Signal to Noise ratio
SB	Sequence Boundary
SEM	Scanning Electron Microscope
SH-waves	Horizontally polarized shear waves velocity
STP	Shut-in tubing pressure
Sv	Vertical principal stress
SV-waves	Vertically polarized shear waves velocity
Tmax	Temperature at maximum release of hydrocarbon during pyrolysis
TOC	Total Organic Content
TSE	Transgressive Surface of Erosion
TST	Transgressive System Tract
Vs	Shear velocity
VSP	Vertical Seismic Profile
W_f	Fracture width
X_f	Fracture half-length
XRD	X-ray diffraction

Appendix D: List of units

bbls	barrels
bpm – bbl/min	barrels per minute
ft	foot
Hz	Hertz
in	inches
km/s	kilometers per second
lb	pounds
m	meter
mm	millimeters
ms	milliseconds
Nm	Newton meters
ppa	pounds per proppant added
ppg	parts per gallons
psi	pounds per square inch
psi/ft	pounds per square inch per foot